MODULATION OF THE TRANSCRIPTIONAL CONTROL OF THE CARBON CONCENTRATION MECHANISM WITHIN *SYNECHOCYSTIS* SP. PCC 6803

By

SHAWN M. E. DALEY

Bachelor of Science in Biochemistry
Colorado State University
Fort Collins, CO
2002

Submitted to the Faculty of the
Graduate College of the
Oklahoma State University
in partial fulfillment of
the requirements for
the Degree of
DOCTOR OF PHILOSOPHY
July, 2010

MODULATION OF THE TRANSCRIPTIONAL

CONTROL OF THE CARBON CONCENTRATION

MECHANISM WITHIN

SYNECHOCYSTIS SP. PCC 6803

Dissertation Approved:

Dr. Robert Burnap

Dissertation Adviser

Dr. Robert Matts

Dr. Ulrich Melcher

Dr. Ramamurthy Mahalingam

Dr. Mark Payton

Dean of the Graduate College

ACKNOWLEDGMENTS

I would like to thank my parents, Michael and Darline Daley, for their love, support, and encouragement to pursue my dreams for so many years. I would further like to thank my grandfather, Harold Rogers, who didn't live long enough to see me finish this work, but has been here with me always, and my grandparents, Marjorie Rogers-Welch, Raymond and Mary Daley for all of their love and support over the years. And my girlfriend, Kristen Szabla, for her support during these last couple of years.

Dr. Dean Price is gratefully acknowledged for his assistance and consultation regarding inorganic carbon limitation buffers/depletion and methods of inorganic carbon uptake kinetics. Additional thanks to: Dr. Robert Tabita for his generous gift of control protein expression constructs used during the early stages of the protein expression work. Dr. Archie Portis for his kind gift of 2-PG (Sigma). Dr. Uday DeSilva for his kind gift of the Taq enzyme construct. Dr. Robert Matts for the pET30a vector (CN Biosciences, Inc.). Dr. Drew Dangel, for his assistance with EMSA buffers and protocols. Ms. Marla Carrick for her able assistance with protein expression and gel-shifting.

Additionally, the family and friends who make this kind of effort worth while: Patrick Hampton, Ann Hampton, Hayden Hampton, Brycen Hampton, Sarah Slater, Michael Puckette, Hong Jin Hwang, Jacob Manjarrez, Brent Raisley, and Liang Sun.

Table of contents

Table of Tables

TABLE OF FIGURES

Key Terms

1,3-BPG	=	1,3-Bisphosphoglycerate
2PG	=	2-Phosphoglycolate
3PG	=	3-Phosphoglycerate
α-KG	=	Alpha Ketoglutarate
ATP	=	Adenosine Triphosphate
B_6f	=	Cytochrome B_6f complex
CA	=	Carbonic Anhydrase
CBB	=	Calvin-Bassham-Benson
CCA	=	Carboxysome Carbonic Anhydrase
CCM	=	Carbon Concentration Mechanism
CcmR	=	Carbon Concentration Mechanism Regulator (1); see also NdhR
CHO	=	Carbohydrates
Ci	=	Inorganic Carbon (HCO_3^- and CO_2)
CmpR	=	Cmp operon transcriptional regulator; *Synechocystis* sp. PCC 6803 Gene ID: sll0030 (*2, 3*)
DBD	=	DNA Binding Domain
DCMU	=	3-(3,4-dichlorophenyl)-1,1dimethylurea
DHAP	=	Dihydroxyacetone Phosphate
DLS	=	Dynamic Light Scattering
EMSA	=	Electrophoretic Mobility Shift Assay (DNA gel shift assay)

EZ = Ethoxyzolamide

G3P = Glyceraldehyde-3-Phosphate (a.k.a. GAP)

GAP = see G3P

GLY = glycolaldehyde

$[HCO_3^-]_{cyt}$ = Cytosolic bicarbonate

HPLC = High-performance liquid chromatography

HTH = Helix-Turn-Helix; DNA binding motif

IPTG = Isoproply-β-D-thiogalactopyranoside

LTTR = LysR-Type Transcriptional Regulators

NdhR = NADPH dehydrogenase regulator (select subunits); *Synechocystis* sp. PCC 6803 Gene ID: sll1594 (*2, 3*)

PAM = Pulse-Amplitude-Modulation

PDC = Pyruvate Dehydrogenase Complex

PSI = Photosystem I

PSII = Photosystem II

RD = Regulatory Domain

Rubisco = Ribulose 1,5-Bisphosphate Carboxylase/Oxygenase

RuBP = Ribulose 1,5-Bisphosphate

SAP = shrimp alkaline phosphatase

SPR = Surface Plasmon Resonance

TCA = Tricarboxylic Acid Cycle

Ycf30 = LysR family transcriptional regulator; Gene ID: sll0998 (*2, 3*)

I. INTRODUCTION

Aquatic photosynthetic organisms are generally dependent upon active transport of inorganic carbon to supply sufficient amounts of CO_2 to the major carbon fixing-enzyme of oxygenic photosynthesis, ribulose 1,5-bisphosphate carboxylase/oxygenase (Rubisco). This active uptake of inorganic carbon (Ci), in the form of CO_2 or HCO_3^-, is a physiological necessity due to the low affinity of Rubisco for its substrate, CO_2, and the fact that concentrations of CO_2 typically found in aquatic environments are very low. This problem is compounded by the fact that Rubisco, besides having a low affinity for its substrate, carbon dioxide (CO_2), also exhibits a competing alternative oxygenase activity that combines O_2 with RuBP, instead of adding CO_2 (Figure 1). Because of the competition between CO_2 and O_2 at the active site of Rubisco, a large fraction of the photosynthetic substrate is directed towards the alternative oxygenation reaction (photorespiration) instead of the biosynthetically productive carboxylase reaction, particularly at low ambient CO_2/O_2 ratios. Since this is a competitive reaction, the fraction directed down one or the other pathway depends upon the local concentrations of these alternative substrates. Therefore, the active uptake of inorganic carbon minimizes the oxygenation reaction and enhances the productive carboxylase reaction. This dual specificity of the Rubisco is an intrinsic and ubiquitous characteristic of all orthologs in nature. The topic of this thesis is the regulation of the mechanism responsible for the uptake of inorganic

carbon in the cyanobacterium, *Synechocystis* sp. PCC6803, an experimental model used in many studies of oxygenic photosynthesis. Cyanobacteria maintain a very high relative concentration (~30 mM) of inorganic carbon (Ci) in the cytoplasm to mitigate the problem of the dual specificity of Rubisco outlined above (4). However, this active uptake of inorganic carbon is intricately regulated and my project concerns the nature of the transcriptional control over the expression of the transport proteins and enzymes that exert the uptake activity.

Figure 1

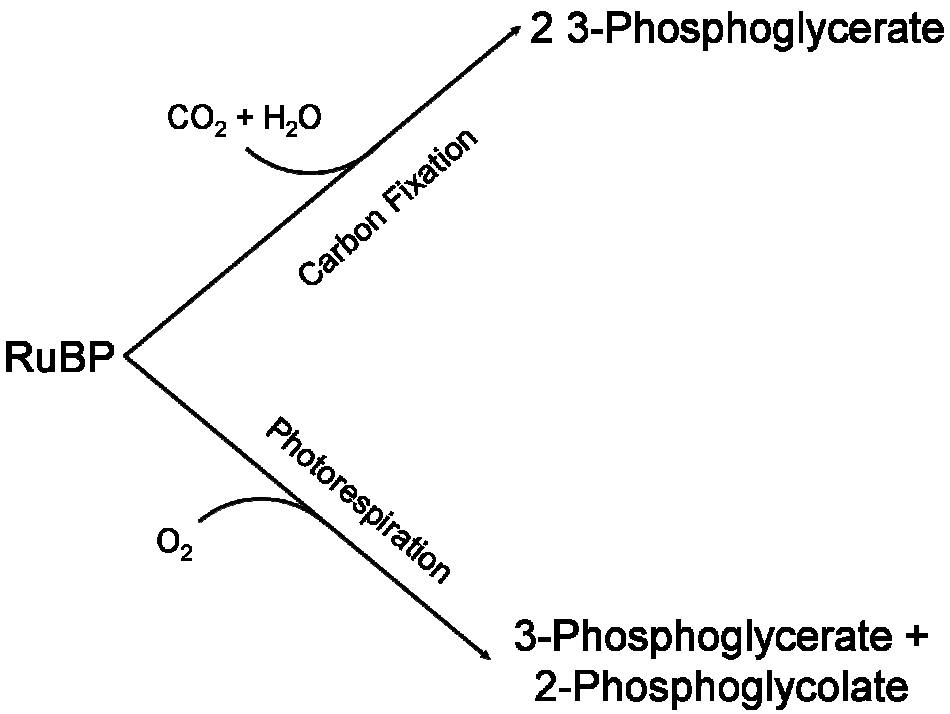

Figure 1. Competing carboxylase and oxygenase reactions catalyzed by Rubisco, the major carbon fixing-enzyme of oxygenic photosynthesis. The co-substrate, ribulose 1,5-bisphosphate (RuBP) may be alternatively carboxylated (yielding two 3-Phosphoglycerate) or oxygenated (yielding 3-Phosphoglcyerate and 2-Phosphoglycolate) (adapted from (5)).

The intracellular Ci concentration is approximately 1000 times that of CO_2 normally found dissolved in water (6). As noted, the oxygenase activity occurs because of the relatively low affinity (15 – 200 μM) of Rubisco for CO_2 and an appreciable affinity for O_2 (6). Higher plants have localized Rubisco to the stromal portion of the chloroplasts, while cyanobacteria localize it within a special protein compartment called a carboxysome (see below) (7-13). Cyanobacteria, green algae and higher plants contain the type I Rubisco comprising both 8 large and 8 small subunits (*7, 8, 14*). Within higher plants, the large subunits are nuclear-encoded and the small subunits are encoded within the chloroplast genome (14). Within *Synechocystis* sp. PCC 6803 (the model organism used for thesis research, see next section), both the large and small subunit coding sequences are part of an operon which includes a gene for a putative Rubisco chaperone [*Synechocystis* sp. PCC 6803 open reading frames (orfs) slr0009, slr0011, slr0012] (*2, 3*). It should also be noted that, given their common ancestry, the stromal portion of chloroplasts is the equivalent of the cytosolic portion of a cyanobacterium (*15, 16*).

Experimental Model: *Synechocystis* sp. PCC 6803

Synechocystis sp. PCC 6803, hereafter *Synechocystis*, is a glucose-tolerant freshwater cyanobacterium that contains a 3.6 meganucleotide genome who's sequence was published in 1996 (*2, 3*). This organism, popular for genetic work because it is naturally transformable and has an endogenous recombination system (via a homologous double cross-over event), can be used in gene replacement strategies. Current evidence supports that cyanobacteria have a

common ancestor with the symbiotic predecessor to the plant chloroplast (*15, 16*). Indeed, apart from differences in the light-harvesting antennae[1], many of the basic components of the photosynthetic mechanism are highly homologous between higher plants and cyanobacteria. *Synechocystis* is a good model system for oxygenic photosynthesis given that we are able to experiment with the active Photosystems (PSI/PSII), and the associated electron transport chains.

Photorespiration activity of Rubisco causes it to produce 3-phosphoglycerate (3PG) and 2-phosphoglycolate (2PG), three- and two-carbon compounds, respectively, by the addition of molecular oxygen (O_2), to ribulose-1,5-bisphosphate (RuBP). The production of 2PG leads to the net loss of inorganic carbon and the generation of H_2O_2 from the salvage pathway (Figure 3). Besides the loss of substrate incurred during the production of serine, the expenditure of an ATP is required for the production of glyceraldehyde phosphate (GAP) (Figure 2) (17). The GAP can then be converted back into RuBP through the remaining steps of the CBB cycle. Overall, there is a net loss of carbon and energy during this process and therefore it is of critical importance that the active site of Rubisco is saturated with CO_2 whenever it is active. Although evolutionary pressure to minimize the oxygenase activity has not successfully eliminated it, the version of Rubisco in cyanobacteria has a Km for CO_2 that is approximately 200 μM while Rubisco in C3 plants have a Km of 15 – 25 μM (6).

[1] Cyanobacteria possess blue colored bilin-containing complexes situated on the thylakoid membrane surface that serve as the major light-harvesting structures, whereas higher plants and green algae use membrane intrinsic chlorophyll a/b complexes for this function.

Figure 2

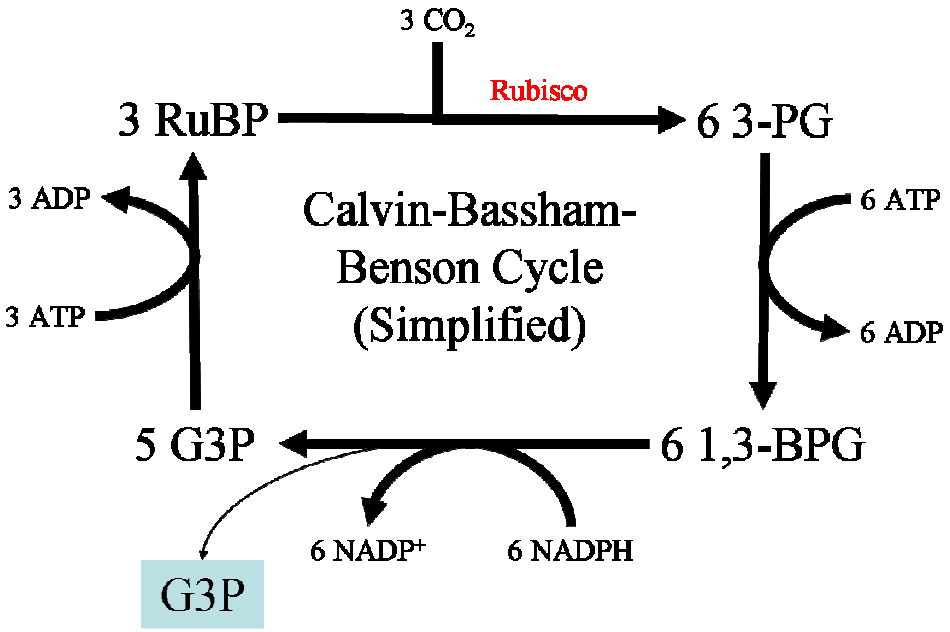

Figure 2: Simplified diagram of the Calvin-Bassham-Benson cycle, illustrating the ratios of substrates to products for the cycle. The highlighted compound glyceraldehyde-3-phosphate (G3P) is the product of the cycle, created from the reaction of 3 RuBP with 3 CO_2 yielding 6 molecules of 3-phosphoglycerate (3-PG), which are phosphorylated to produce 6 molecules of 1,3 bisphosphoglycerate (1,3-BPG) , which is subsequently reduced to produce 5 G3P (used for regeneration of the RuBP) and 1 which is pulled off for biosynthetic processes. This extra G3P is not required to regenerate the RuBP used in the initial reaction by Rubisco and may be pulled off for biosynthesis, within glycolysis or gluconeogenesis. The critical enzyme (Rubisco) of the cycle, responsible for the addition of CO_2 to RuBP, is indicated in red.

Figure 3

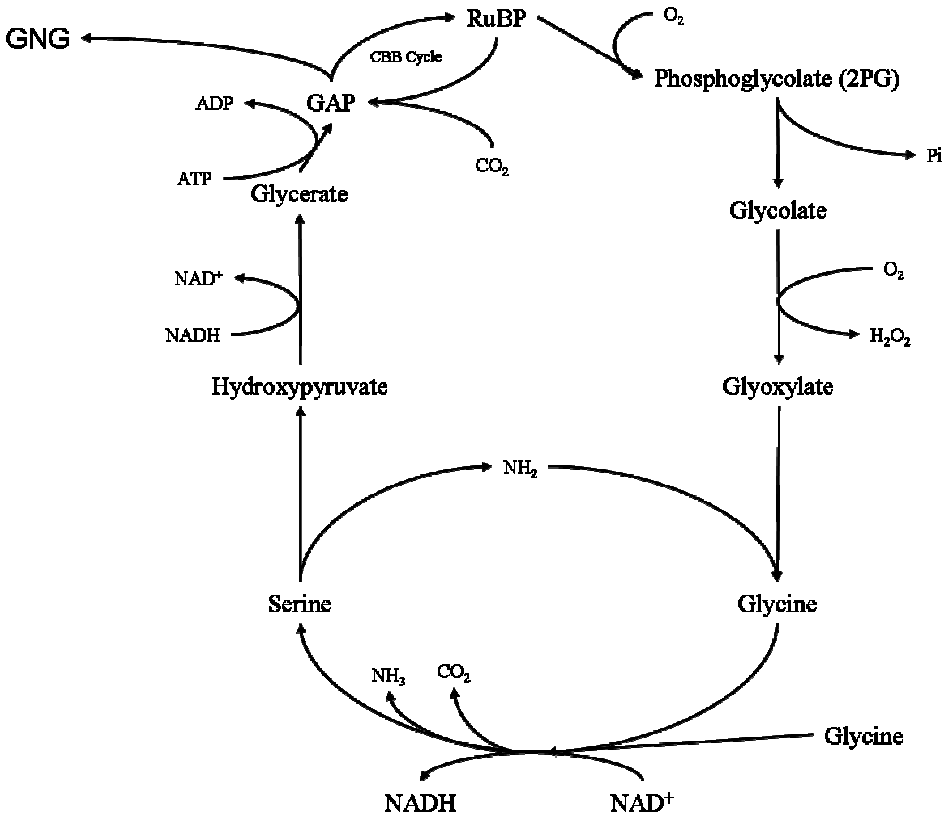

Figure 3. Simplified diagram of the photorespiratory cycle. Glyceraldehyde phosphate (GAP a.k.a. G3P), gluconeogenesis (GNG). Adapted from (18).

Carbon Concentration Mechanism (CCM)

Inorganic carbon (Ci) is found primarily in the biosphere as either carbon dioxide (CO_2) or bicarbonate (HCO_3^-). As mentioned, cyanobacteria maintain a very high relative concentration of inorganic carbon in the cytoplasm to provide Rubisco with enough CO_2 to avoid wasteful photorespiration. Both CO_2 and HCO_3^- are substrates of the CCM with each substrate using a different mechanism of transport into the cell. Dedicated transporters bring extracellular HCO_3^- into the cell using ATP hydrolysis (*cmpA*) or Na^+ symporter (*sbtA*) (see Transport Groups Low and High Affinity for a more detailed description). The transport of CO_2 into the cell is carried out by passive diffusion using water channels within the plasma membrane down the concentration gradient created by CO_2 consumption (see Transport Groups Low and High Affinity for a more detailed description). This consumption is initiated in the cytoplasm by a dedicated protein complex (NdhF3 a.k.a. CupA), which catalyzes the hydration of the CO_2 into HCO_3^- (*6-8, 19-24*). The hydration takes place on the thylakoid membranes of the cell and utilizes NADPH as an energy source (*6-8, 19-24*). The overall CCM (Figure 4), involves the development of high concentrations of bicarbonate HCO_3^- (~30mM) in the cytoplasm, where it can be transported into a sub-cellular microcompartment, termed the carboxysome, which contains the cellular complement of Rubisco. Rubisco can only use CO_2 and therefore a carboxysome carbonic anhydrase (CCA) function is to convert the HCO_3^- to usable CO_2 inside the carboxysome (*8-13, 23-30*). Whether or not the other enzymes of the CBB cycle are also contained within the carboxysome remains a

matter of debate. However, the net result is that once the inorganic carbon is in the cell it may be converted into carbohydrates (CHO) by the CBB cycle.

The CCM involves two structurally distinct, yet complementary transport groups, one high affinity and the other low affinity, of transporter proteins, with each group having at least one HCO_3^- transporter and one CO_2 transporter (31-33) as mentioned above. Basically, for each of the several transporter types (either HCO_3^- or CO_2 transporter), there are two forms, a low affinity protein variant and a high affinity protein variant. These transporters are differentially expressed depending upon the ambient Ci conditions, as discussed below. Functionally, this allows for additional uptake under Ci limiting conditions through the activity of the high affinity transporters. However, the high affinity transporters are not sufficient to meet all needs of the cells inorganic carbon and the low affinity system is expressed under all conditions (31-33). Thus, the high affinity transporters are expressed to augment, but not replace the low affinity transporters. Depending upon the type of transporter, either ATP or NADPH is thought to be the source of energy for the active uptake. However, most of the details of the transport mechanisms remain to be established and the exact bioenergetic costs remain to be determined. The entire CCM, including the carboxysome, is depicted in Figure 4, illustrating only the high affinity variants of each transporter type. What is known of the mechanism and expression of each is discussed more thoroughly in the next few sections.

Figure 4

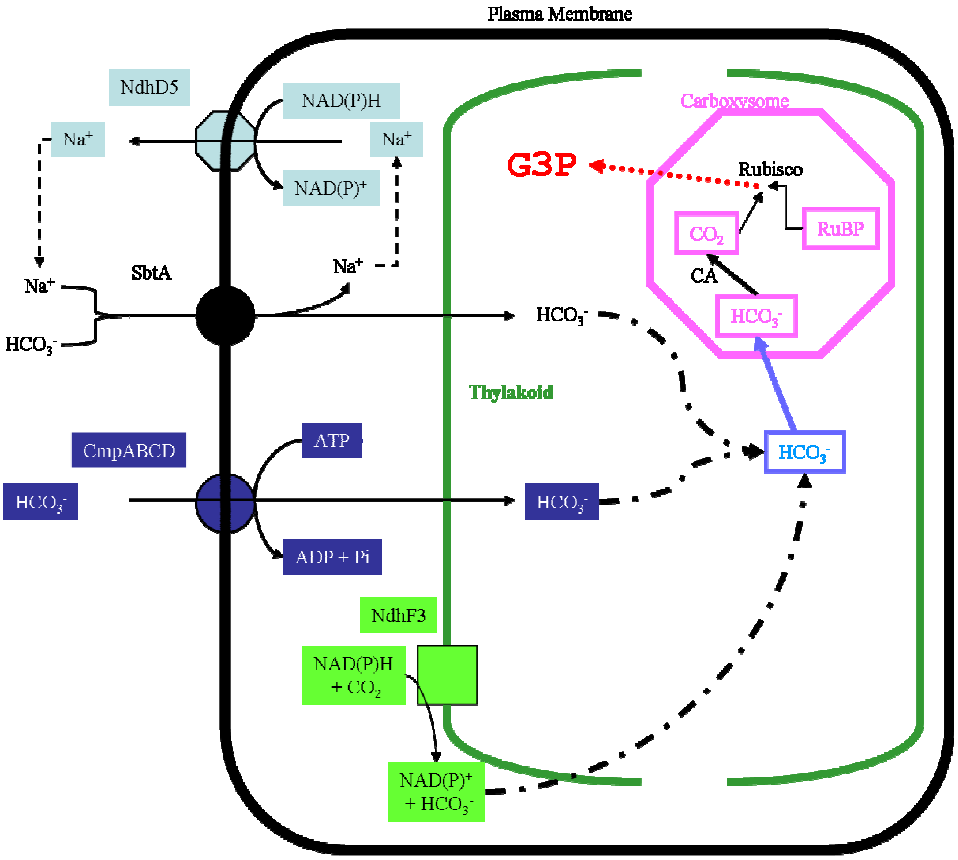

Figure 4: Diagram of the inorganic carbon uptake system including the interaction with the carboxysome and the primary product of the Calvin-Bassham-Benson (CBB) cycle, 3-Phosphoglycerate (G3P) indicated in red. Only the high affinity transporters are illustrated in this diagram, for both the HCO_3^- and CO_2 transport groups. Adapted from (8).

Transport Groups (Low and High Affinity)

The low affinity transporters, are constitutively expressed, and can be divided into two types, one transporting CO_2 (*6-8, 19-24*), and the other HCO_3^- (*6, 8, 19, 20, 22-24, 34-43*). The high affinity transporters are inducible, and are likewise divided into two distinct types; one transporting CO_2 (*6-8, 19-24*), and the other transporting HCO_3^- (*6, 8, 19, 20, 22-24, 34-43*). Induction of the high affinity transporters occurs under conditions of carbon limitation/stress (*1, 6, 8, 19, 20, 22-24, 34-43*). ***The signal transduction pathway for the induction of the high affinity components of the CCM is not known and this is a topic of my thesis project.*** Collectively, the transport mechanisms increase the cytoplasmic HCO_3^- concentration and it is this species of inorganic carbon that is transported into the carboxysome.

High Affinity Transport Genes

LysR-type transcriptional regulators (discussed later in this chapter) have been identified as controlling CCM genes (*19, 32, 44-46*). One of these, CcmR, is theorized to control several different sets of genes that have related, but individually distinct high-affinity Ci uptake functions within the cell (Figure 5) (*1, 19*), and is of primary interest to this thesis project. The first set includes two members that are multicistronic and are directly involved in the acquisition of inorganic carbon (*sbtA* and *ndhF3*) (*1-3, 8, 19, 37, 38*). These encode the proteins for the presumptive sodium-bicarbonate symporter and the CO_2 uptake (CUP) proteins, respectively. The second set of genes that appear to be controlled by CcmR, includes a Na^+ transporter used to establish the Na^+

gradient (*ndhD5*) which *sbtA* uses and a Na^+/H^+ antiporter that is thought to be used in maintaining the intracellular pH (*nhaS1*) (*1-3, 8, 19, 37, 38*). This Na^+ transporter is a multicistronic gene (*ndhD5*) (*1-3, 8, 19, 37, 38*). The third and final set consists of single genes of CcmR, and a quinone synthesis gene (*ubiX*) (*1-3, 19, 37, 38*). Physical evidence for the interaction of CcmR and specific DNA targets shown in Figure 5 is largely hypothetical and is based upon earlier DNA microarray data. Indeed, one of the main aims of my thesis project is to provide direct physical evidence for these hypothesized interactions.

Induction of physiological states of increased affinity for Ci appears to be complex and probably involves both transcriptional and post-transcriptional mechanisms. My research focused on the transcriptional mechanisms, with earlier work showing that post-transcriptional mechanisms do exist (at least in some species of cyanobacteria). It has been shown that a higher affinity state is produced within 10–15 min. of the challenge event in some species (*32-34, 42, 47*). This time interval is sufficient for either *de novo* synthesis of new transport protein(s), or chemical modification of existing protein complexes. Several experiments were conducted to determine if the high affinity transporters are indeed *de novo* synthesized, or if there are chemical modifications (e.g. phosphorylation) occurring by some unknown mechanisms (*34, 42, 47*). One speculative possibility is that the constitutive low affinity transporters have their activity modulated by post-translational modifications, but this has yet to be explored.

Figure 5

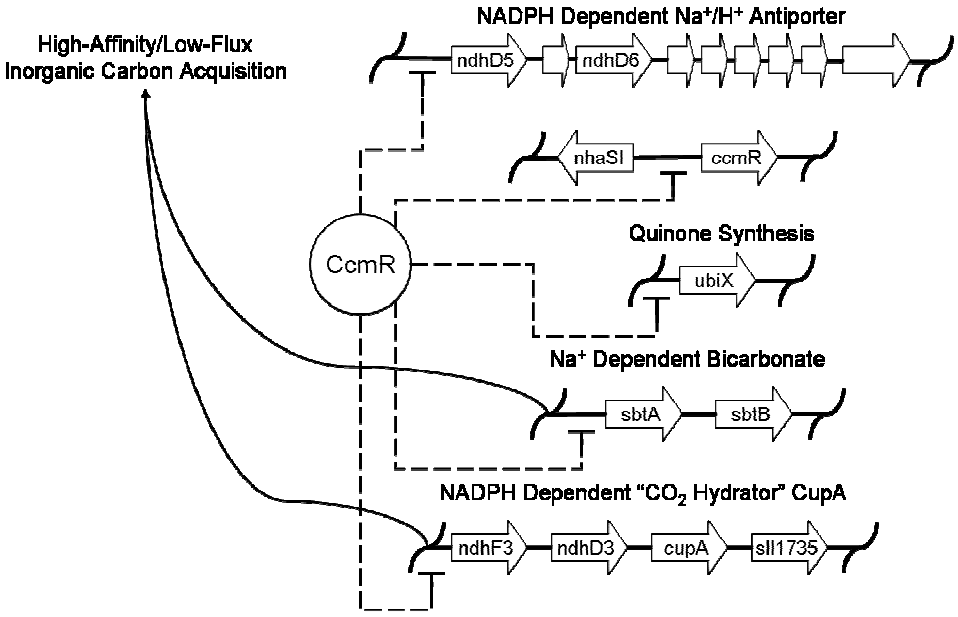

Figure 5. Proposed regulon for CcmR based on microarray analysis of global transcriptional changes following a downshift in inorganic carbon availability (1). CcmR was proposed, based upon these microarray results, as a repressor of all the genes/operons under its regulatory control. The identified genes are *ccmR* (self) and *ubiX* (quinone synthesis) - as monocistronic products. Additionally *sbtA* and *ndhF3* are multicistronic operons that are directly involved in the uptake (HCO_3^-) or hydration (CO_2), respectively, for inorganic carbon acquisition. The final member of the regulon is *ndhD5* which is another multicistronic operon that maintains a sodium gradient for use by the *sbtA* operon.

The determination of whether or not *Synechocystis* has a post-transcriptional mechanism for increasing the affinity for Ci has been especially controversial. Addition of the translational inhibitor chloramphenicol to the cells at the time of carbon downshift (34) did not cause any hindrance in the activation of the high affinity transporters, which would indicate that the transport proteins are not being synthesized *de novo*, and thus are post-translationally controlled. The addition of K252a (a eukaryotic ser/thr protein kinase inhibitor), using the same carbon downshift, no measurable increase in carbon uptake affinity could be detected indicating that post-translational modification (phosphorylation) is involved in the activation of the high affinity uptake system (34). However, these results were disputed: the Badger group published data indicating that the addition of chloramphenicol prevents the induction of the high affinity transport systems which would suggest that *de novo* protein synthesis is required to activate the high affinity system (47), these results are in direct contradiction to the data showing the requirement of post-translational modification using phosphorylation (34). In contrast to the disagreement regarding the situation in *Synechocystis*, the existence of a chloramphenicol-insensitive induction of a high affinity state has been shown using two *Synechococcus* species, the freshwater *Synechococcus* sp. PCC 7942 and the marine *Synechococcus* sp. PCC 7002 (42). Thus, while the existence of post-translational regulation is in dispute in *Synechocystis*, such mechanisms are likely to exist in other cyanobacterial species. On the other hand, regulation at the level of transcription has been unequivocally shown in all cyanobacterial species examined to date.

In addition to the abovementioned regulatory mechanisms for the regulation of the CCM, a third possible mechanism requiring the protease FtsH (Slr0228) was recently described (48). This work was based on a knockout of the gene encoding the FtsH protein (*Synechocystis* orf sll0228) and an analysis of the high-affinity transporter activity in the mutant. Like all FtsH proteins, the protein encoded by orf sll0228 is a protease, but in this case, it is crucial for the degradation of damaged photosystem II proteins. The authors' main conclusion is that the high-affinity carbon transport system requires FtsH in order to become induced when HCO_3^- levels are low within the cell (48). However, while the experiments are technically well executed, I believe the authors misinterpreted a key piece of their data (failure of the system to induce the high-affinity transporters) to indicate that FtsH is required for activation of the high-affinity transporters by way of CcmR degradation (48). The biochemical demonstration that FtsH is required is not presented and it appears that the authors have overlooked that without FtsH the D1 protein of Photosystem II (PSII) is not turned over following photodamage. This causes PSII to become inactive and prevents the accumulation/regeneration of both ATP and NADPH from subsequent complexes which rely on the electrons extracted from H_2O by PSII. Without ATP or NADPH neither of the high-affinity transport systems will become active (see Energy Requirements for the CCM). Not only are the transporters themselves dependent on ATP or NADPH but the CBB cycle requires both to function (Figure 3). Without sufficient reserves/turnover of ATP and NADPH, the CBB cycle will not function and the intracellular [HCO_3^-] will not drop low enough for the high-

affinity system to become active (see above). It is this detail that is missing from the conclusion/interpretation made by (48). Failure to consider these points causes the conclusions stated by the authors (48) to be flawed, which is most unfortunate given the excellent technical skill of the experiments themselves, and that FtsH has no direct role in the high-affinity transport system. However, I have not addressed this issue in my thesis.

Energy Requirements for the CCM

Evidence regarding the details of the energy requirements (ATP or NADPH) for the inorganic carbon transport mechanism remains scarce for all the transporters and most of the information remains tentative and is based upon protein homologies. While two transporters (CmpABCD and NdhF3) appear to use a direct coupling of energy (ATP and NADPH, respectively), the sodium bicarbonate transporter (SbtAB) uses the Na^+ gradient that is established by another protein complex (22) (Figs. 5 and 6). In order to help establish this Na^+ gradient CcmR appears to control a protein complex, NdhD5, which seems to function as a redox-driven (NADPH) Na^+ transporter (*1, 38*). Because it appears to be co-regulated with the other components of the CCM, the NdhD5 complex appears to function primarily for establishing the Na^+ gradient for SbtA (8).

It is interesting to note that while several of the transporters use Na^+ gradients to perform their transport of Ci they may also use Li^+ but not K^+ (*8, 43, 49, 50*). That K^+ has a larger radius than Na^+ or Li^+ might explain why it can not be used by the transporters. It should be noted that although Li^+ can bind and be used by the transport proteins it is not as effective as Na^+ (*43, 49, 50*).

The ATP and NADPH used to provide energy for the active transport by these complexes comes primarily from the light reactions of photosynthesis. CcmR controls proteins involved with the NADPH-driven transport of CO_2 and HCO_3^- (NdhF3 and SbtA, respectively), while CmpR controls proteins involved with the ATP driven transport of HCO_3^- (CmpABCD) (*6, 8, 19, 20, 22-24, 34-43*).

Carboxysomes

The carboxysomes are small unilamellar protein-bound structures (a.k.a. microcompartments) found within many different photoautotrophic and chemoautotrophic bacterial species (*13, 51-55*). Although, microcompartments have been observed for over 40 years their functions are only now beginning to be understood (56). Within *Synechocystis*, the proteins which make up the structural portion are CcmK1-4LMNO (orf sll1028-1032, slr1838-1839, slr0436), while the Rubisco proteins are RbcLS (orf slr0011-0012), along with a specific carboxysome carbonic anhydrase CcaA (orf slr1347) (*2, 3, 8, 55, 57-59*). The carboxysomes contain the majority of the Rubisco (*7-9, 57*). Carboxysome shells have recently been divided into two classes based on the form of Rubisco and the form of carboxysome proteins they contain (8). This division has held true in all of the photoautotrophic bacteria which have been examined (8). Based on this division, *Synechocystis* is a member of the β-cyanobacterial family and contains the 1B version of Rubisco (*7, 8*).

The carboxysome appears to allow for the free diffusion of HCO_3^- through the protein shell and the conversion into CO_2 by the carboxysome carbonic anhydrase (*7, 8*). This allows for a net flow of inorganic carbon into the

carboxysome for consumption by Rubisco. Recent evidence suggests that the surface of the carboxysomal proteins are charged and contain small pores which may allow for the controlled diffusion of small anions through the protein shell, although this remains conjecture at the present time (*7, 8, 58, 59*).

LysR-Type Transcriptional Regulator Proteins (LTTRs)

As mentioned, LTTRs have been shown to be important for the regulation of the CCM in cyanobacteria. LTTRs have been described as being among the largest and most widely distributed families of prokaryotic transcription factors (60). Six paralogous LTTRs have been identified in *Synechocystis*; sll1594 (*ccmR*), sll0030 (*cmpR*), sll0998 (*ycf30*), slr0395 (*ntcB*), slr1871, and slr1245 (Appendix B; Figure B1a-e, B2). LTTRs contain two functional domains: a DNA Binding Domain (DBD) and a Regulatory Domain (RD), which are connected by a short α - helical linker (coil-coil).

The wide distribution of these proteins in the eubacteria (including cyanobacteria) argues for their presence from the early stages of life on earth (*7, 8*). The known high resolution structures of these proteins reveal that they share similar structural characteristics despite considerable sequence divergence (61-65). Additionally, LTTRs have been found encoded within the genomes of chloroplasts in some algae. Examples of repressor and activator activities are found in this large family of transcriptional regulators. Indeed, of the two proteins that I have studied in this thesis project, one is a repressor (CcmR) and one is an activator (CmpR).

In all instances where the action of an LTTR has been studied in detail, the protein has been found to bind one or more small ligand molecules that serve as co-activator or co-repressor molecules, depending upon the mode of transcriptional regulation. These ligands modulate the DNA binding properties of the LTTR to its cognate transcriptional regulatory region of the DNA near the

gene being regulated. Recently it was determined that within *Synechococcus elongatus* PCC 7942, both RuBP and 2PG acted as the ligand molecules for CmpR while controlling the CmpABCD operon (66). Although, both RuBP and 2PG are acting as co-regulators for CmpR, they are acting with very different affinities (66). The photorespiratory metabolite 2PG appears to bind with a nearly 1000 fold higher affinity than does RuBP (66). The 2PG affinity was determined by electrophoretic mobility shift assay (EMSA) and thus contains a high degree of uncertainty about the exact value and difference between these affinities. As discussed later, my efforts to see if I could apply this technique for identifying the ligand(s) of CcmR proved problematic, although I was able to use the EMSA technique for evaluating the specificity binding of CcmR to particular chromosomal DNA fragments. Although co-regulatory molecules have now been identified for CmpR, this molecule controls only a small portion of the total high affinity uptake system. It is still unknown how many other regulatory molecules could be regulating different components of the CCM and specifically, what ligand serves to control the activity of CcmR. It is probable that the set of agents controlling the CCM may contain several different regulatory molecules acting in concert allowing for multiple levels of regulatory control.

LTTR Structural Characteristics

DNA Binding Domain (DBD)

Structurally the DBD of an LTTR is located in the N-terminal region of the protein and is composed of approximately 65 amino acids. The three dimensional structure of the domain contains a Helix-Turn-Helix (HTH) motif (67-

69). It is responsible for the actual contact with the DNA, and binds directly to 50 – 60 bp of DNA (19). The binding sequences are known to be approximate palindromes of 10 – 20 bp (*19, 70*). The consensus sequence for CcmR in cyanobacteria has been tentatively (small sample size) determined as 5' TCAATG-N_{10}-ATCAAT 3' (19).

The DBD shows the highest proportion of conserved residues when the paralogous inorganic carbon uptake regulators CcmR and CmpR are compared (Appendix B; Figure B1b). When looking at all six of the *Synechocystis* proteins, the degree of DBD amino acid sequence conservation is considerably less, but this region still contains the majority of the conserved residues (Appendix B; Figure B1a). The majority of the sequence differences are seen within the regulatory domain of the proteins, including CcmR/CmpR which show an overall sequence identity of more than 50%. But, within the DBD, these two proteins have a sequence identity of almost 68% (Appendix B; Figure B1b). This conservation within the DBD is not surprising given that this family of proteins binds and regulates the expression of genes at the transcriptional level, and would therefore require common situational elements.

Regulatory Domain (RD)

The RD comprises the largest segment of the protein, with approximately 200 amino acids, and is located in the carboxyl terminal portion of the protein. This domain contains the binding site(s) for the ligand molecule(s). The binding of the ligand(s) to the protein is thought to change its conformation, altering the function of the protein (71).

The DBD must maintain a structural conformation to bind with the DNA, while the RD must control the behavior of the protein with respect to the DNA sequence to which it is bound. The changes in RD sequence have likely occurred in order to facilitate the observed differences in the regulation and binding characteristics among various members of the LTTR family without sacrificing structural stability. In a random, chemical mediated mutagenesis study, no mutations leading to constitutive activation within the DBD were detected (72). The majority of the mutations are located in the RD with two located in the carboxyl-terminal end of the coil-coil linker (72). The locations of the mutations do not follow any predictable pattern and the side chain chemistries are not conserved (72).

Known ligand molecules are as varied as the pathways that are being regulated and include sulfate, thiosulfate, succinate, ribulose 1,5-bisphosphate, etc. (71-77). In the case of CcmR it is logical to propose that its ligand is bicarbonate (HCO_3^-) given its control over inorganic carbon transporters. However, in Chapter 3, I show this is not the case and that other small molecules function in the regulation of CcmR.

Coil-Coil Linker

The coil-coil linker is a small (~20 residues) α-helical linker between the DBD and RD, which has no known function apart from connecting the two domains. However, dimer/tetramer interactions with other LTTRs have been shown and these interactions could have their structural origins within the coil-coil linker (*45, 63, 71*). Additionally, substantial bending of the DNA has been

shown by (71) and, based on the crystal structure of a related LTTR (1iz1 (62)), the linker may be involved in the conformational shift upon ligand binding (see 'Activity' below).

LTTR Function

The activation mechanism is unknown for most members of the LTTR protein family. It is known that some (perhaps all) use a DNA bending action to cause regulatory changes in gene expression as illustrated by van Keulen (71) (Figure 6) and their study of the LTTR CbbR from *Xanthobacter flavus*. This bending involves the formation of a dimer/tetramer interaction, and uses three inverted repeats (71). Within these three sequences the protein binds with different affinities and this causes two dimers to be placed at position 1 and 3 (IR1 and IR3) which bends the DNA an angle of ~64° (71). In this configuration the target operon (*cbbLSXFPTAE*) is not actively transcribed (71). Once the ligand (NADPH) is added, the DNA bend relaxes to ~55^{o} and the operon is actively transcribed (Figure 6) (71). This activation is accomplished by a shifting of the second dimer (position 3) toward the 5' end of the intergenic region, relative to the gene start, which creates a tetramer like interaction (using positions 1 and 2 [IR1 and IR2]) (Figure 6) (71).

The determination of DNA bending can be calculated by measuring the migration of the protein:DNA complexes on EMSA, and using a simple formula to determine the angle of bending (see Materials and Methods, Chapter II) (78). The migration measurements are done on DNA fragments that have the binding sites in the middle of the DNA or at the ends. This yields two migration distances

that can be converted into a ratio of bending (*71, 78-80*). Using the formula and knowing the location of bending allows for the calculation of the angle that the protein bends the DNA from the migration distance of the DNA:Protein complex (see below, Materials and Methods) (71).

Given that members of the LTTR family of proteins are found throughout the cyanobacterial world their evolution most likely predates the evolution of the different cyanobacterial species as we know them today. While some of these occurrences of LTTRs may be the results of horizontal gene transfer (HGT), it is unlikely that HGT can be used to explain the strong conservation seen in some members of the families across the diverse genera of cyanobacteria.

The identification of the ligand molecules for CcmR, and its direct binding to the promoters of the putative CcmR Regulon, remain to be determined. The control of these proteins is of interest given their transcriptional control of protein complexes involved in the high-affinity transport of inorganic carbon into the cell. The determination of direct DNA binding, part of my thesis project, will allow for the regulatory network of the CCM to be mapped, for the first time, to completion, with the addition of CcmR to the information already discovered about CmpR.

Figure 6

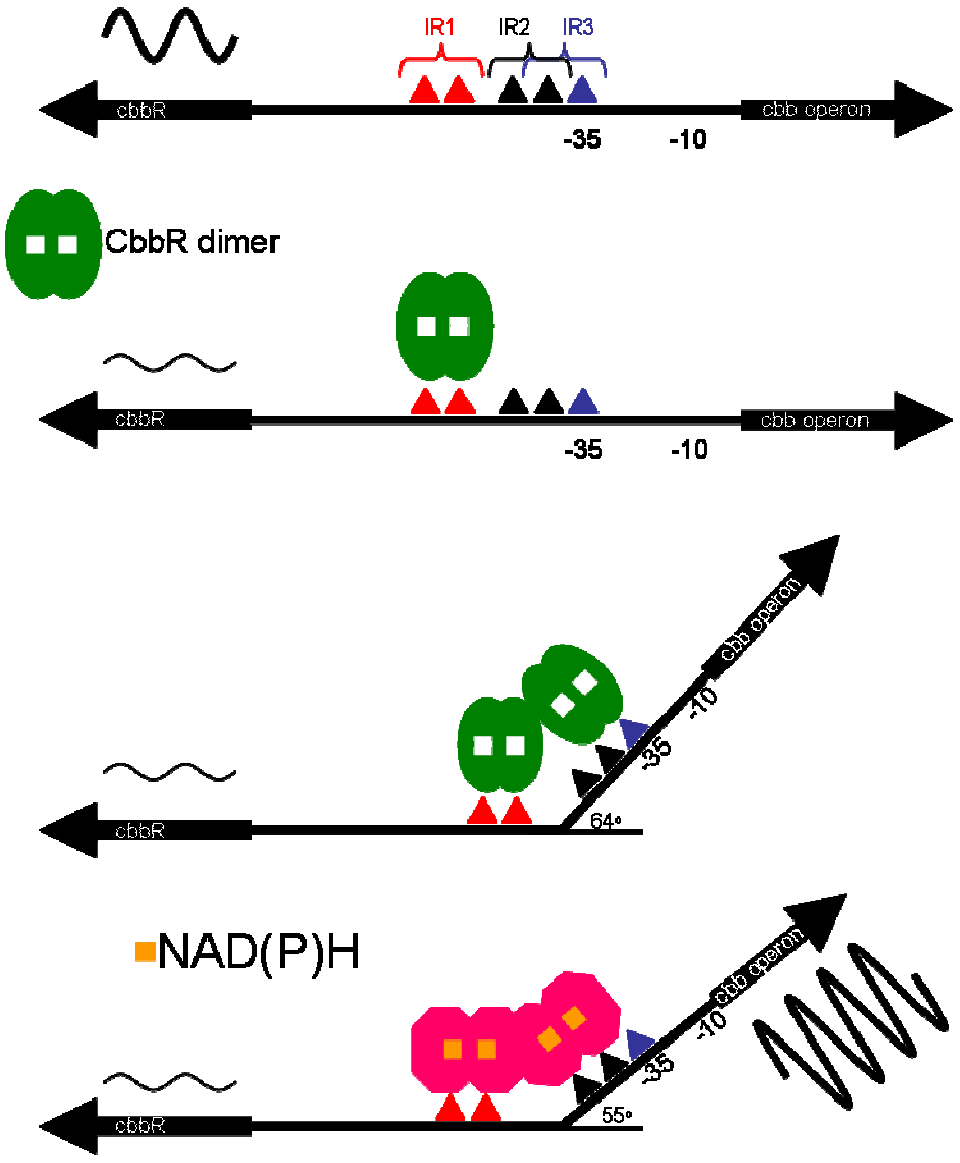

Figure 6: Illustration of the proposed DNA bending model of CbbR. Locations in red are the high affinity sites of the binding region (IR1). The IR3 (blue) is the low affinity binding region which overlaps with IR2 (black). The second dimer binds to the IR3 site only after the IR1 site is occupied. Upon addition of a second dimer DNA bending occurs between the IR1 & IR2 sites. Addition of the ligand molecule causes a conformational shift in the CbbR dimers allowing for an altered interaction which moves the IR3 binding dimer to IR2 allowing for transcriptional activation of the target gene. Adapted from (71).

II. MATERIALS AND METHODS

Cloning

Cloning of CcmR from Synechocystis PCC 6803 (N-Term His-Tag)

Full length *CcmR* was cloned from genomic DNA isolated from wild-type cells. *ccmR* was PCR amplified by Platinum *Pfx* DNA polymerase (Invitrogen) according to standard protocols supplied by the manufacturer using primers listed/described in Appendix A. Cloning into a plasmid was facilitated by the addition of unique 5' and 3' restriction enzyme sites (*Nde*I and *Xho*I, respectively) for ligation into *Nde*I and *Xho*I digested pET15B vector (CN Biosciences, Inc.). Restriction digestion of both insert and vector was carried out using 5 µL of NEB4 reaction buffer, 15 µL of DNA sample, 2.5 µL of *Nde*I (20,000 units mL^{-1}) and *Xho*I (20,000 units mL^{-1}) (New England Biolabs (NEB)), and 2 µL 100x BSA (New England BIolabs) in a 50 µL total reaction volume in distilled H_2O (dH_2O). Digestion was carried out in sequential steps starting with *Nde*I for 4 hours at 37 °C followed by addition of *Xho*I for 12 hours at 37 °C. Digestion products were subsequently subjected to electrophoresis using a 1% agarose gel to confirm the presence of DNA fragments before ligation and before DNA quantity was determined using a microspectrophotometer (Nanodrop Technologies, Inc). Ligations were performed following verification using 2 µL of 10x buffer, 1 µL T4 ligase, 3 µL pET15B, 3 µL *ccmR*, and 11 µL dH_2O. Ligations were carried out at 18 °C overnight, and then electrocompetent *Escherichia coli* DH5α cells were

transformed with ampicillin resistant plasmids containing the newly ligated DNA fragments by means using a MicroPulser (BioRad) following the manufacturer's instructions. Transformants were screened using alkaline lysis plasmid preparations followed by restriction analysis using standard protocols (81). Constructs were verified by sequencing at the Oklahoma State University Recombinant DNA/Protein Resource Facility. The verified *ccmR*/pET15B construct was subsequently used for all *in vitro* assays described below. However, due to a primer design error it should be noted that this recombinant protein contains an additional methionine residue at what would be the N-terminus of the CcmR protein itself. This mutation has shown no indication of impairing the function of the recombinant protein in any assay currently performed.

Cloning of CmpR from Synechocystis PCC 6803 (N-Term His-Tag)

Cloning of *cmpR* with an N-Terminal His-Tag was carried out essentially as described above for the *ccmR* N-Term His-Tag with the following modifications. The *cmpR* gene fragment was PCR amplified using in-house produced Taq polymerase (see Taq isolation). Following digestion the pET15B fragment was treated with shrimp alkaline phosphatase (SAP) (United State Biochemical (USB)). Phosphatase treatment was carried out using 16 µL dH_2O, 13 µL 10x SAP Buffer, 6 µL SAP, and 95 µL pET30a with the reaction carried out at 37 °C for 1 hour. Enzymes were then heat killed at 65 °C for 20 minutes. Digested *ccmR* and pET15B fragments were purified by phenol:chloroform extraction using standard protocols, and the fragments were subjected to

electrophoresis using 1% agarose gels to confirm the successful purification with the concentration being determined by microspectrophotometer (Nanodrop Technologies, Inc) before ligation. Ligations were performed at 25 °C for 5 min using Quick T4 ligase (NEB) following protocols supplied by the manufacturer, and then $CaCl_2$ treated *Escherichia coli* DH5α cells were transformed with plasmids encoding ampicillin resistance and containing the newly ligated DNA fragments using a MicroPulser (BioRad) to introduce the DNA by electroporation following the manufacturer's instructions. Transformants were screened using colony PCR essentially as described in (81). DNA constructs were verified by sequencing at the Oklahoma State University Recombinant DNA/Protein Resource Facility. The verified *cmpR*/pET15B construct was subsequently used for all *in vitro* assays described below

Generation of Intergenic DNA Fragments from Synechocystis PCC 6803

The intergenic regions of the genes and oligonucleotide primers were listed in Appendix A, and were amplified by PCR using in-house produced Taq polymerase (see Purification of Taq Polymerase) or Taq supplied by Fermentas according to standard protocols. The resulting fragments were concentrated using Sodium Acetate/Ethanol (NaOAc/EtOH) precipitation (0.1 volume NaOAc + 2.5 volumes 100% EtOH, stored at -20 °C overnight and centrifuged at 14,000 x g for 10 min.; decanted and washed with 1 mL 70% EtOH (-20 °C) then centrifuged as before. DNA samples were then dried in a Speed Vac (Savant) for at least 15 minutes. DNA samples were subsequently solubilized in either 10

mM Tris-HCl, pH 8.5, or dH_2O. The fragments were subjected to electrophoresis using 1% agarose gel to confirm successful amplification and concentrations were determined by spectroscopic means before use in gel-shifting or SPR [see below].

Purification of Taq Polymerase

A single colony of the Taq construct (*82*) was inoculated into 3 mL of Luria-Bertani (LB) media + 100 µg/mL ampicillin and allowed to grow overnight at 37 °C with shaking (225 rpm). An aliquot (0.6 mL) of the overnight culture was transferred to 500 mL of LB media with a final concentration of 100 µg/mL ampicillin and allowed to grow further. Once the cells reached the OD_{600} = 0.8, Isopropylthio-β-D-galactoside (IPTG) was added (0.5 mM final concentration) and the cells were allowed to incubate for an additional 12 hours at 37 °C with shaking at 225 rpm. Cells were harvested by centrifugation at 12,000 x g for 10 min, decanted and resuspended in 50 mL of Buffer A (50 mM Tris-HCl pH 7.9; 50 mM Dextrose; 1 mM etheylenedinitrilo-tetraacetic acid (EDTA). Cells were re-harvested at 12,000 x g for 10 min. and re-suspended in 25 mL of Buffer A + 4 mg/mL lysozyme, then allowed to incubate at room temperature for 15 min. Then 25 mL lysis buffer (10 mM Tris-HCl pH 7.9; 50 mM KCl; 1 mM EDTA; 0.5% Tween 20; 0.5% NonIdet P40; 1 mM phenylmethanesulfonyl fluoride (PMSF) was added and the cells were incubated at 75 °C for 1 hour. The lysis mixture was centrifuged at 14,000 x g for 10 min at 4 °C and the supernatant liquid was transferred to a flask. Ammonium sulfate (30 g per 100 mL) was added gradually over a period of 30 minutes while stirring. The precipitated protein mixture was

centrifuged at 14,000 x g for 10 minutes at 4 °C. The pellet was dried by inverting the centrifuge bottle for 10 minutes before resuspension in a total of 55 mL storage buffer (50 mM Tris-HCl pH 8.0; 12.5 mM dextrose; 75 mM NaCl; 0.325 mM EDTA; 0.375 mM dithiothreitol (DTT); 0.75% Triton X-100; 50% glycerol). DNA polymerase activity was verified by PCR of GS28 fragment using a 100 mM Tris-HCl, pH 8.3; 500 mM KCl buffer.

Protein Expression

CcmR Expression

Protein expression of CcmR was accomplished using electrocompetent BL21 (DE3) pLysS cells (CN Biosciences, Inc.) transformed with the *ccmR* containing plasmid (see above). The transformants were plated on nutrient agar plates containing 125 µg/mL ampicillin, and allowed to grow overnight at 37 °C. Resulting colonies were then used to inoculate 50 mL LB in 250 mL flasks with 100 µg/mL ampicillin, and incubated overnight at 37 °C with ~250 rpm shaking. Resulting cultures were used to inoculate 1000 mL LB with 100 µg/mL ampicillin and grown with aeration at 37 °C with ~250 rpm shaking until reaching an OD_{600} of 0.4 – 0.6; when the cultures were induced with 1 mM IPTG, and allowed to incubate for a further 3 hours. Following induction cells were harvested by centrifugation, frozen with liquid nitrogen, and stored in a -20 °C freezer until needed.

CmpR Expression

Protein expression of CmpR was carried out essentially as described for CcmR with the following modification. Following induction of the culture with IPTG the cells were allowed to incubate for a further 5 hours.

Recombinant Protein Purification

CcmR Purification

CcmR was purified using the cell pellets that were stored at -20 °C. Cell pellets were lysed with the addition of 1 mL room temperature (RT) native lysis buffer (see Appendix D) per 100 mL of cell culture volume. To ensure the compete lysis of the cells, and disruption of genomic DNA, sonication was performed with 10 – 15 second pulse durations at a power setting of 8 watts from 6 to 8 times. Following each pulse the tube was placed in an ice/water bath to be cooled for at least 1 minute before the next pulse. Following sonication the suspension was centrifuged at 14,000 x g for 5 minutes at RT. The resulting pellet was discarded and the supernatant was applied to 100 µL of Ni-NTA Superflow resin (Qiagen) per 100 mL original cell culture for affinity binding. Affinity binding was carried out in batch mode in 1.6 mL tubes (Eppendorf) by adding the supernatant from the lysis to Ni-NTA Superflow resin (Qiagen) and incubating at 4 °C for 15 – 60 minutes with gentle rocking. The suspension was spun at 14,000 x g at 25 °C for 10 – 15 seconds, and the supernatant was removed. The resin was subsequently washed 3 times with 1 mL wash buffer (see Appendix D) per 100 mL original culture volume using the same centrifugation settings. Once the washes were completed, the resin was

resuspended in 1 mL elution buffer (see Appendix D) per 100 mL original cell culture with centrifugation steps as above repeated for a total of 4 elution fractions. Elution fractions were combined and ammonium sulfate was added for protein precipitation up to 30 % of final concentration. Ammonium sulfate precipitation was carried out at 4 °C with gentle rocking for at least 1 hour; then the precipitate was centrifuged at 6,000 x g for 15 – 30 minutes at 4 °C. The supernatant was discarded and the pellet was solubilized in storage buffer (see Appendix D). Protein concentration was determined by measuring absorption at 260 nm and 280 nm using spectroscopic techniques and the protein samples were subsequently aliquoted and snap frozen with liquid N_2.

CmpR Purification

CmpR was purified essentially as described for CcmR with the following modifications. Elution fractions were combined and a final concentration of 50% ammonium sulfate was added for protein purification.

Electrophoretic Mobility Shift Assay (EMSA, a.k.a DNA gel shift assay)

Gel-shift reactions were carried out in a final reaction volume of 50 µL; 10 µL of 5x buffer (developed in-house based upon Molecular Probes, Invitrogen, EMSA Kit E33075) plus a range of concentrations (0 – 200 nM) of double stranded DNA target sequence (see Generation of Intergenic DNA Fragments from Synechocystis PCC 6803) (1 – 5 µL), a range of concentrations (0 – 7500 nM) transcriptional regulatory protein (see CcmR or CmpR Purification) (0 – 20 µL) ,a range of concentrations (0 – 5 mM) ligand molecule (1 – 10 µL), 0.1x xylene cyanol [loading dye] (5 µL), 1.5x BSA (0 – 15 µL) [relative to target

protein] and 10 – 20 µL 80% sucrose (30% final W/V). All components were mixed and centrifuged at 14,000 x g for 5 seconds. Reactions were incubated at RT for 20 minutes and centrifuged at 14,000 x g for 5 minutes. Samples (30 µL) were then loaded onto 6% native polyacrylamide gels (pH 8.5) for electrophoresis (PAGE) at 125 – 200 volts for 35 – 60 minutes at 4 – 25 °C. All gels were run using a BioRad Protean system. Gels were then stained with ethidium bromide or according to the EMSA kit (Invitrogen E33075) (*83, 84*), and imaged using a GelDoc-It (TS Imaging System). All DNA samples for gel-shifting were solubilized in 10 mM Tris-HCl pH 8.5. For a complete list of buffers see Appendix D.

Migration distances were used in the following formula to determine bending angles of DNA in the presence of a protein.

$$\alpha = 2 (\cos^{-1} (\mu m \times \mu e^{-1}))$$

µm = mobility of DNA molecules with bends in the middle

µe = mobility of DNA molecules with bends at the ends

α = bending angle

Surface Plasmon Resonance (SPR)

SPR is an optical method of detecting interactions between an injected free biomolecule flowing over an immobilized biomolecule on the surface of a biosensor. SPR is based on the fact that when photons strike the surface of a thin layer of gold at a certain angle it is able to excite a plasmon on the opposite side of the metal surface thereby generating an evanescence field (118). The loss of reflected photons at a specific set of angles from the light striking the

surface of the metal is reported as response units (RU), which is dependent on the refractive index of the biomolecule immobilized on the metal surface and the interaction with the injected free biomolecule along the flow path within the evanescence field.

All SPR assays were carried out using the SensiQ instrument (ICX Nomadics). Consistent data could not be generated using Ni-NTA coated carboxylic acid (COOH) chips, therefore direct DNA coupling using amine modified fragments was attempted using COOH chips. DNA fragments could not be directly coupled to the surface of COOH chips, so the COOH chip procedure was discarded in favor of protein coupling reactions. Pre-coupled Neutravidin chips were purchased from Nomadics for use with biotinylated DNA fragments. Normalization of chips was carried out using protocols developed in partnership with Ms. Kristen Szabla (OSU Biochemistry and Molecular Biology department). In order to prevent index shifts from occurring, the velocity of the system should not change before and after injections, association and disassociation flow rates need to remain uniform in order to accurately determine kinetic constants. Where required, interacting protein was removed from the surface using 0.1% SDS. Data exported into Excel (Microsoft) had baseline normalization applied to all values within each experimental set. Normalized data were then imported into Microcal Origin 6.0 and plotted. Mathematical processing beyond normalization was also completed in Excel for the determination of kinetic constants, with the results being exported either to Origin 6.0 (Microcal) or KaleidaGraph 3.5 to generate specific curve plots.

Biotinylated DNA was added to the neutravidin surface using a discrete injection of DNA at 5 – 10 µL/min for 25 – 50 minutes. If the surface was not saturated then additional injections (2 – 3 minutes) were made until no additional DNA binding was observed, typical saturation occurred at 400 – 800 RU's. DNA (see Generation of Intergenic DNA Fragments from Synechocystis PCC 6803) was dissolved in 10 mM Pipes pH 7.4, 300 mM NaCl immediately prior to use.

Protein samples were prepared using standard storage buffer with sucrose (see protein isolation [above] and Appendix D). Protein samples were exchanged on in-house produced gel-filtration spin columns (P6DG resin (BioRad)) for buffer exchange into running buffer (10 mM Pipes pH 7.4, 300 mM NaCl, 0.02% Tween-20 (CcmR) or 0.02% Triton X-100 (CmpR)). Post-exchange protein concentration was determined spectroscopically. All centrifugations were carried out at RT at 2000 x g for 4 minutes. The exchange columns were equilibrated using at least 2 washes of 100 µL each with running buffer. Once the columns were equilibrated, protein samples (75 – 80 µL) were applied to the resin surface and centrifuged.

CcmR or CmpR (1.5 µM) was injected into the system at 25 µL/min for 240 seconds. Ligand molecules were incubated with CcmR or CmpR for at least 5 minutes on ice before injection into the system. The interacting surface was regenerated using a 0.1% SDS (Protein) or 10 mM Pipes, pH 8.5; 1 mM EDTA (Ligand) wash. Data exported into Excel had baseline normalization applied to all values within each experimental set. Normalized data were then imported into Microcal Origin 6.0 or KaleidaGraph 3.5 to generate specific curve plots.

Scatchard Analysis

Following baseline normalization (see above) the data was imported into Excel and the values for Scatchard plots were calculated for each time point (100, 150, 200, 250, 275, 290 and 300 sec.). Y-axis = Response Units x (CcmR (nM))$^{-1}$ while the X-axis = Response Units. The Scatchard values were then imported into Origin and plotted for each promoter target. Linear regressions were then performed to determine the slope at each time point for each promoter target, using the formula:

Slope = 1 x $(k_D)^{-1}$.

Chlorophyll-a fluorescence and NADPH fluorescence measurements

Simultaneous measurements of chlorophyll-a fluorescence and NADPH fluorescence were made using a pulse amplitude modulated (PAM) fluorometer (DUAL-PAM-100, Walz) and an emitter-detection-cuvette assembly (ED-101US) with a DUAL-ENADPH emitter (Walz) hosting the NADPH (365 nm) and Chlorophyll-a fluorescence (620 nm) excitation source and an LED Array (producing light at a wavelength of 635 nm) for continuous actinic light. The attached detector heads included the DUAL-DNADPH with a filter sandwich (BG39, KV418, DT Cyan for 420-550 nm light) and a photomultipler for detection of NADPH fluorescence and the DUAL-DR with a PIN photodiode (999 nm) for measuring chlorophyll-a fluorescence changes.

Cells were prepared by harvesting 250 mL of high carbon (cultures bubbled with 3% CO_2 supplemented air), mid-log-phase cells grown in standard BG-11 media buffered with HEPES-NaOH, pH 8.0 via centrifugation at 8,000 x g

for 5 minutes and resuspended in fresh BG-11 to a final concentration of 100 µg of Chl mL^{-1}. The cells were placed on a rotary shaker (100 rpm) under constant illumination at room temperature. Individual samples were prepared by diluting the cells to a concentration of 3 µg of Chl mL^{-1} in a cuvette and then placed within the cuvette assembly with a stir bar allowing mixing. The samples were untreated or treated with Glycolaldehyde (GLY) to a final concentration of 10 mM, Ethoxyzolamide (EZ) to a final concentration of 200 µM, or 3-(3,4-dichlorophenyl)-1,1-dimethylurea (DMCU) to a final concentration of 20 µM and incubated in the dark without measuring or actinic light for 30 minutes while mixing. The excitation sources were activated 20 seconds prior to recording. The actinic light was activated 20 seconds after start of recording and deactivated 180 seconds after start of recording, followed by an 80 second dark period with excitation sources active before recording was terminated.

Gel-Filtration Chromatography

HPLC Gel-Filtration was performed using a Superdex 200 hr column within the OSU Protein DNA Core facility (Akta). Two hundred (200) µL of each sample was injected into the system, containing between 3.80 – 76.0 µL of CcmR (1 µg μL^{-1}), 5.94 µL of pCcmR (GS28) plus sufficient buffer to reach 200 µL (50 mM Na_2HPO_4 pH 8.0; 300 mM NaCl; 20% sucrose (w v^{-1})) or (50 mM Na_2HPO_4 pH 8.0; 300 mM NaCl).

Dynamic Light Scattering (DLS)

DLS was performed using a Malvern Instruments Zetasizer µV, Dr. Deng (OSU). All DLS samples were prepared identically as those for EMSA; except

that all samples were spun at 14,000 x g for 15 minutes at 4 °C before loading. Five (5) µL of each sample was placed into the cuvette and loaded into the instrument. Once the assay was finished the sample was removed and the cuvette was washed at least 6 times with dH_2O followed by 70% EtOH washes (at least 6 times). The cuvette was blown dry with compressed air or N_2 and the next sample loaded. All data were exported into Excel (Microsoft) for mathematical calculations and visualized following importation into Origin 6.0 (Microcal).

III. $NADP^+$ AND ALPHA-KETOGLUTARATE ACT AS CO-REPRESSORS FOR CCMR

INTRODUCTION

For aquatic photosynthetic autotrophic organisms such as cyanobacteria, Ci is an often limiting, essential substrate for oxygenic photosynthesis. Cyanobacteria have evolved an ability to overcome low ambient Ci concentrations by acquiring, through active transport, Ci in the form of bicarbonate (HCO_3^-) or as dissolved carbon dioxide (CO_2), and to increase the localized CO_2 concentration around the inefficient carbon-fixing enzyme Rubisco housed within the carboxysome. These adaptations to overcome the low affinity of Rubisco for CO_2 and increase the carboxylase activity are collectively called the carbon concentrating mechanism (CCM) (see *85, 86-88, 89 for review*).

Currently, five different Ci uptake systems have been identified (with a variety of uptake flux and net affinity characteristics) and extensively studied within the cyanobacteria *Synechococcus sp.* PCC 7002 (hereafter *Synechococcus* PCC 7002), *Synechococcus elongatus* PCC 7942 (hereafter *Synechococcus* PCC 7942), and *Synechocystis sp*. PCC 6803 (hereafter *Synechocystis*), with all five systems allowing the cystolic levels of Ci to be maintained at levels 1000-fold greater than extracellular concentrations (*89*). While grown under high carbon conditions where Ci is sufficient there is a basal constitutive level of low-affinity transport activity which is up-regulated when

grown under Ci limiting conditions (*28, 44, 49, 90-96*). The transcriptional regulators responsible for the basal level of CCM activity were identified through mutants with high-CO_2-requiring (HCR) physiological phenotypes requiring excess quantities of Ci to reach rates of photosynthesis compared to that of wild type cells (*28, 44, 49, 90-96*). In *Synechocystis*, the basal level of Ci transport activity is related to the expression of the constitutive transporters, a Na^+-dependent HCO_3^- transporter BicA encoded by *sll0834* (33) and the CO_2 uptake system NDH-I_4 based on a specialized NDH-I complex encoded by the genes *ndhF4* (*sll0026*), *ndhD4* (*sll0027*), and *cupB* (*slr1302*) (*31, 97*) which do not show increases in expression when shifted from high carbon conditions to low carbon or carbon limiting conditions. The inducible Ci transporters which show increased expression upon shift from high carbon conditions to low carbon conditions corresponding to increased CCM activity and the increased affinity of Ci transport are the high affinity HCO_3^- transporter, BCT1, encoded by the *cmpAB(porB)CD* (*slr0040-44*) operon (32), the high affinity Na^+-dependent HCO_3^- transporter, SbtA, encoded by *slr1512* (41), and high affinity CO_2 uptake system NDH-I_3 encoded by the genes *ndhF3* (*sll1732*), *ndhD3* (*sll1733*), *cupA* (*sll1734*), and *sll1735* (*31, 97-100*).

While considerable advances have been made in defining the structural genes required for the CCM, there has been little progress in the understanding of their transcriptional regulation. The expression of the inducible Ci transporters is controlled by one of two LysR-family regulators known as CmpR and CcmR (NdhR) (*1, 19, 46, 101*). The LysR-family of transcriptional regulators are a large

family of DNA binding proteins that act as either as an activator or repressor of transcription by interacting with RNA polymerase at the promoter region for which a co-inducer or co-repressor is necessary for activation or repression. The co-inducer or co-repressor is usually a product or intermediate of the metabolic pathway controlled by the LysR-type transcriptional regulator (*102, 103*). CmpR has been shown to increase the expression of the Ci responsive *cmp* operon encoding the BCT1 transporter during carbon limiting conditions in *Synechocystis* and *Synechococcus* PCC 7942 (46). However, CmpR appears to be absent from the genome of *Synechococcus* PCC 7002 (*101*). CmpR from *Synechococcus* PCC 7942 was determined to bind the regulatory region upstream of the *cmp* operon using electrophoretic mobility shift assays and it was shown that the presence of the small molecules ribulose-1,5-bisphosphate (RuBP) and 2-phosphoglycolate (2-PG) enhanced binding (*104*). The proposed action of CmpR under low CO_2 conditions is as follows: oxygenase activity of Rubisco increases causing oxygenation rather than carboxylation of the substrate RuBP forming the product 2-PG causing activation of the *cmp* operon through the actions of CmpR. This has yet to be demonstrated in other cyanobacteria, including *Synechocystis*. In *Synechocystis,* CcmR acts as a negative regulator of CO_2 responsive genes including the Ci transporters, NDH-I_3 and SbtA (1). CcmR in *Synechococcus* sp. PCC 7002 acts as a negative regulator for all the known CO_2 responsive genes including the *cmp* operon (*101*). CcmR appears to be absent from the genome of *Synechococcus* PCC

7942, suggesting that CmpR acts as a regulator of the genes encoding the SbtA and NDH-I3 transporters or a yet unidentified regulator is responsible.

In this study, we demonstrate that the ligand molecules for CmpR (Sll0030) from Synechocystis are consistent with those previously identified for CmpR from Synechococcus PCC 7942 (*104*), suggesting the conserved nature of the low CO_2 signal that is detected through CmpR. We show direct physical interaction between CcmR (Sll1594) and the proposed genes comprising the putative CcmR regulon previously identified by microarray analysis of a strain of Synechocystis lacking the *ccmR* gene. A molecular characterization of CcmR binding to the putative CcmR regulon including the enhanced binding caused by the presence of $NADP^+$ and α-KG is demonstrated and the role of these molecules as signals for adaptation to CO_2 limiting conditions in cyanobacteria is discussed.

RESULTS

EMSA shows specific binding of CcmR to DNA fragments bearing the upstream regions of the putative CcmR regulon.

In order to determine if CcmR directly binds to the regulatory and promoter regions of the members in the putative CcmR Regulon, as proposed by (1), EMSAs were employed. The basis of EMSA is that DNA bound by protein, such as a transcriptional regulator, will migrate through a native-PAGE more slowly than unbound or free DNA allowing the determination whether a complex between a particular protein and a specific target DNA fragment is possible. Further, by addition of a competing DNA fragment that is not specifically bound by the protein, in excess of the specific target DNA fragment, it is possible to demonstrate that the protein bound is specific for the target DNA fragment if the competing DNA fragment fails at decreasing the abundance of the specific complex (*2, 3*).

The image of the ethidium bromide stained native-PAGE in Figure 7A is representative of EMSA data showing specific binding of the transcriptional regulator, CcmR, to different DNA fragments containing the intergenic regions upstream relative to the translational start sites of genes and operons of the putative CcmR regulon in table S3 (supplemental data), as summarized and modeled in Figure 7B. The EMSA in Figure 7A demonstrates the specific binding of CcmR to a DNA fragment (pccmR-1) containing the region from -110 bp to +65 bp relative to the transcriptional start site of the gene *ccmR*, encoding the LysR-type transcriptional regulator CcmR, in the presence of a 5 fold molar

excess of a competitor DNA fragment (prim-1) containing the coding region of a homolog of the 16S rRNA processing protein RimM, (*slr0808) (1),* from the +30 bp to +243 bp relative to the translational start site in the presence and absence of $NADP^+$. Along the bottom of the gel image, bands belonging to either the target DNA fragment, pccmR-1 (FDT), or the competing DNA fragment, primM-1 (FDC) are visible. These positions within the native-PAGE mark the extent of migration through the gel during electrophoresis of the unbound DNA fragments. We identified PCR based artifacts for the competitor DNA fragment, primM-1, that were visualized on the polyacrylamide gel as two bands (CI and CII) that did not change in position nor relative intensity upon addition of CcmR, and therefore, were not included in further analysis. Addition of CcmR to the competitor DNA fragment, rimM-1, showed a band (CIII) that migrated a shorter distance as compared to the free DNA fragment (FDC) indicating a shifted complex containing bound CcmR and competitor DNA fragment, primM-1, in the absence (lane 5) and in the presence (lane 8) of $NADP^+$. A shifted band (CIV) representing a shifted complex of the pccmR-1 DNA fragment bound by CcmR in the absence (lane 4) and an increased abundance in the presence of $NADP^+$ (lane 7) is visible. The increased abundance of the complex was also observable in the lack of visible unbound DNA fragment (FDT, lane 7). These results demonstrate an increase in abundance of the CcmR bound DNA fragments in the presence of $NADP^+$.

Figure 7

A)

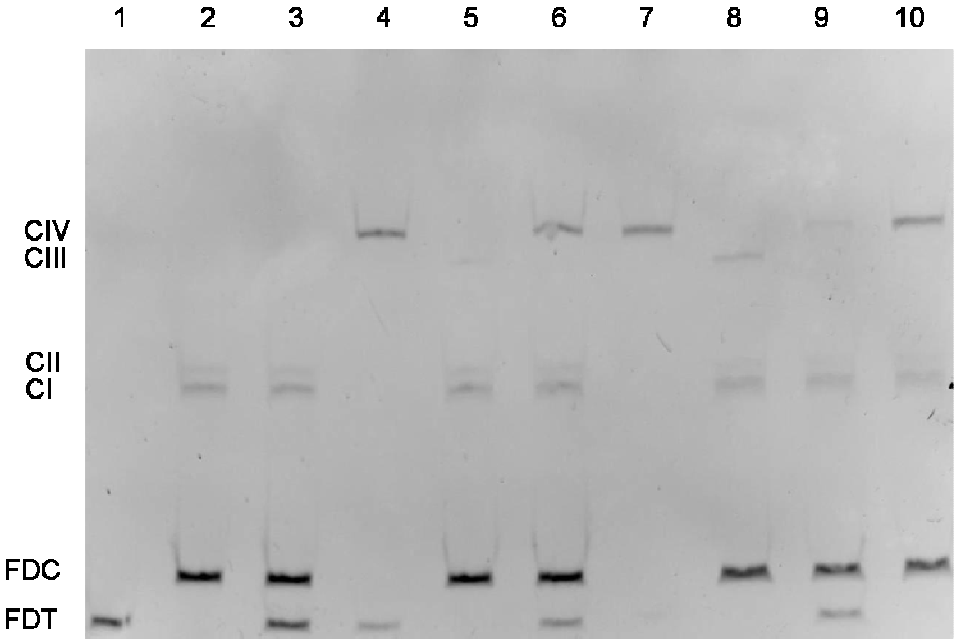
1
2
3
4
5
6
7
8
9
10
CIV
CIII
CII
CI
FDC
FDT

B)

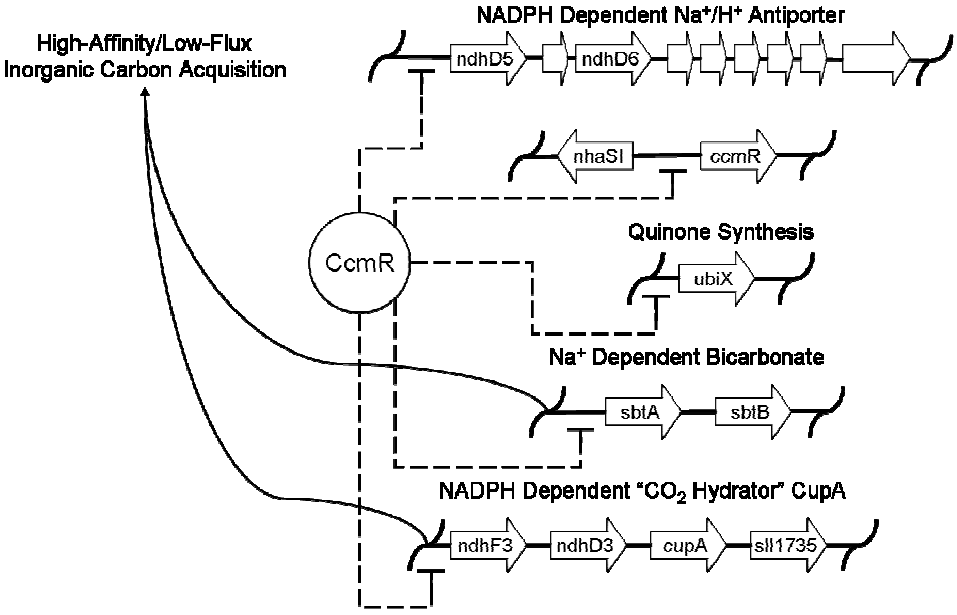
High-Affinity/Low-Flux
Inorganic Carbon Acquisition
NADPH Dependent Na+/H+ Antiporter
ndhD5
ndhD6
nhaSI
ccmR
CcmR
Quinone Synthesis
ubiX
Na+ Dependent Bicarbonate
sbtA
sbtB
NADPH Dependent "CO2 Hydrator" CupA
ndhF3
ndhD3
cupA
sll1735

Figure 7 A) EtBr stained 6% Native PAGE-EMSA illustrating CcmR binding to the promoter of its own gene (pccmR) in the presence of excess competitor containing the coding region of an rRNA processing protein (rimM), with and without one of the identified ligand molecules ($NADP^+$). All components were mixed and allowed to incubate at RT for 20 minutes before a quick centrifugation, then processed at 125 V for 60 minutes at RT. FDT, Free DNA pccmR (-110, +65 relative to transcriptional start site); FDC; Free DNA rimM (+30, +243 relative to translational start site); CI and CII; PCR artifacts of rimM, CIII; rimM shifted band; CIV; pccmR shifted band. Lanes 1, 3, 4, 6, 7, 9, 10 contain 20 nM pccmR. Lanes 2, 3, 5, 6, 8, 9, 10 contain 100 nM rimM. Lanes 4 – 8, 10 contain 200 nM CcmR. Lane 9 contains 100 nM CcmR. Lanes 7 – 10 contain 5 mM $NADP^+$. The shifted bands indicate that in the presence of the ligand molecule, CcmR causes an increase in binding to the target DNA fragment even in the presence of molar excess competitor DNA.

B) Proposed regulon for CcmR based on previous microarray analysis (*105*). CcmR was classified as a repressor of all the genes/operons under its regulatory control. The identified genes are ccmR (self) and ubiX (quinone synthesis) as monocistronic products. Additionally sbtA and ndhF3 are multicistronic operons that are directly involved in the uptake (HCO_3^-) or hydration (CO_2), respectively, for inorganic carbon acquisition. The final member of the regulon is ndhD5 which is another multicistronic operon that maintains a sodium gradient for use by the sbtA operon.

To demonstrate specific binding of CcmR to the target DNA fragment, pccmR-1, over that of the competing DNA fragment, primM-1, 5 fold molar excess of primM-1 was added to the binding assay with pccmR-1 before the addition and incubation of CcmR in the absence (lane 6) or presence (lane 10) of $NADP^+$. The band formed by primM-1 and CcmR (CIII) was not visualized while the pccmR-1 fragment bound by CcmR (lane 6 and lane 10) was of equal abundance to that without the addition of primM-1 (lane 4 and lane 7). The successful competition of the pccmR-1 DNA fragment over that of the excess abundant primM-1 DNA fragment for CcmR binding, demonstrated specific binding of CcmR to the region from -110 bp to +65 bp relative to the transcriptional start site of *ccmR.*

The EMSA data (representative gel image see Figure 7A) showed that CcmR binds specifically to the upstream region of all five of the putative regulon members including: -110 bp to +65 bp upstream of *ccmR* relative to the transcriptional start site, -300 bp to +1 bp upstream of *ndhF3* relative to the translational site (pndhF3-1), -425 bp to -125 bp upstream of *sbtA* relative to the translational site (psbtA-1), -350 bp to -50 bp upstream of *ndhD5* relative to the translational site (pndhD5-1), and -350 bp to -50 bp upstream of *ubiX* relative to the translational site (pubiX-1), as previously hypothesized (Figure 7B) (*83, 84, 106*).

Surface Plasmon Resonance (SPR) illustrating binding characteristics of CcmR to DNA fragments bearing the upstream region of members of the putative CcmR regulon.

Although EMSA can be used to demonstrate specific binding of proteins to DNA, the binding reactions are not at chemical equilibrium during electrophoresis, causing dissociation of the complexes and underestimation of band density leading to error in determining binding affinity kinetics (*107-118*). In order to confirm binding of CcmR to the putative regulon members and to determine the different affinity of CcmR for the upstream region of the members of the putative CcmR regulon under chemical equilibrium conditions, we employed SPR.

Using SPR, the DNA fragments of the five members of the putative CcmR regulon were tested to determine binding under equilibrium conditions (Figure 8 & 3, A - E) and their subsequent kinetic constants (Figure 9F). The flow surface of the SPR biosensor was prepared by immobilizing single end 5' biotinylated-DNA fragments containing different upstream regions of the putative CcmR regulon to the pre-coupled neutravidin coated slides, exposing the DNA to the injection flow path.

Figure 8

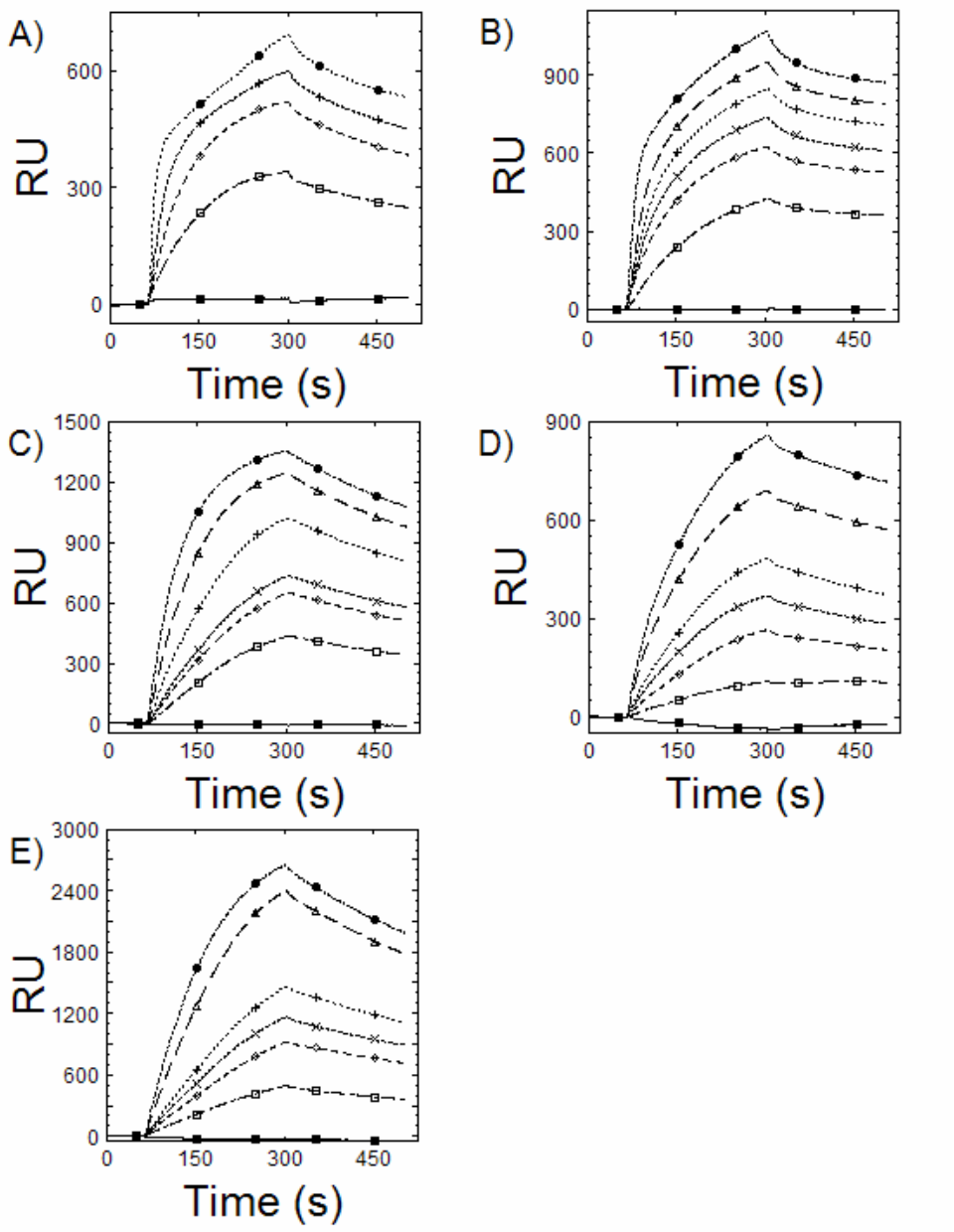
A)
RU
600
300
0
0
150
300
450
Time (s)
B)
RU
900
600
300
0
0
150
300
450
Time (s)
C)
RU
1500
1200
900
600
300
0
0
150
300
450
Time (s)
D)
RU
900
600
300
0
0
150
300
450
Time (s)
E)
RU
3000
2400
1800
1200
600
0
0
150
300
450
Time (s)

Figure 8. Surface Plasmon Resonance curves illustrating binding of CcmR to each member of the proposed regulon (see Figure 7B.). Promoters of each gene were amplified using 5' modified (biotin) primers (IDT). Pre-coupled Neutravidin chips were obtained from Nomadics. Biotinylated DNA fragments were subsequently injected over the surface until no additional binding occurred. All DNA fragments are approximately 150 bp in length. All injections began at 60 seconds and continue for 240 seconds, at 25 uL min^{-2}. Regeneration of the surface using 0.1% SDS, following 360 seconds of buffer flow after the end of each protein injection. 1 RU = 1 pg mm^{-2}. Plots displayed using KaledíaGraph 3.5. Protein (CcmR) concentration for each target is as follows, markers are for visualization only; 0 nM (Closed Square), 250 nM (Open Square), 500 nM (Open Diamond), 750 nM (X), 1000 nM (+), 2000 nM (Open Triangle), 3000 nM (Closed Circle). A) pccmR. B) pndhF3. C) pndhD5. D) psbtA. E) pubiX.

Figure 9

A)

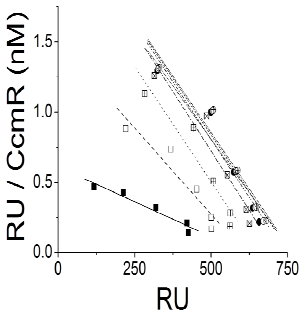

B)

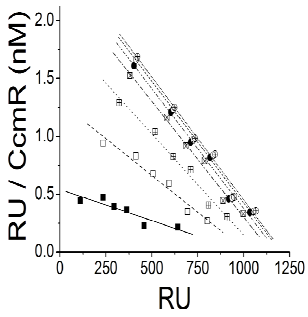

C)

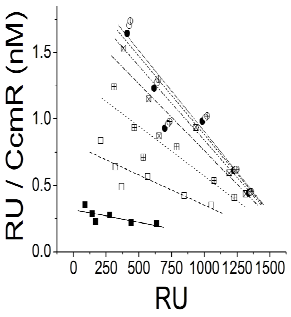

D)

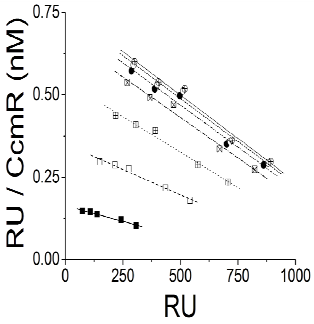

E)

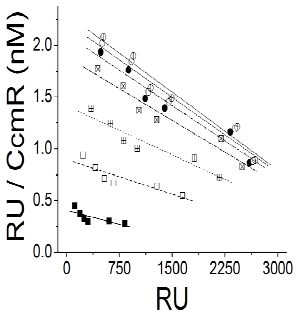

F)

Calculated Affinity for CcmR Regulon		
Promoter Fragment	K_D (nM)	N
pccmR	308.0 ± 3.8	3
pndhF3	477.0 ± 5.7	3
pndhD5	853.3 ± 36.9	3
psbtA	1922. ± 29.	3
pubiX	2086. ± 103.	3

Figure 9. Scatchard analysis of the CcmR regulon. SPR data (Figure 8.) was re-plotted to allow for the determination of k_D values for each member of the regulon. At the indicated time points the data was analyzed, for all concentrations, to determine the change in k_D over the injection. This method was employed given the apparent lack of protein saturation on the surface regardless of the injection time (1 – 10 min.). Plots of the linear regressions showed that although the protein injections had not reached saturation they had reached a steady state and showed no change (parallel lines) over time. The K_D for each promoter was determined from the Scatchard plot given that $K_D = -1 \times \text{slope}^{-1}$. The average of the last 25 seconds of each injection was used to determine the k_D for each promoter fragment. Linear regressions on each data set were calculated using Microcal Origin. All plots show both the raw data and the calculated linear regression, markers indicate actual data values. Data points: 100 sec. (Closed Square), 150 sec. (Open Square), 200 sec. (Open Square with +), 250 sec. (Open Square with X), 275 sec. (Closed Circle), 290 sec. (Open Circle), 300 sec. (Open Circle with +). Linear Regression: 100 sec. (—), 150 sec. (— —), 200 sec. (• • •), 250 sec. (— - —), 275 sec. (— - -), 290 sec. (- - - -), 300 sec. (· · ·). A) pccmR. B) pndhF3. C) pndhD5. D) psbtA. E) pubiX. F) Table of calculated k_D values. Values are average of 275, 290 and 300 sec. time points ± (s.d.).

A range of concentrations of CcmR (0 to 3000 nM) were injected into the flow path of the biosensor with immobilized DNA fragments of the upstream region of the five putative CcmR regulon members causing an increase in response units (RU), as shown in figure. 8. The response curve during the association phase (60 to 300 sec) and dissociation phases (361 to 500 sec.) showed semi-linear increase and decrease in RU, respectively, at the lower concentrations of CcmR. At higher concentrations of CcmR, the response curves during the association phase were hyperbolic without reaching saturation of signal and the dissociation phase shows an initial drop in signal followed by a slow semi-linear decrease in response units. The shape of the curves in both the association and dissociation phases suggested an interaction between CcmR and the five putative CcmR regulon DNA fragments.

It was not possible to use the software provided by the manufacturer, QDAT. QDAT uses the Langmuir isotherm model to determine the kinetic constants for the association (k_a) and dissociation phase (k_d), and calculation of the binding affinity constant (k_D). The Langmuir isotherm model assumes signal saturation as the steady-state binding between CcmR and the DNA fragment (Nomadics). CcmR does not obey the assumptions needed to utilize the Langmuir isotherm model and therefore a different analysis method was needed. To determine the binding affinity constant, k_D, we employed Scatchard plot analysis, which is a linear transformation of kinetic data that relies only on the association phase of the kinetic curve. In the Scatchard plot analysis, Figure 9, the X-axis represents the binding of CcmR to the DNA fragment in response

units (RU) and the Y-axis represents the binding in RU divided by the injected concentrations of free CcmR. The plot is analyzed by linear regression and k_D, the negative reciprocal of the slope, is calculated.

The analysis was performed on each promoter at various time points during the association phase to determine if a steady state was achieved. The Scatchard plots (Figure 9) show the linear regression for each member of the regulon at 100, 150, 200, 250, 275, 290 and 300 seconds. The linear regression showed increasingly similar slopes as visualized by the parallel regression lines after 250 seconds during the association phase, indicating that the binding affinity (k_D) of CcmR for the DNA fragments approximated a steady state after 250 seconds.

The estimated k_D for each target was then calculated as the average of the 275, 290, and 300 second time points (Figure 9F). See Figure 9F for the calculated values.

Although, the k_D values were calculated from the Scatchard analysis they yielded interesting and puzzling results. These results suggest that the binding affinity of CcmR can not be accurately determined at this time using this type of analysis given the putative conformational changes that are occurring along the surface of the protein during its interaction with the DNA. Additional work will need to be done to attempt to unravel this complex system of protein and DNA interactions involving conformational changes.

SPR screening identifies α-KG and $NADP^+$ as ligand molecules for CcmR.

Previous work has suggested two main hypotheses for the possible ligand molecules for the regulators of the high-affinity CCM; one that they directly detect the intracellular Ci, and the other that they are directly sensing photorespiratory intermediates (review by *119*). We therefore used SPR to screen different biologically relevant molecules in carbon fixation and carbon transport in an effort to determine the ligand molecule for CmpR (appendix C6) and CcmR (appendix C7) from *Synechocystis*. The use of SPR technology allowed the determination of the ligand molecules for CcmR and CmpR under chemical equilibrium conditions allowing less consumption of the putative ligand and the development of a quicker, more reliable screening assay than EMSA.

Prepared SPR biosensors with immobilized single end 5'-biotinylated DNA fragments consisting of either the upstream region of *ndhF3* from -333 bp to -191 bp relative to the translation start site (pndhF3-2) or the upstream region of the *cmp* operon from -275 bp to +25 bp relative to the translational start site (pcmpA-2) were used to screen for the ligand molecules for CcmR and CmpR, respectively. A baseline for the CcmR and CmpR binding for pndhF3-2 and pcmpA-2, respectively, were established by injection of 1.5 µM of the transcriptional regulator in the absence of putative ligand. The surface of the SPR biosensor was washed to remove bound transcriptional regulator with regeneration solution (10 mM Pipes, pH 8.5; 1 mM Na_4-EDTA) resulting in no apparent change in binding affinity in the subsequent screenings, allowing reuse of the surface to test multiple putative ligands. The binding of CcmR to pndhF3-2

was tested in the presence of: Pyruvate, 2-PG, NADPH, PEP, $NADP^+$, and α-KG at a concentration of 500 µM. CcmR showed increases in RU in the presence of $NADP^+$ and α-KG after double referencing, which is the subtraction of CcmR binding to the DNA fragment without the ligands present (Figure S5). HCO_3^-, RuBP, and 2PG were tested as putative ligands that augmented the binding of CmpR to the DNA fragment, pcmpA-2, at concentration of 500 µM. In the presence of RuBP and 2PG, CmpR showed an increase in response units (RU) compared to the CmpR only baseline (Figure S2).

To observe the effects of $NADP^+$ and α-KG on CcmR binding to the upstream regions of the putative CcmR regulon, a fixed concentration of CcmR (with increasing concentrations of $NADP^+$ or α-KG) was assayed for binding to the upstream region of *ccmR* from -50 bp to +87 bp relative to the transcriptional start site (pccmR-2) and *ndhF3* from -333 bp to -191 bp relative to the translational start site (pndhF3-2). Injection of 1.5 µM CcmR in the absence of the ligand molecule for both, pccmR-2 and pndhF3-2, allowed for the establishment of a baseline of CcmR binding to be used in double referencing (Figure 10). Injection of CcmR after 5 minute incubation on ice with 10 µM $NADP^+$ or α-KG showed no change in RU for the pccmR-2 DNA fragment (Figure 10A and C) nor the pndhF3-2 DNA fragment (Figure 10B and D). Addition of 100 µM $NADP^+$ shows a slight increase in signal with pccmR-2 (Figure 10A), while the pndhF3-2 shows a greater increase in the signal (Figure 10B). The addition of 500 µM $NADP^+$ to both the pccmR-2 and pndhF3-2 fragments caused a greater increase in the signal obtained without $NADP^+$ (Figure 10A and B),

however, the increase in signal was greater for pndhF3-2 than for pccmR-2. Addition of 100 µM α-KG caused no increase in signal for the pccmR-2 fragment while only a slight increase in signal occurred with the pndhF3-2 fragment (Figure 10C and D). Addition of 500 µM α-KG shows a greater increase in signal for both fragments (Figure 10C and D), however the increase in signal was greater for the DNA fragment pccmR-2 than for pndhF3-2 in the presence of increasing concentrations of α-KG.

Figure 10

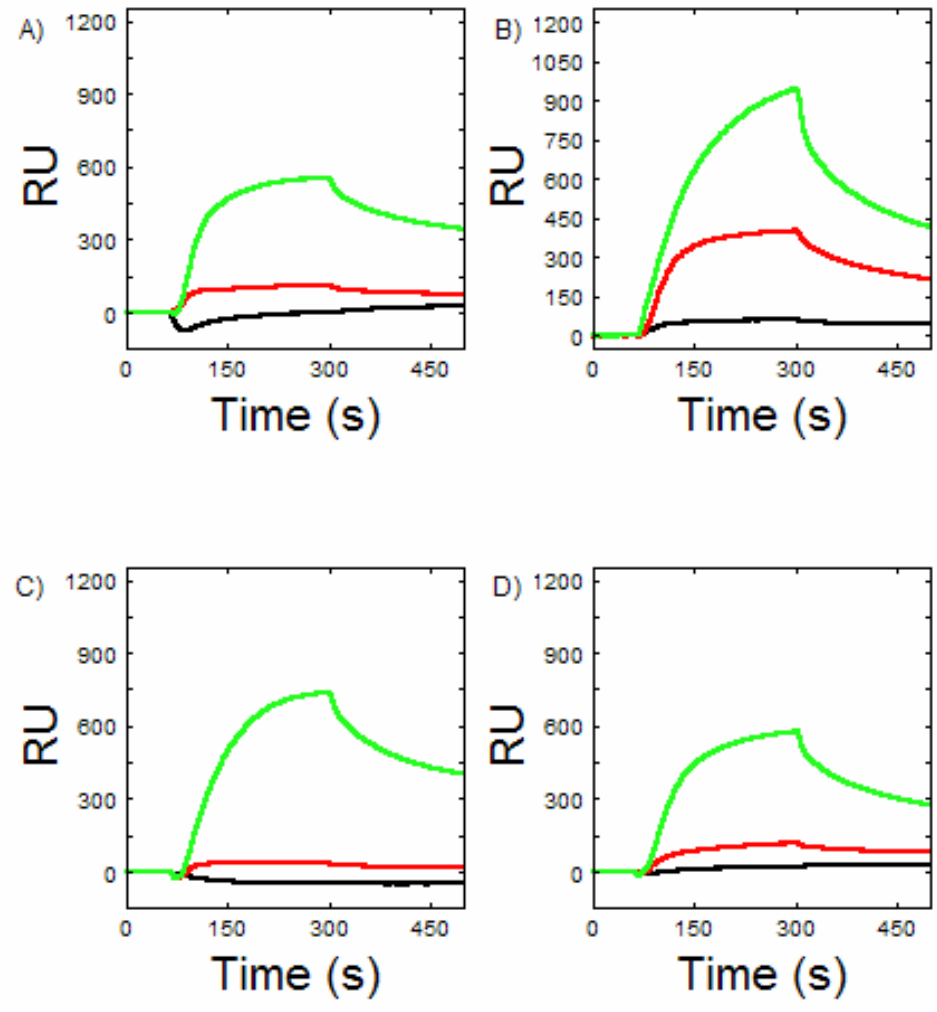

Figure 10. SPR curves illustrating protein binding to immobilized biotinylated DNA fragments (pndhF3 or pccmR) with increasing concentrations of ligand molecule. DNA immobilization as described in Figure 8. For assay method see Figure 8. All curves are double referenced (*105*). Proteins were incubated with the indicated ligand molecule on ice for at least 5 minutes before injection. All injections contain 1.5 μM of CcmR and 10 μM (Black), 100 μM (Red), or 500 μM (Green) of the indicated ligand molecule. A) pccmR with $NADP^+$. B) pndhF3 with $NADP^+$. C) pccmR with α-KG. D) pndhF3 with α-KG. These results have allowed for the identification of $NADP^+$ and α-KG as the ligand molecules for CcmR. Based on their affect on CcmR (increasing signal) these molecules are hereby named “co-repressors” within the regulation system. This identification of the ligand molecules for CcmR allows, for the first time, the integration of the two high-affinity/low-flux inorganic carbon concentration mechanism regulators. See Figure 12 for the proposed integration of the pathways.

The level of sbtA transcript abundance is related to the level of $NADP^+$

We wanted to test the relationship between decreased levels of $NADP^+$ and established effects of known carbon metabolism inhibitors on CcmR regulon transcript abundance. The Dual-PAM-100 (Heinz Walz GmbH) fluorometer was configured for concurrent detection of chlorophyll and NADPH fluorescence was used to measure the relative level of NADPH within the cells of *Synechocystis* grown under high carbon conditions (3% CO_2 supplemented air) and subjected to treatment with the chemical agents 3-(3,4-dichlorophenyl)-1,1dimethylurea (DCMU), ethoxyzolamide (EZ), and glycolaldehyde (GLY). An increase in the level of NADPH would signify a comparable decrease in $NADP^+$, as well as, an increase in the NADPH:$NADP^+$ ratio.

The chlorophyll a and NADPH fluorescence traces of high carbon adapted *Synechocystis* cells are representative of common traces achieved using the PAM flourometer (*120, 121*). Treatment with DCMU showed a similar shape in chlorophyll fluorescence trace under non-saturating actinic light as others have shown (*1, 19*). The slow increase in chlorophyll fluorescence is due to blocking of the transfer of electrons from PSII to electron carriers downstream. The DCMU treatment showed an initial increase in NADPH fluorescence followed by a decrease and a constant low level until the deactivation of the actinic light. Treatment with EZ and GLY produced a similar shape in the chlorophyll fluorescence trace to that of non-treated cells. The NADPH fluorescence traces of high carbon adapted cells treated with EZ and GLY showed increases in

NADPH fluorescence compared to no treatment (EZ treatment fluorescence was greater than GLY treatment fluorescence).

Figure 11

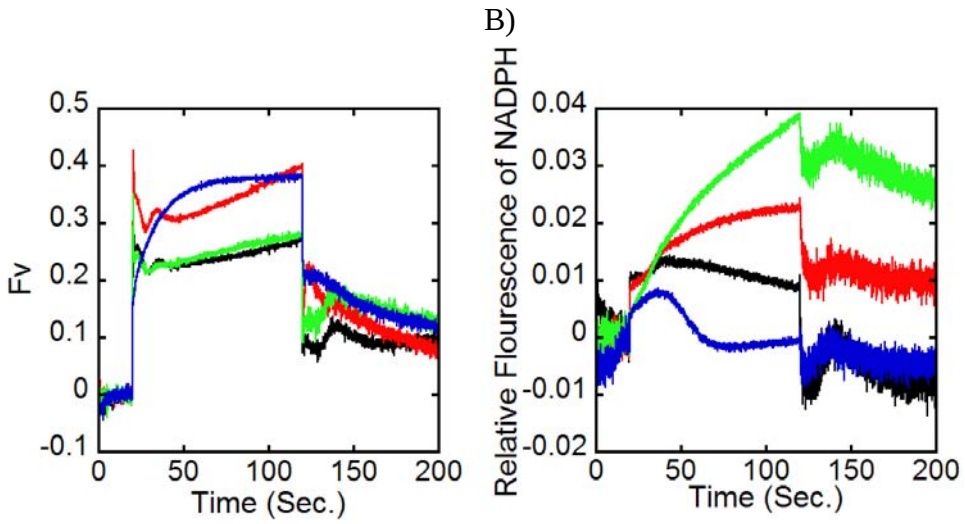

Figure 11. Dual-PAM traces for high-carbon grown cells (3% CO_2 in air) illustrating A) Chlorophyll-a fluorescence and B) NADPH fluorescence under different conditions. All measurements were carried out using high-carbon adapted cells washed with 100 mM HCO3- containing BG-11. All samples were pre-illuminated with a 100 sec actinic light within the measuring cuvette, to determine viability of sample. Compounds were added as indicated and the cells allowed to mix and remain in the dark for 30 minutes before assay. Excitation sources for both chlorophyll-a and NADPH were turned on at 0 sec and remained on for the whole assay, with the actinic light turned on at 20 sec. The actinic light remained on for 100 sec. No addition (Black), DCMU (Blue), GLY (Red), and EZ (Green).

A) Fv for each of the samples illustrating the reduction state of Q_A^-. Shown here is the change in re-oxidation of QA upon addition of DCMU, a known blocker of the QA to QB transfer of electrons within PSII. This change illustrates that the other samples are not blocking the transfer of electrons into the PQ pool.

B) Relative level of fluorescence of NADPH. With the addition of DCMU the NADPH concentration goes down, as expected given that the transfer of electrons has been blocked. The level of NADPH goes up in both the GLY and EZ treatments as expected by blocking the CBB and CCA (respectively).

DISCUSSION

There has been a comprehensive focus for the last two decades on increasing the understanding of the structural aspects of the CCM. Although the research has been ongoing, the control and regulation of the CCM is still poorly understood, especially in the nature of the signal detected.

The results presented herein provide additional insight into the transcriptional regulation and control of the inducible inorganic carbon transporters by the LysR-type transcriptional regulators, CcmR and CmpR in *Synechocystis*. In this study, the upstream region of the five members of the putative CcmR regulon were shown to be bound by CcmR in a specific manner and that this binding was modulated by the presence of the small molecules, $NADP^+$ and α-KG. It was shown that chemical inhibitors of carbon metabolism (EZ, GLY, and DCMU), which were previously shown to modulate the transcriptional level of *sbtA*, a member of the putative CcmR regulon, also modulated $NADP^+$ levels in a manner indicating an inverse relationship between the level of $NADP^+$ and *sbtA* transcript abundance, most likely through the actions of CcmR. This study also shows that CmpR specifically binds to the upstream region of the *cmp* operon and is modulated by the presence of 2-PG and RuBP in *Synechocystis*. Together, these results suggest that transcription of the inorganic carbon transporters is not regulated directly by internal or external inorganic carbon levels, but is indirectly regulated by the internal inorganic carbon levels through the direct detection of the levels of metabolites from reduced efficiency of RuBisCO, 2PG and RuBP, through detection by CmpR and

the direct detection of decreased photosynthetic reduction of $NADP^+$ or the accumulation of carbon skeletons for the assimilation of nitrogen, α-KG, from the shunting of fixed carbon to the partial oxidative Krebs cycle, through detection by CcmR.

Since the identification of the members of the putative CcmR regulon consisting of the gene clusters *sbtA*/*sbtB*, *ndhF3*/*ndhD3*/*cupA*/*sll1735*, *slr2006*/*ndhD5*/*ndhD6*/*slr2009*/*slr2010*/*ssr3409*/*ssr3410*/*slr2011*/*slr2012*/*slr2013* and the genes c*cmR* and *ubiX* in *Synechocystis*, it was expected that CcmR would directly bind to the upstream regions of these member gene clusters (*122*). For all five members of the putative CcmR regulon, this scenario was consistent with our analysis of DNA fragments from the upstream region of the members of the putative regulon used in competitive EMSA analysis (Figure 7A). CcmR showed specific binding to all five members of the putative regulon. This evidence of physical contact between CcmR and the putative regulon members supports the hypothesis that CcmR is a direct repressor of transcription for these genes and gene clusters.

While a qualitative analysis of binding affinity was possible with the use of EMSA, a more quantitative approach that was under chemical equilibrium, SPR, was used to identify the binding characteristics of CcmR and CmpR. The kinetic curves of the SPR data for all CcmR regulon components showed a common curvature which lacked saturation of the primary signal indicated by the increasing response units (RU) over the late period of the association phase. The lack of saturation of signal did not allow the use of the manufacturer's program

which uses the Langmuir isotherm model that assumes steady state for the binding kinetics. As a result, Scatchard plot analysis was used instead. The plots indicated that at the late association phase the binding kinetic reached a steady-state and was obscured. Based on the design of the SPR biosensor, the cause of the obscured steady-state was most likely due to conformational changes within CcmR and/or bending of the DNA fragment during binding (1).

Calculation of the binding affinity constant based on Scatchard Plot analysis (Figure 9) which is a linear transformation of data that can cause distortion of the experimental error leading to violations of several assumptions of linear regression and can give estimations that are still far from the actual constant, however, the general relationship of the intrinsic binding affinity of CcmR for the putative regulon can be interpreted. CcmR has the highest affinity for its own promoter, which suggests, along with the previous microarray comparison, that this promoter is not only controlled by the signal through the action of CcmR, but the concentration of CcmR itself. The next members of the putative regulon for which CcmR has high affinity for are the *cupA* operon (with the initiation of transcription upstream of *ndhF3*) and the *ndhD5* operon, followed by the gene *ubiX,* and the *sbtA* operon, the members of the putative regulon with an estimated binding affinity constant a fold higher than *cupA* and *ndhF3* operons. Interestingly, (*102*) results from reverse transcriptase PCR (RT-PCR) showed relatively the highest starting transcript abundance levels of *ccmR* (*ndhR*) followed by *ndhF3*, and *ndhD3* before the shift to low carbon conditions than the transcript abundance for *sbtA* which remained undetectable until 60

minutes after the shift. This shows an inverse relationship between the initial transcript abundance of the putative regulon members and the estimated intrinsic binding affinity constant value of CcmR for these operons. Apo-form of LTTR usually binds one binding site as two interacting dimers and, upon interaction with the co-inducer or co-repressor ligand molecule, a second site is bound causing bending of the DNA (*119*). It is possible that the inverse relationship between HCi transcript abundance of the putative regulon members and the relative binding affinity of the apo-form of CcmR is caused by stabilization of the RNA polymerase initiation complex by the action of CcmR without ligand molecules present. It is also just as likely that another regulator is causing the observed differences of transcript abundance and that there is no relationship between the observed initial transcript abundance with the binding affinity of CcmR. Further analysis of the promoters, possible transcriptional regulators, and the interaction of CcmR for the putative CcmR regulon is necessary to develop a better understand of the intricate regulation of the regulon members.

Through screening by SPR (appendix C7), $NADP^+$ and α-KG were identified as the ligands for CcmR that caused increase binding to the putative regulon components. It was expected that the presence of each ligand would modify the binding of CcmR to different putative regulon members in the same quantitative way. However, SPR data with a fixed concentration of CcmR and increasing concentration of either $NADP^+$ or α-KG showed that α-KG increased CcmR binding to the upstream region of *ccmR* to a greater extent than *ndhF3* while $NADP^+$ increased CcmR binding to the upstream region of *ndhF3* greater

than *ccmR*. This suggests that the ligand effects on CcmR binding are DNA sequence dependent. Further analysis of the effects of the two ligands on CcmR binding of the other members of the putative regulon would increase insight into this phenomenon.

While chlorophyll-a fluorescence and NADPH fluorescence measurements were made to determine the effects of various chemical agents on the photosynthetic electron transport chain and the relative level of NADPH, respectively, and the broad effects are reported and discussed, the physiological complexities of these traces are not. Several reviews of the physiological implications of the chlorophyll a traces are available (*123*) and the physiological implications of the NADPH fluorescence traces are starting to be understood (*120, 121*). Treatment with DCMU showed a similar shape in chlorophyll fluorescence trace under non-saturating actinic light as others have shown (27). The slow increase in chlorophyll fluorescence is due to the blocking of the transfer of electrons from PSII to electron carriers downstream. The DCMU treatment showed an initial increase in NADPH fluorescence followed by a decrease and a low level until the deactivation of the actinic light, which is supported by the activity of DCMU which blocks linear electron transport required for the reduction of $NADP^+$. The hypothesis that low levels of NADPH fluorescence reflect a higher level of $NADP^+$, we expect repression of the putative CcmR regulon under conditions of low NADPH fluorescence. This scenario is supported by the lack of increased transcript abundance of *sbtA*, a component of the CcmR regulon in Woodger et, al.(27) with addition of DCMU to

high carbon adapted cells in *Synechococcus elongatus* PCC 7942. Chlorophyll-a fluorescence produced similar traces before and after treatment with EZ and GLY. The NADPH fluorescence traces of high carbon adapted cells treated with EZ and GLY show increases in NADPH fluorescence compared to no treatment, with EZ treatment causing a greater increase than GLY treatment. This is consistent with the hypothesis that increased levels of NADPH fluorescence, which corresponds to a decrease level in $NADP^+$ would cause a derepression of the CcmR regulon which was demonstrated by (*124*) with a small increase in the CcmR regulon component *sbtA* transcript abundance with treatment with GLY and a greater increase with EZ. These results support the hypothesis that the regulation of the putative CcmR regulon is through the direct detection of the level of $NADP^+$ within the cell, presumably through the action of CcmR.

While the putative CcmR regulon is negatively regulated through CcmR, additional transcriptional regulations of these genes by yet unidentified signals are likely. The upstream region of the gene cluster *sbtA*/*sbtB* between -301 bp to -137 bp relative to the translational start site has been shown to bind the transcriptional regulators LexA (Sll1626) and two CyAbrB proteins (Sll0359 and Sll0822) (*124*). While a deletion mutant of *sll0359* (*124*) is non-viable, suggesting it is necessary for normal growth it was shown to bind to the promoter of the *hox* operon encoding bidirectional hydrogenase. The transcriptional regulator LexA from *Escherichia coli* is involved in SOS response. However, this is not the case in *Synechocystis* and LexA was identified as regulating the *hox* operon and the RNA helicase, *crhR*. The deletion mutant of *sll0822* showed low constitutive

expression of *sbtA*, *ndhF3*, and *cmpA* through detection by reverse transcriptase PCR (*104*).

The results of the EMSA and SPR using CmpR and the DNA fragments containing the upstream region of the *cmp* operon from *Synechocystis*, showed specific binding of CmpR and the DNA fragment (data not shown) and indicated that the presence of 2PG and RuBP increased binding. This is consistent with data acquired from *Synechococcus* PCC 7942 (1).

Figure 12 represents our current working model of regulation of the inducible Ci transporters by CmpR and CcmR. During Ci replete conditions, the constitutive Ci transporters are able to supply enough CO_2 to the inefficient RuBisCO to decrease the oxygenation of RuBP to 2-PG, increasing the carboxylation of RuBP to 3-PG and accumulating carbon skeletons in the form of α-KG for the purpose of nitrogen assimilation. Photosynthetic production of NADPH is being utilized for the purposes of carbon fixation, carbon metabolism, and nitrogen assimilation causing a low $NADPH:NADP^+$ ratio. Because of the reduced levels of 2-PG, and the utilization of RuBP, CmpR is not binding upstream of the *cmp* operon and activation is not taking place. Upon depletion of Ci, the constitutive transporters are not able to overcome the decrease in Ci causing the oxygenase activity of RuBisCO to increase therefore increasing the levels of 2-PG. This causes the activation of the *cmp* operon through the detection of 2-PG and the action by CmpR. There is a decrease in carbon fixation and active carbon metabolism causing an increase in the $NADPH:NADP^+$ ratio as the abundant sink for reducing power (NADPH) is not being utilized. The

lack of carbon metabolism also decreases the pool of α-KG. The decrease in $NADP^+$ and α-KG is detected through CcmR and the transcription of the putative CcmR regulon is derepressed. The activation of the *cmp* operon and derepression of the putative CcmR regulon cause active transcription of the inducible Ci transporters causing an increase affinity for Ci and increase the internal concentrations of Ci and increase carbon fixation and the efficiency of Rubisco.

Figure 12

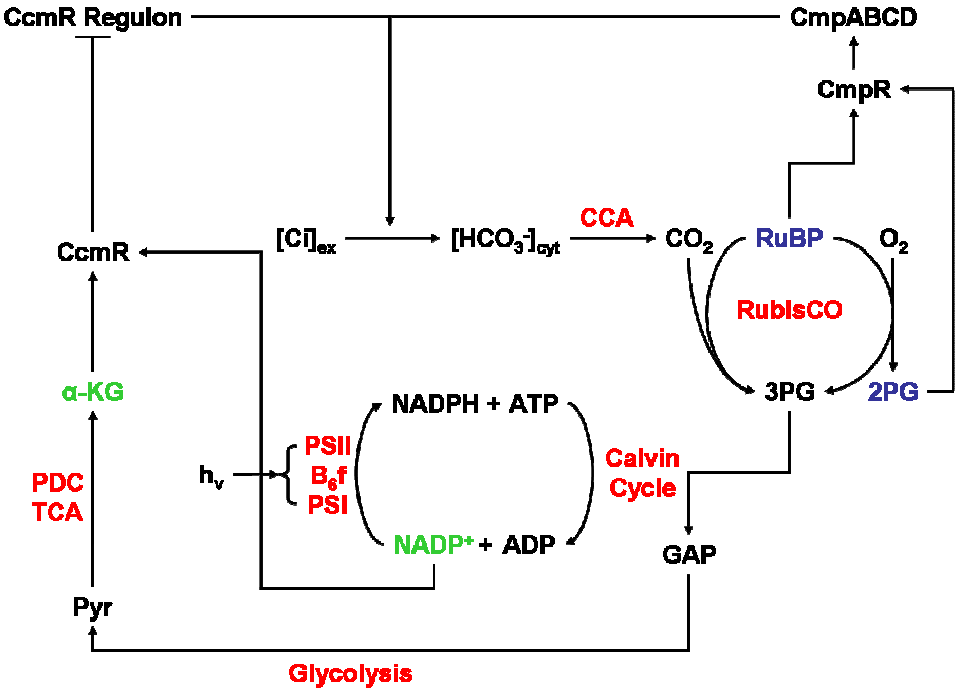

Figure 12. Diagram of the proposed regulatory network within Synechocystis sp. PCC6803, showing both CcmR and CmpR (along with their ligand molecules and the relevant metabolic pathways). Enzyme/complex or metabolic pathways involved in the given step are indicated in red. Ligand molecules for CcmR are indicated in green, while those of CmpR are indicated in blue.

IV. BINDING CHARACTERISTICS OF CCMR TO NON-SPECIFIC DNA (RIMM)

Given that important regulatory ligand molecules for CcmR, $NADP^+$ and α-KG, have now been identified, major questions arise about their mode of action upon CcmR and how they are affecting the function of the protein. How does the binding of the ligand molecule affect the protein's ability to act as a repressor? Why do we see such large differences in the binding characteristics of CcmR to non-specific DNA sequences as compared to the specific regulatory sequences upstream of the genes of the members of the CcmR regulon? If a conformational change is occurring upon binding of CcmR to the DNA fragments, as suggested by the Surface Plasmon Resonance (SPR) experiments presented in the previous chapter, would this change be large enough to be detected or do the changes simply indicate additional units of CcmR binding to the fragment? The main focus of this chapter is on the question: Why do we see such large differences in the binding characteristics of CcmR to non-specific DNA sequences (rimM, see Chapter 3) as compared to the DNA fragments containing cognate regulatory binding site sequences for CcmR, such as the promoter region of *ndhF3*?

In this chapter, I present addition SPR experiments probing the interaction between CcmR and non-specific DNA sequences (rimM). Additionally, I present initial studies using Dynamic Light Scattering (DLS), which is used to estimate

hydrodynamic radii and has the advantage utilizing very small samples and rapid measurements.

RESULTS

DLS was performed to determine the hydrodynamic radius CcmR and its complexes under different conditions. The aim was to evaluate whether hydrodynamic radius changes occur in CcmR upon binding DNA. In the DLS experiment, changes in the angle of light scattering are used to determine the hydrodynamic radius or radius of gyration or Stokes radii (indicators of the volume displaced by the macromolecule as it tumbles through space). I relied upon calculations (using the manufacturer's software) that assumed that the protein complexes may be modeled by a perfect sphere (globular complex) although many proteins, including CcmR, do not share this idealized symmetry. Based on the crystal structure (1IZ1) of a homologous protein, this protein family is generally described as 'dumb bell' shaped. Nevertheless, I felt that DLS might afford the opportunity to observed the changes in conformation that we speculated to exist upon bind DNA (see Chapter 3).

DLS was performed to determine the hydrodynamic radii of CcmR alone and when complexed with DNA during an incubation on ice. Early in the course of performing these experiments it was noticed that the hydrodynamic radius values were unexpectedly high under certain conditions indicative very large complexes and that the formation of these large complexes was occurring in minutes time range. These fragments and the buffers used are similar to those

used in the SPR assays as described in Chapter 3, and the formation of large complexes under similar buffer conditions was not observed during preliminary gel filtration experiments (not shown). Therefore this DLS experiment was conducted to determine if any changes might be seen in the molecular size of the complex formed over time with the idea that during gel filtration the formation of large complexes might be prevented due to turbulence in the buffer during the chromatography. Recent analysis has shown that other LTTRs are prone to forming specific high molecular weight multimeric assemblies in solution and this likely explains why intact complexes are difficult to crystallize (*71-75, 90*). These are not non-specific protein interactions, but instead seem to result from specific and reversible interface interactions between CcmR molecules coming into contact in solution.

In order to determine the hydrodynamic radii of CcmR in solution both with and without a DNA fragment present along with an incubation of ice for the measurement of changes within the oligomeric form of the protein. This change oligomeric form has been previously reported (71-75) for other LTTR's. In order to determine if CcmR also exhibited these features the sample, both with and without a DNA fragment (pndhF3), samples were incubated on ice for 0, 20 or 40 minutes and the radii determined (Table 1). Using software available from the manufacture (Malvern) the molecular weight was calculated for each of the samples (Table 1). It should be noted that although this calculation was performed automatically by the system the resulting molecular weights do not correspond to the expected values for CcmR alone nor when bound to the DNA.

The calculations assumptions do not appear to fit the true shape of CcmR in solution or when bound to a DNA fragment.

During the time course when CcmR was allowed to incubate on ice without any DNA present the radii (nm) increased over time, indicating a larger complex being formed. All four shape models (i.e. globular) supplied by the manufacture (Malvern) show an increase in the molecular weight to levels which would most probably be larger multimeric complexes. The possibility of aggregation forming within the sample during this time can not be ruled out although no evidence was observed for aggregates within the sample prior to loading.

When CcmR is bound to DNA (pndhF3) the overall radii of the complex is lower than without DNA and this is true for each time point (Table 1). This would suggest that the protein:DNA complex has entered into a new configuration possibly by conformational change causing the free arms of the DNA to wrap around the protein and thus create a more compact structure which would sweep a small volume in solution. Even with the smaller overall size of CcmR when bound to DNA the same trend is observed with regards to changes in radii over time. As the sample is allowed to incubate on ice the radii of the complex becomes larger over time (Table 1). Although, the presence of DNA appears to slow this process it does not appear to have the ability to prevent the increase in apparent radii of the complexes that are formed. It is worth emphasizing that the sizes are much larger than expected for a complex between the DNA fragment and a tetramer (151.96 kDa) or even an octomer (303.92 kDa) of CcmR.

Therefore, I conclude that the complexes observed by DLS are artifacts of CcmR's oligomerization into higher order structures that have no biological meaning within the cell. The observed results are the direct consequence of protein sub-units interacting and creating a complex that has no biological meaning.

Table 1

Calculated DLS Radii Time course incubation on ice					
Sample	r. nm	Globular (kDa)	Linear (kDa)	Starburst (kDa)	Branched (kDa)
CcmR + 0 min on ice	10.72	866.2	150	1911.3	401.8
CcmR + 20 min on ice	29.62	9370.5	950.1	58383.6	4054.3
CcmR + 40 min on ice	35.63	1439.9	1325	108113.8	6149.1
CcmR + pndhF3 0 min on ice	4.866	137.8	36.1	136.4	67.5
CcmR + pndhF3 20 min on ice	12.31	1197.2	192.8	3041.9	550.1
CcmR + pndhF3 40 min on ice	9.330	625.9	116.6	1198.7	293.1

Table 1. Table summarizing the exclusion volumes and calculated molecular mass for CcmR (2 μM) with and without DNA (pndhF3) incubated on ice for 0, 20 or 40 minutes. Molecular mass was determined by set standards from within the DLS data analysis software as supplied by the manufacture (Malvern).

Previous studies with LTTRs have shown that the interaction between the transcriptional regulator and DNA causes the DNA to bend (71). In order to determine the bending angle of the DNA upon addition of CcmR an EMSA assay (Figure 13) was performed essentially as described previously (71). The ratio of the migration distances of the DNA fragments with binding points at either the 3' or 5' end as compared to those with binding points in the middle allow for the determination of the bending angle for the DNA fragments. At lower protein concentrations (lanes: 3, 5, 8) the EMSA shows a single shifted band (CI) while at higher protein concentrations (lanes: 4, 6, 9) the EMSA shows a higher shifted band (CII). Note that in lane 6 both shifted bands occur at the higher protein concentration, although they do not occur in lanes 3 and 9 with the other fragments. The fragments used in lanes 1 – 3 have the binding site located near the 5' end, while lanes 4 – 6 have it near the 3' end, and lanes 7 – 9 have it localized in the middle.

The average bending angle for CI (Figure 13 Lane 2, 5) is 120^{o}, while the average bending angle for CII (Figure 13 Lane 3, 6) is 90^{o} based on the formula as described in materials and methods (Chapter 2). While DNA cannot bend 90 or 120^{o} over just the few bases of the recognition sequence, the values show here are applied across the entire length of the fragment. This indicates that over the length of these DNA fragments (225 bp) the bending angle is much larger than those reported for CbbR binding to its target promoter (71). While it is possible that multiple sub-units of CcmR are binding to the DNA fragment, SPR

calculations of binding ratios support a 4:1 molar ratio of protein binding to the available DNA on the surface of the chip (Table C 1).

This support for a 4:1 ratio of DNA on the surface of the chip when used in SPR does not explain the two different sets of bands shown. However, it should be noted that the protein concentration used during EMSA assay is much higher than that used during SPR experiments. For the CI band the ratio is 5:1 while for the CII band the ratio is 15:1. It can not be discounted that this difference, especially in the CII band, is the result of additional protein sub-units binding to the DNA fragment, which we do not observe in the SPR. Taken in concert with the results show above for the DLS it is possible that the multimeric complex observed previously could be responsible for the changes observed in the EMSA data (Figure 13).

Figure 13

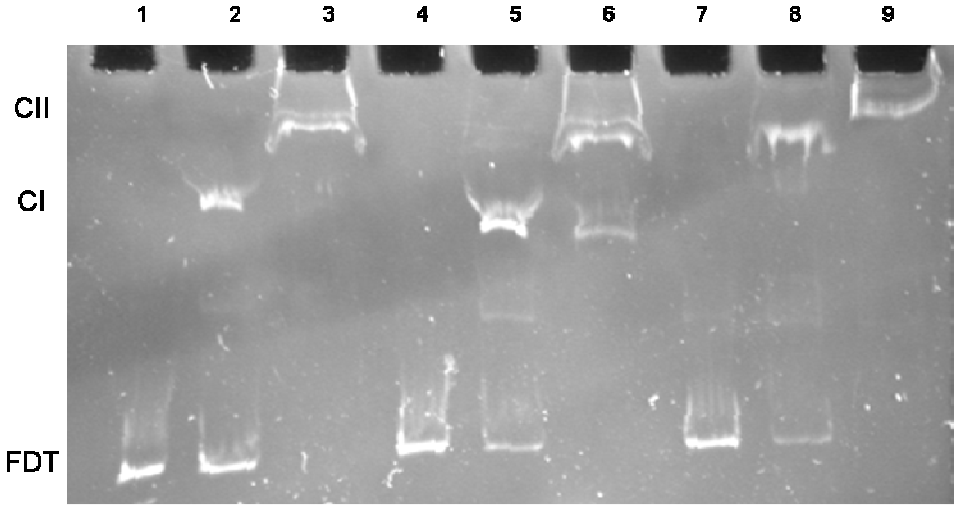

Figure 13 A) EtBr stained 6% Native PAGE-EMSA illustrating CcmR binding to the promoter of its own gene (pccmR) with the binding site located at the 5' end of the fragment (Lane 1 – 3), located in the 3' end the fragment (Land 4 – 6), or located at the middle of the fragment (Lane 7 – 9). All components were mixed and allowed to incubate at RT for 20 minutes before a quick centrifugation, then processed at 125 V for 60 minutes at RT. FDT, Free DNA pccmR; CI, 1st shifted band; CII, 2nd shifted band. All lanes contain 100 nM of DNA. Lanes 1, 4, 7 contain 0 µM CcmR. Lanes 2, 5, 8 contain 0.5 µM CcmR. Lanes 3, 6, 9 contain 1.5 µM CcmR. Using the migration distances on the gel of the DNA bound by the protein, the bending angle of the DNA can be calculated, based on the ratio of migration for a fragment with the binding site located in the middle of the fragment relative to the migration of the fragment with the binding site at either the 3' or 5' end of the fragment. The average bending angle for CI (Lane 2, 5) is 120^{o}, while the average bending angle for CII (Lane 3, 6) is 90^{o} based on the formula as described in materials and methods (Chapter 2).

Using a *rimM* fragment modified with a 5' Biotin tag, which was immobilized onto the surface of the chip, as all of the other previous SPR targets, we attempted to determine the binding affinity of CcmR for this non-specific DNA fragment. The resulting kinetic curves for rimM (Figure 14) show a completely different pattern to those obtained for each of the members of the regulon (Figure 8). The binding of CcmR to the non-specific DNA clearly exhibited saturation. In contrast, the binding of CcmR to the promoters of the specific DNA does not show saturation. The lack of saturation behavior in the CcmR-target DNA interaction may be due to conformational changes making the analysis of binding unsuited to the simple Langmuir isotherm that the model is built upon within the main analysis software provided by Nomadics. The Langmuir isotherm model assumes pseudo-first order kinetics, which CcmR does not obey when binding to its regulon targets. However, when CcmR is bound to the non-specific fragment the kinetic curves showed pseudo-first order binding and also showed that the system is saturating at relatively low concentrations of the protein (Figure 14 A). This is consistent with the interpretation that the binding of CcmR involves are comparatively simpler interaction with non-specific DNA compared to its interaction with DNA containing specific target sequences.

The simpler binding kinetics of CcmR to non-specific DNA has allowed for the determination of the kinetic value for binding using both the analysis software from Nomadics and the Scatchard analysis employed for use with the non-saturating curves of the regulon. These values are similar to each other and indicate what could be the inherent DNA affinity of CcmR. For the Scatchard

(Figure 14 B) analysis the values were 74.7 ± 7.0 nM while the QDAT (Nomadics) yielded a value of 56 ± 4 nM. This value is lower than that for CcmR binding to the specific targets themselves as calculated by Scatchard analysis (Figure 8, 9), which range from 308 nM to 2 µM. Therefore we conclude that the affinity values obtained from the analysis the binding curves of CcmR interacting with specific targets are likely greatly higher than the actual affinities, because other kinetic features of the interaction obscure the analysis that I applied. The binding ratio of CcmR to the non-specific fragment was calculated at 0.52 CcmR monomers per non-specific fragment. The ratio calculated for CcmR binding to the promoter of a regulon target was approximately 4 monomers per DNA fragment (Table C1).

Figure 14

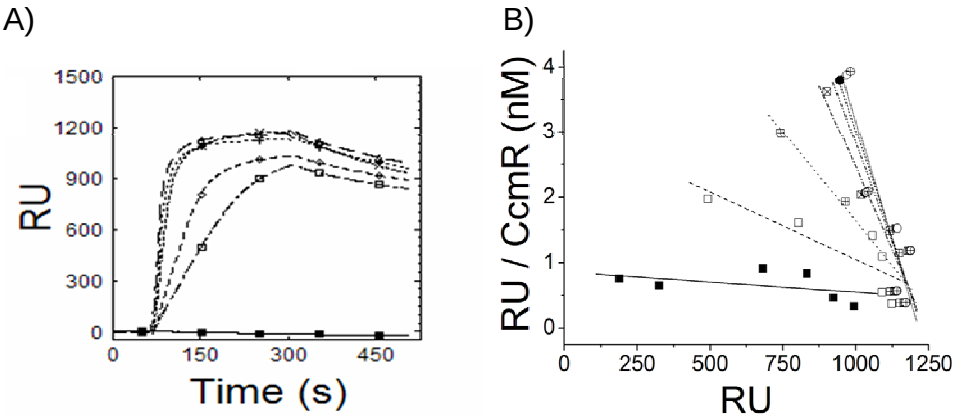

Figure 14. Surface Plasmon Resonance curve illustrating binding of CcmR to the coding region of rimM. Essentially as described in Figure 8. A) Titration of CcmR binding to the rimM fragment with the markers for visualization only; 0 nM (Closed Square), 250 nM (Open Square), 500 nM (Open Diamond), 750 nM (X), 1000 nM (+), 2000 nM (Open Triangle), 3000 nM (Closed Circle). B) Scatchard analysis of CcmR binding to the rimM fragment. SPR data (Figure 14 A) as described in Figure 9. Data points: 100 sec. (Closed Square), 150 sec. (Open Square), 200 sec. (Open Square with +), 250 sec. (Open Square with X), 275 sec. (Closed Circle), 290 sec. (Open Circle), 300 sec. (Open Circle with +). Linear Regression: 100 sec. (—), 150 sec. (— —), 200 sec. (• • •), 250 sec. (— - —), 275 sec. (— - -), 290 sec. (- - - -), 300 sec. (· · ·).

This result was very puzzling and subsequently a ligand molecule injection was done to determine whether the ligand molecule could be promoting a conformation that allowed for the specificity of the protein. A simple titration was performed using $NADP^+$ and CcmR exactly as done previously during the screen for the ligand molecule (Figure 10). Upon addition of the $NADP^+$ and CcmR we found that over all binding to the non-specific decreased by about 350 RU's (Figure 15). Given that the initial blank injection containing only CcmR went to approximately 800 RU's, the value when the ligand molecule was included showed a decrease of nearly 50% (Figure 15).

Figure 15

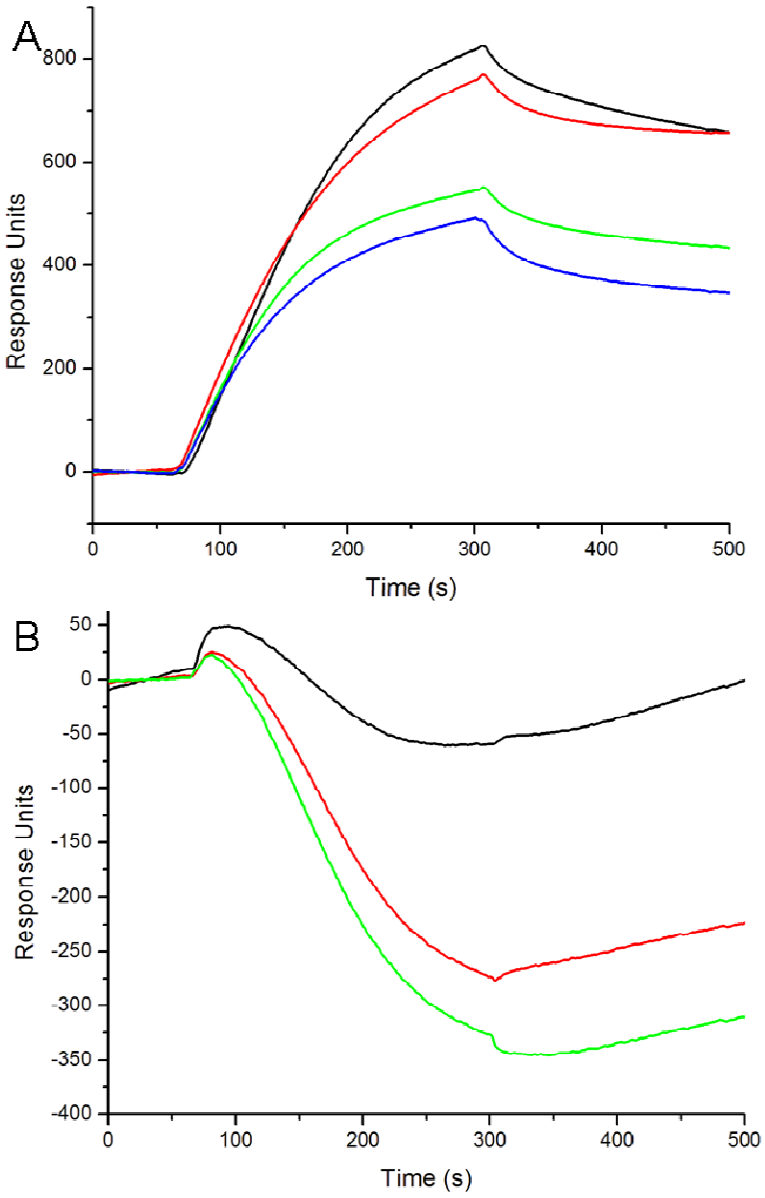

Figure 15. SPR curves illustrating binding of CcmR to rimM can be disrupted by $NADP^+$.

A) Titration of CcmR onto the immobilized rimM fragment, in the presence of $NADP^+$. All injections contain 1 μM CcmR; 0 μM (Black), 10 μM (Red), 100 μM (Green), 500 μM (Blue).

B) Double reference subtraction for the curve shown in panel A; 10 μM (Black), 100 μM (Red), 500 μM (Green).

DISCUSSION

Why do we see such large differences in the binding characteristics of CcmR to non-specific as compared to the specific fragments? The differences in the binding of CcmR (Figure 16) to the non-specific control fragment and to the specific promoter fragments represent a highly complex system that is not fully understood at the present time and the experiments presented here will hopefully contribute to the resolution of this difficult problem. Taken together the other recent results (71-75) combined with the DLS data presented above (Table 1), suggests that CcmR is also capable of oligomerization and the formation of these complexes will require careful future study in order to determine the true binding kinetics and characteristics of this complex system.

Two possible, but not mutually exclusive, explanations for positive contributions to SPR signals can be considered. The first possible explanation is simply that more mass has been added to the surface of the chip through the interaction of the protein with the DNA. A second alternative explanation is that binding of the protein to the DNA causes a conformational change to occur which causes a change in the magnitude of the signal as the CcmR:DNA complex moves within the evanescent field generated on the surface of the chip (*109-113, 118*). In the following discussion, I will try and take these alternative processes to explain the contrasting binding behavior of CcmR to the DNA fragments (non-specific and specific).

The first possible explanation involves the addition of more units of CcmR onto the DNA molecule attached to the surface of the chip. In the case of the

binding of CcmR to non-specific DNA (i.e. rimM), the first explanation most likely accounts for the signal characteristics, which has a classic binding curve shape that shows saturation. The binding of CcmR to non-specific binding of the protein to the DNA presumably occurs through the DNA binding domain of CcmR, but without specific interactions with DNA sequence. This would cause the increase in signal that is observed. The binding curve exhibits saturation, which is best explained by assuming that a quasi-steady state is reached and this steady state is due to a balance between the number of new molecules binding being balanced by the number of molecules that had been bound, that are now being released into the buffer flowing over the SPR chip. In contrast, when looking at the curves for the CcmR titrations onto the specific DNA no clear saturation occurs, but upon closer examination the curves show a fast and a slow kinetic phase (see Chapter 3). The fast kinetic phase would most likely be the initial binding of CcmR to the recognition sequence of the promoter. This first phase of addition appears to occur during the initial 60 seconds of the protein binding to the DNA fragment (Figure 16 and Chapter 3). While this initial phase does not reach saturation of the target DNA fragment the signal increases approximately 500 to 600 units depending on the protein concentration. This increase is 60–65% of the total increase in signal observed over the entire 240 second injection (Figure 16 and Chapter 3).

During the remaining period of the injection (180 seconds) the rate of increase in the signal goes down, perhaps indicating that fewer proteins are binding to the DNA fragment during this phase of the injection. It is during this

phase that the remaining 35 – 40% of the positive signal is observed (Figure 16 and Chapter 3). One possibility is that there is the binding of additional subunits of CcmR to the DNA fragment may be occurring along the entire length of the DNA fragment and results in transient binding which gives the constant increase in signal as more and more subunits bind to available free locations on the fragment without regard to the sequence. Given the known binding sequence of CcmR (19) and allowing for the protein to bind over the entire length of the DNA fragments (without overlap) used during the SPR assay a total of approximately 6.8 CcmR DNA binding units could occur on 150 bp of DNA. If we assume that the binding unit of CcmR is a tetramer than the total would be 27.2 CcmR monomers per 150 bp. Another possibility is that the DNA protein complex is undergoing a re-arrangement that causes the signal to be altered. In other words, the second cause for the signal to increase mentioned above would be a change in shape to the DNA-protein complex.

Turning to the dissociation phase after the protein is no longer in the stream of buffer flowing over the surface of the SSR chip and the protein begins to dissociate without replacement by new subunits. As the injection finishes and the protein begins to dissociate from the DNA fragment without replacement, we also observe two basic portions, a fast phase and a slow phase in the case of the CcmR-specific DNA complex. These phases could entail either a fast off and slow off kinetics, or it is possible that they are representing a fast off and slow rearrangement. However, during the disassociation this difference between the fast and slow phases is more tentative. The drop in signal following this first fast

phase will continue at a very slow rate, which never reaches the initial starting level, indicating that the affinity of the protein for the DNA is relatively high. Calculations performed using Scatchard analysis support k_D values in the nanomolar to low micromolar range, but it should be noted that Scatchard analysis relies on the association phase for calculation (Chapter 3). As noted below, the application of Scatchard analysis to these complex kinetics seems to result in a gross underestimation of the actual affinities in the case of the specific DNA-CcmR interaction.

The observed pattern for CcmR binding to the non-specific fragment shows a different trend in the kinetic curves. Within the same time frame were the fast phase for the regulon targets was observed we see nearly 90% of the signal occurring. This would appear to indicate a much tighter binding of CcmR to this DNA fragment than was observed for the specific fragments themselves. This seems nonsensical and probably reflects the complexity of the binding signal, which is comprised of two kinetic phases in the specific interaction. No clear slow phase exists for the binding of CcmR to the non-specific fragment (Figure 16 and Chapter 3). The remaining signal increase is spread over such an extended period of time and with such a small increase that it probably represents proteins that are simply in physical proximity with the DNA rather than actually interacting.

The observed off rate for the CcmR bound to non-specific also shows a different kinetic pattern than does the specific fragment (Figure 16 and Chapter 3). In the case of the off rate it would appear to be a single phase, no clear

immediate drop is observed and the rate remains relatively uniform over the following 200 seconds. The observed curves for CcmR bound to non-specific would indicate that the proteins are simply dissociating from the fragment with a single off rate, as indicated by the single phase of the curve, whereas with the regulon targets (Chapter 3) it has at least two phases indicating two different rates.

For this data (association phase of CcmR to DNA) the second possible explanation involves a conformational change occurring on the surface of the chip. This conformational change would show on the curves as an increase or decrease in signal depending on the nature of the conformational change (*109-113, 118*). If the CcmR:DNA complex was brought closer to the surface of the chip the signal would increase, if the complex was brought further from the surface the signal would decrease (*109-113, 118*). This is based on the dielectric field constants and the interaction with the evanescent field (*109-113, 118*).

For the specific fragment data the two phases as described would now have a binding (fast) and conformational (slow) interpretation to them. The binding of the protein to the DNA would account for the fast phase and the subsequent conformational changes occurring in the CcmR:DNA complex would require additional time and this would be indicated by the gradual increase in signal observed in the slow phase of the on rate. The inability of the signal to reach saturation has been observed previously and generally indicates conformational changes (*109-113, 118*). The rapid drop in signal follows the termination of the injection may still be the removal of associated subunits that

have either not bound to the DNA or not undergone conformational change, which allows them to dissociate from the DNA at a much faster rate. The slow phase of the dissociation maybe the result of the protein:DNA complex in a different conformation that reduces the exposure of the protein to the buffer flow and thus reduces the off rate, yielding a slower release from the DNA fragment.

The non-specific binding data again shows only a single basic rate for the binding of CcmR and this ability to saturate the surface would tend to indicate that no conformational changes are occurring, or if they are occurring that the conformational changes are much less extensive and thus not causing a great perturbation of the DNA structure and movement within the evanescent field. The single off rate would also tend to support this idea of no or limited movement of the CcmR:DNA complex, as again there is only a single observed phase to the dissociation.

This apparent dichotomy of CcmR and its binding characteristics with both the specific and non-specific fragments is enhanced by the DNA bending assay (Figure 13) which shows that CcmR is causing a conformational change in the specific DNA. This bending would appear to favor the interpretation of the SPR data for the changes in conformation and movement within the evanescent field, however the EMSA data upon which this bending assay is based uses higher protein concentrations (relative to the DNA) and this may have induced differences in the conformation that are not observed for the binding under the equilibrium conditions that exist along the surface of the SPR chip.

The function of the ligand molecule upon binding to CcmR has also shown very interesting trends in relation to the difference between the specific and non-specific fragments. With the addition of $NADP^+$ CcmR binds with kinetic curves that show saturation (Figure 10), whereas, in the absence of the ligand molecule no saturation was observed. This change can also have two possible explanations; 1) That the conformation of CcmR has been altered allowing for increased binding to the DNA fragment or 2) that the on and off rates have been altered which allows increased protein binding to the fragment. The concentration of CcmR remains constant during the injections with different ligand molecule concentrations. This shows that in the presence of these increased concentrations that binding changes are due to the ligand molecule and its effects on the protein.

Unfortunately, there is no way to positively determine which scenario is the correct function of the ligand molecule with the current data. A change in the conformation of CcmR which allows additional subunits to bind to the DNA fragment in the higher affinity state would show an increased binding to the fragment and be observed as a saturation kinetic curve. This increased binding could reflect the change in conformation allowing for the bending of the DNA to occur among a greater population of the CcmR almost instantly given the nature of the injection that would allow for the saturation to occur without the two phase kinetics observed earlier.

When looking at the changes (specific vs. non-specific) in the off rate kinetics is much less dramatic than those of the on rate. The basic

shape/characteristics of the off rate appear very much like those of the off rate in the absence of the ligand molecule. The major difference involves the first few seconds following the injection termination, were an even larger decrease in signal is observed followed by the gradual loss of signal as seen previously. This major drop in signal again probably corresponds to the removal of loosely bound protein which is in simple proximity to the DNA.

Upon binding of CcmR to the non-specific fragment in the presence of the ligand molecule several interesting observations have been made. The first is that the signal goes down in the presence of increasing concentrations of the ligand molecule (Figure 15) which would appear to indicate that the protein is not binding to the DNA. This change may be caused by changes in either the on or off rate of the protein for the DNA fragment. In all probability the observed change is in fact an alteration in both kinetic constants for the interaction between CcmR and the non-specific fragment.

This change can be observed in the on rate as shown in the simple change in the kinetic curve of the binding. The curves do not show the appearance of a second kinetic phase simply the reduction in the maximum signal achieved in the presence of the ligand molecule. During this phase of the kinetic curve the primary factor influencing this shape is the on rate itself. Following the conclusion of the injection the kinetic curves show a change in the kinetic phase. This change is generally regarded as being controlled by the off rate, and here shows a basic change in the shape of the curve in the presence of the ligand molecule but of interest is that the curves themselves are fairly similar

just at lower values based on the association kinetics. This would appear to indicate that although the on and off rates have changed, the on rate has been effected more than the off rate.

Given the changes in conformation that are known to occur in other LTTR's upon ligand molecule binding it is reasonable to assume that CcmR also responds to the presence of its ligand molecule by altering its conformation. This alteration in conformation is the most likely explanation for the changes that have been observed for both the on and off rates shown (Figure 15). The ability of the ligand molecule to control the selectivity of CcmR for the sequence of DNA it is binding to has given this process a new dimension. Previously, it was assumed that CcmR would be able to 'read' the sequence of DNA that it was bound to by interactions between the surface amino acids and the nucleotide bases themselves. This has proven to be a difficult prospect to accept given the extremely high affinity of CcmR for the non-specific fragment, which is higher than for those of the regulon itself (see above and Chapter 3). The process of binding to the DNA could involve a conformational change in CcmR, and this change may be induced by the ligand molecule. It would appear that this new ligand molecule induced conformation allows for the selectivity of CcmR for the DNA sequence it is binding to.

Two main theories for the interaction of CcmR with ligand and DNA have emerged from the results described in this thesis: 1) CcmR in the presence of the ligand molecule adopts a conformation that is only stable when DNA is wrapped around the tetramer core; 2) CcmR adopts a conformation in the presence of the

ligand that alters the interaction with the DNA in a DNA sequence specific manner. Both theories are similar in their molecular interactions between CcmR and DNA, but have distinct molecular differences in how those interactions are modulated by the ligand molecule.

Theory number one involves the change in intermolecular interactions between CcmR sub-units such that the tetramer configuration of the protein is only stable when DNA is wrapped around the protein. In the absence of the ligand molecule the tetramer conformation is stable. In the absence of the DNA the new conformation of CcmR is no longer stable and this causes the tetramer to disassociate. This theory could be applied to the observed kinetic curves generated by the non-specific DNA interactions, where we do not believe DNA wrapping/bending to be occurring.

Theory number two involves the change in conformation causing a difference in the interactions of the protein to the DNA allowing for the specificity of the interaction. This allows the protein to differentiate between specific and non-specific DNA sequences. This conformation than allows for the wrapping of the DNA only when the specific target sequences is present.

Given these two competing theories for the molecular interaction between CcmR and DNA (specific and non-specific) the calculated ratio of binding of the protein to the DNA becomes even more interesting. Upon binding to specific DNA, calculations have shown that the protein is binding at approximately 4 to 1 molar ratio (see above). When the non-specific DNA is used the molar ratio decreases to approximately 0.5 to 1 (see above). This major change in the

molar binding ratio of the protein in the presence of the specific vs. non-specific DNA fragments allows for the supposition that the calculated kinetics affinities shown in Figure 9 and discussed above are actually much lower than the true values for the binding of CcmR to specific DNA targets. The true value is most likely in the pM range for the interactions between CcmR and specific DNA targets, which has been masked by possible conformational changes, yielding the much lower affinity values shown (Chapter 3).

The current assay required the binding of the protein to the DNA target already bound on the surface of the SPR chip and the determination of the ligands affinity for the protein could not be determined based on the simplified model used by the analysis software (Nomadics, Icx). It is very likely that the more complex kinetic model already under development (Nomadics, Icx) will be able to make these determinations of the ligand binding kinetics. The conformational changes that maybe occurring on the surface can cause increases or decreases in the signal that can not be entirely distinguished from additional protein sub-units binding or unbinding from the DNA fragment (*109-113, 118*). The direct binding of the protein to the surface of the chip may allow for a better determination of the binding kinetics for both the protein:DNA interaction and the protein:ligand interaction. Although, this assay may allow for the kinetics to be determined the oligomerization tendency of the LTTR's and the conformational changes seen here and with other LTTR's would make the direct coupling problematic (see Chapter 1 and 3). The possible use of an antibody mediated coupling system could allow for the direct assay of the ligand molecule

and DNA interaction kinetics, although the potential for restriction in conformational changes upon binding of the protein to the antibody can not be ignored.

In summary the binding of CcmR has been shown to be more complex than originally theorized and this complexity will require additional work beyond the scope for this thesis to fully unravel the molecular interactions occurring between CcmR and DNA.

Figure 16

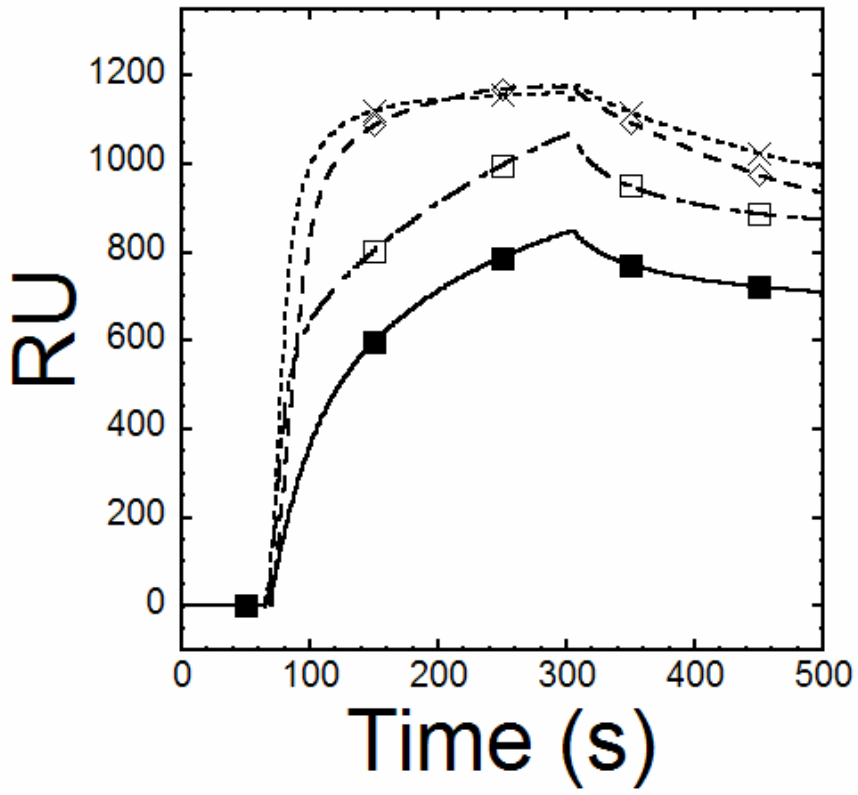

Figure 16. Surface Plasmon Resonance curve illustrating binding of CcmR to the coding region of rimM vs the promoter of ndhF3. Essentially as described in Figure 8. Titration of CcmR binding to the rimM and pndhF3 fragment with the markers for visualization only; CcmR (1 μM)- pndhF3 target (Closed Square), CcmR (3 μM)-pndhF3 target (Open Square), CcmR (1 μM)-rimM target (Open Diamond), CcmR (3 μM)-rimM target (X).

V. CONCLUSIONS AND FUTURE DIRECTIONS

A major question has persisted within the literature regarding how conditions of limiting inorganic carbon availability are sensed by cyanobacteria. The most extensive studies on this topic were performed by the Badger and Price research groups in Australia. Looking at transcriptional regulation of the major Ci transporters and using a variety of metabolic inhibitors, this group concluded that the regulation responded to the size of the cytoplasmic pool of Ci and the response was dependent upon oxygen. These authors suggested that HCO_3^- could be directly sensed by the transcriptional regulatory mechanism. About that time, the Burnap group published a global gene expression study of Ci limitation in *Synechocystis*, including the analysis of a mutant lacking CcmR. It was concluded that CcmR may function as the major transcriptional repressor of the high affinity transport systems. My thesis project aimed to verify the regulon of CcmR and use CcmR to identify the regulatory signal. It was hypothesized that CcmR would change its repressor activity in response to binding a small molecule that signaled the inorganic carbon status of the cell since other LTTRs act in this way. During the course of my studies, the Omata group, one of the first groups to identify LTTRs as important for Ci regulation, used EMSA to show that one of the intermediates of photorespiration, 2PG and the CBB cycle intermediate, RuBP, acted to control the DNA binding properties of CmpR. CmpR was previously shown to activate the transcription of one of the other

bicarbonate transporters. Therefore, it seemed that the main candidates for the regulation of the high affinity system via CcmR could be bicarbonate, RuBP, and 2PG. The identification of α-KG and $NADP^+$ as the co-repressors within *Synechocystis* has now answered this question. Typically for the LTTR family, the ligand molecules have come from the regulated metabolic pathways under their control . Neither protein is responding directly to the inorganic carbon concentration of the cell, HCO_3^- or CO_2, and only one molecule is directly from the photorespiratory pathway (2PG). This set of results is in direct contradiction to the theorized ligand molecules for both CcmR and CmpR. However, the mechanism proposed in this thesis makes sense in that inorganic carbon limitation would tend to deplete the cytoplasm of α-KG and $NADP^+$ thereby allowing the de-repression of the high affinity system.

While the identification of functionally important ligand molecules for CcmR has been achieved, the work has not eliminated the possibility that other regulatory molecules act upon CcmR. Furthermore, the complete kinetic picture of the proteins is still largely unknown at the molecular level. We have seen no synergistic effect on the binding to target sequences, where a stronger effect by $NADP^+$ over α-KG can be seen. Nothing is yet known on the location of the binding sites of these effectors. Yet the question remains, why do both CcmR and CmpR have two distinct ligand molecules when we see no synergistic effects from them? Presumably, it simply reflects the fact that more than one metabolic pathway is being affected by the availability of inorganic carbon. It is interesting to compare CcmR and CmpR. CmpR controls the expression of an ABC-

cassette type transporter of bicarbonate and is thought to contribute a relatively small fraction of the cell's uptake capacity. On the other hand, CcmR controls a much larger set of the inorganic uptake genes, and because it is modulated by the level of α-KG and because α-KG is a key metabolic precursor for nitrogen assimilation, the CcmR regulon is linked to the activity of the nitrogen assimilation pathway.

The thesis work also provides physical evidence for the operation of the regulon proposed earlier based upon microarray experiments. This was accomplished using EMSAs to show that CcmR specifically interacts with the promoter regions of each of the proposed operons of the regulon. Furthermore, I have provided evidence that the binding affinity of CcmR for each of the promoters is slightly different. At the same time, the SPR gave puzzling results regarding the affinities: according to the SPR kinetic analysis, a non-specific control fragment of DNA showed a higher affinity for CcmR than any of the specific promoter sequences for the genes that were under its direct control. This apparent contradiction can be explained, by the major conformational changes that CcmR undergoes when binding to its regulon targets and subsequent ligand molecule binding. These conformational changes have prevented the accurate determination of the true binding constant for CcmR and the cognate promoters of the high affinity CCM regulon. The inclusion of the control DNA fragment has given us the opportunity to determine what the intrinsic binding affinity of CcmR for DNA actually is. This fragment has the highest affinity of all fragments tested and yet our very ability to determine these kinetic

constants shows us that the control DNA is not undergoing these massive conformational changes. The picture becomes even more intriguing when the ligand molecule is added and we see a major decrease in binding of CcmR to the DNA fragment. From this we can conclude that the ligand probably induces a conformational change in CcmR that reduces the affinity in the absence of specific sequences. Perhaps, CcmR undergoes a similar conformational change when bound to the specific DNA sequences, but instead of causing the protein to fall off, the specific sequences provide 'traction' and cause the DNA to bend even further than EMSA bending assays have indicated.

It is interesting to realize that the high affinity CCM appears to be controlled by both $NADP^+$ and by α-KG. The affect of the fundamental redox carrier $NADP^+$ probably reflects the central role that the $NADP^+$/NADPH ratio plays in regulating this important process. We now have identified an additional integration point between the carbon and nitrogen metabolism within *Synechocystis*, in the form of the ligand molecule for CcmR (α-KG). As noted, this molecule is a known interlink point between carbon and nitrogen metabolism and now we have identified it as a co-repressor of a key inorganic carbon regulator. It is interesting to note that neither co-activator molecule that modulates CmpR, is functioning in this fashion.

Overall the study of these two proteins has shown us some very interesting facets of the metabolic control of the cell with regards to the acquisition of inorganic carbon, and the subsequent reduction into organic carbon. The cross-talk occurring on multiple levels of the cellular metabolism

between these two regulators and the nitrogen metabolism has opened exciting new avenues of research to be pursued in the future.

REFERENCES

(1) Wang, H. L., Postier, B. L., and Burnap, R. L. (2004) Alterations in global patterns of gene expression in Synechocystis sp. PCC 6803 in response to inorganic carbon limitation and the inactivation of ndhR, a LysR family regulator. *J Biol Chem 279*, 5739-51.

(2) Kaneko, T., Sato, S., Kotani, H., Tanaka, A., Asamizu, E., Nakamura, Y., Miyajima, N., Hirosawa, M., Sugiura, M., Sasamoto, S., Kimura, T., Hosouchi, T., Matsuno, A., Muraki, A., Nakazaki, N., Naruo, K., Okumura, S., Shimpo, S., Takeuchi, C., Wada, T., Watanabe, A., Yamada, M., Yasuda, M., and Tabata, S. (1996) Sequence analysis of the genome of the unicellular cyanobacterium Synechocystis sp. strain PCC6803. II. Sequence determination of the entire genome and assignment of potential protein-coding regions. *DNA Res 3*, 109-36.

(3) Kaneko, T., Sato, S., Kotani, H., Tanaka, A., Asamizu, E., Nakamura, Y., Miyajima, N., Hirosawa, M., Sugiura, M., Sasamoto, S., Kimura, T., Hosouchi, T., Matsuno, A., Muraki, A., Nakazaki, N., Naruo, K., Okumura, S., Shimpo, S., Takeuchi, C., Wada, T., Watanabe, A., Yamada, M., Yasuda, M., and Tabata, S. (1996) Sequence analysis of the genome of the unicellular cyanobacterium Synechocystis sp. strain PCC6803. II. Sequence determination of the entire genome and assignment of potential protein-coding regions (supplement). *DNA Res 3*, 185-209.

(4) Badger, M. R., and Andrews, T. J. (1982) Photosynthesis and Inorganic Carbon Usage by the Marine Cyanobacterium, *Synechococcus* sp. *Plant Physiol 70*, 517-523.

(5) Lodish, H., Berk, A., Zipursky, L. S., Matsurdaira, P., Baltimore, D., and Darnell, J. (2000) *Molecular Cell Biology*, Fourth Edition ed.

(6) Moroney, J. V., and Somanchi, A. (1999) How Do algae concentrate CO2 to increase the efficiency of photosynthetic carbon fixation? *Plant Physiol 119*, 9-16.

(7) Badger, M. R., and Price, G. D. (2003) CO_2 concentrating mechanisms in cyanobacteria: molecular components, their diversity and evolution. *J Exp Bot 54*, 609-622.

(8) Badger, M. R., Price, G. D., Long, B. M., and Woodger, F. J. (2006) The environmental plasticity and ecological genomics of the cyanobacterial CO2 concentrating mechanism. *J Exp Bot 57*, 249-65.

(9) Cannon, G. C., Bradburne, C. E., Aldrich, H. C., Baker, S. H., Heinhorst, S., and Shively, J. M. (2001) Microcompartments in prokaryotes: carboxysomes and related polyhedra. *Appl Environ Microbiol 67*, 5351-61.

(10) English, R. S., Lorbach, S. C., Qin, X., and Shively, J. M. (1994) Isolation and characterization of a carboxysome shell gene from Thiobacillus neapolitanus. *Mol Microbiol 12*, 647-54.

(11) Ogawa, T., Marco, E., and Orus, M. I. (1994) A gene (ccmA) required for carboxysome formation in the cyanobacterium Synechocystis sp. strain PCC6803. *J Bacteriol 176*, 2374-8.

(12) Price, G. D., Howitt, S. M., Harrison, K., and Badger, M. R. (1993) Analysis of a genomic DNA region from the cyanobacterium Synechococcus sp. strain PCC7942 involved in carboxysome assembly and function. *J Bacteriol 175*, 2871-9.

(13) Shively, J. M., Ball, F., Brown, D. H., and Saunders, R. E. (1973) Functional organelles in prokaryotes: polyhedral inclusions (carboxysomes) of Thiobacillus neapolitanus. *Science 182*, 584-6.

(14) Garcia-Murria, M. J., Karkehabadi, S., Marin-Navarro, J., Satagopan, S., Andersson, I., Spreitzer, R. J., and Moreno, J. (2008) Structural and functional consequences of the replacement of proximal residues Cys(172) and Cys(192) in the large subunit of ribulose-1,5-bisphosphate carboxylase/oxygenase from Chlamydomonas reinhardtii. *Biochem J 411*, 241-7.

(15) Andersson, J. O., and Roger, A. J. (2002) A cyanobacterial gene in nonphotosynthetic protists--an early chloroplast acquisition in eukaryotes? *Curr Biol 12*, 115-9.

(16) Cavalier-Smith, T. (2002) Chloroplast evolution: secondary symbiogenesis and multiple losses. *Curr Biol 12*, R62-4.
(17) Reumann, S., and Weber, A. P. (2006) Plant peroxisomes respire in the light: some gaps of the photorespiratory C2 cycle have become filled--others remain. *Biochim Biophys Acta 1763*, 1496-510.
(18) Nelson, D. L., and Cox, M. M. (2003) Lehninger Principles of Biochemistry 3rd ed.
(19) Figge, R. M., Cassier-Chauvat, C., Chauvat, F., and Cerff, R. (2001) Characterization and analysis of an NAD(P)H dehydrogenase transcriptional regulator critical for the survival of cyanobacteria facing inorganic carbon starvation and osmotic stress. *Mol Microbiol 39*, 455-68.
(20) Ghoshal, D., and Goyal, A. (2000) Carbon concentration mechanisms in photosynthetic microorganisms. *Indian J Biochem Biophys 37*, 383-94.
(21) Kusian, B., and Bowien, B. (1995) Operator binding of the CbbR protein, which activates the duplicate cbb CO2 assimilation operons of Alcaligenes eutrophus. *J Bacteriol 177*, 6568-74.
(22) Li, Q., and Canvin, D. T. (1998) Energy sources for HCO3- and CO2 transport in air-grown cells of synechococcus UTEX 625. *Plant Physiol 116*, 1125-32.
(23) Ohkawa, H., Sonoda, M., Katoh, H., and Ogawa, T. (1998) The use of mutants in the analysis of the CO2-concentrating mechanism in cyanobacteria. *Can. J. Bot. 76*, 1035-1042.
(24) Price, G. D., Sültemeyer, D., Klughammer, B., Ludwig, M., and Badger, M. R. (1998) The functioning of the CO2 concentrating mechanism in several cyanobacterial strains: a review of general physiological characteristics, genes, proteins, and recent advances. *Can. J. Bot. 76*, 973-1002.
(25) Amichay, D., Levitz, R., and Gurevitz, M. (1993) Construction of a Synechocystis PCC6803 mutant suitable for the study of variant hexadecameric ribulose bisphosphate carboxylase/oxygenase enzymes. *Plant Mol Biol 23*, 465-76.
(26) Shively, J. M., van Keulen, G., and Meijer, W. G. (1998) Something from almost nothing: carbon dioxide fixation in chemoautotrophs. *Annu Rev Microbiol 52*, 191-230.
(27) Woodger, F. J., Badger, M. R., and Price, G. D. (2003) Inorganic carbon limitation induces transcripts encoding components of the CO(2)-concentrating mechanism in Synechococcus sp. PCC7942 through a redox-independent pathway. *Plant Physiol 133*, 2069-80.
(28) Badger, M. R., and Price, D. (1992) The CO2 concentrating mechanism in cyanobacteria and microalgae. *Physiologia Plantarum 84*, 606-615.
(29) Skleryk, R. S., So, A. K., and Espie, G. S. (2002) Effects of carbon nutrition on the physiological expression of HCO3- transport and the CO2-concentrating mechanism in the Cyanobacterium chlorogloeopsis sp. ATCC 27193. *Planta 214*, 572-83.
(30) Badger, M. (2003) The roles of carbonic anhydrases in photosynthetic CO2 concentrating mechanisms. *Photosynth Res 77*, 83.
(31) Maeda, S., Badger, M. R., and Price, G. D. (2002) Novel gene products associated with NdhD3/D4-containing NDH-1 complexes are involved in photosynthetic CO2 hydration in the cyanobacterium, Synechococcus sp. PCC7942. *Mol Microbiol 43*, 425-35.
(32) Omata, T., Price, G. D., Badger, M. R., Okamura, M., Gohta, S., and Ogawa, T. (1999) Identification of an ATP-binding cassette transporter involved in bicarbonate uptake in the cyanobacterium Synechococcus sp. strain PCC 7942. *Proc Natl Acad Sci U S A 96*, 13571-6.
(33) Price, G. D., Woodger, F. J., Badger, M. R., Howitt, S. M., and Tucker, L. (2004) Identification of a SulP-type bicarbonate transporter in marine cyanobacteria. *Proc Natl Acad Sci U S A 101*, 18228-33.
(34) Amoroso, G., Seimetz, N., and Sultemeyer, D. (2003) The dc13 gene upstream of ictB is involved in rapid induction of the high affinity Na(+) dependent HCO(3) (-) transporter in cyanobacteria. *Photosynth Res 77*, 127-38.
(35) Bloye, S., Silman, N., Mann, N., and Carr, N. (1992) Bicarbonate Concentration by Synechocystis PCC6803. *Plant Physiology 99*, 601-606.

(36) Takahashi, Y., Yamaguchi, O., and Omata, T. (2004) Roles of CmpR, a LysR family transcriptional regulator, in acclimation of the cyanobacterium Synechococcus sp. strain PCC 7942 to low-CO(2) and high-light conditions. *Mol Microbiol 52*, 837-45.
(37) Wang, H. L., Postier, B. L., and Burnap, R. L. (2002) Optimization of fusion PCR for in vitro construction of gene knockout fragments. *Biotechniques 33*, 26, 28, 30 passim.
(38) Wang, H. L., Postier, B. L., and Burnap, R. L. (2002) Polymerase chain reaction-based mutageneses identify key transporters belonging to multigene families involved in Na+ and pH homeostasis of Synechocystis sp. PCC 6803. *Mol Microbiol 44*, 1493-506.
(39) Ritchie, R. J., Nadolny, C., and Larkum, A. (1996) Driving Forces for Bicarbonate Transport in the Cyanobacterium Synechococcus R-2 (PCC 7942). *Plant Physiol 112*, 1573-1584.
(40) Maeda, S., Price, G. D., Badger, M. R., Enomoto, C., and Omata, T. (2000) Bicarbonate binding activity of the CmpA protein of the cyanobacterium Synechococcus sp. strain PCC 7942 involved in active transport of bicarbonate. *J Biol Chem 275*, 20551-5.
(41) Shibata, M., Katoh, H., Sonoda, M., Ohkawa, H., Shimoyama, M., Fukuzawa, H., Kaplan, A., and Ogawa, T. (2002) Genes essential to sodium-dependent bicarbonate transport in cyanobacteria: function and phylogenetic analysis. *J Biol Chem 277*, 18658-64.
(42) Sultemeyer, D., Klughammer, B., Badger, M. R., and Price, G. D. (1998) Fast Induction of High-Affinity HCO3- Transport in Cyanobacteria. *Plant Physiol 116*, 183-192.
(43) So, A. K. C., Kassam, A., and Espie, G. S. (1998) Na+-dependent HCO3- transport in the cyanobacterium Synechocystis PCC6803. *Can. J. Bot. 76*, 1084-1091.
(44) Ogawa, T., and Inoue, Y. (1984) A Post-Illumination CO2 Burst in *Anabaena variabilis* as a measure of bicarbonate trasport driven by cyclic photophosphorylation. *Advances in Photosynthesis Research II*, II.7.723 - II.7.726.
(45) Ogawa, T., and Kaplan, A. (2003) Inorganic carbon acquisition systems in cyanobacteria. *Photosynth Res 77*, 105.
(46) Omata, T., Gohta, S., Takahashi, Y., Harano, Y., and Maeda, S. (2001) Involvement of a CbbR homolog in low CO2-induced activation of the bicarbonate transporter operon in cyanobacteria. *J Bacteriol 183*, 1891-8.
(47) Benschop, J., Badger, M., and Dean Price, G. (2003) Characterisation of CO2 and HCO3 uptake in the cyanobacterium Synechocystis sp. PCC6803. *Photosynthesis Research 77*, 117.
(48) Zhang, P., Sicora, C. I., Vorontsova, N., Allahverdiyeva, Y., Battchikova, N., Nixon, P. J., and Aro, E. M. (2007) FtsH protease is required for induction of inorganic carbon acquisition complexes in Synechocystis sp. PCC 6803. *Mol Microbiol 65*, 728-40.
(49) Espie, G. S., and Canvin, D. T. (1987) Evidence for Na-Independent HCO(3) Uptake by the Cyanobacterium Synechococcus leopoliensis. *Plant Physiol 84*, 125-130.
(50) Espie, G. S., Miller, A. G., and Canvin, D. T. (1988) Characterization of the Na-Requirement in Cyanobacterial Photosynthesis. *Plant Physiol 88*, 757-763.
(51) Codd, G. A. (1988) Carboxysomes and ribulose bisphosphate carboxylase/oxygenase. *Adv Microb Physiol 29*, 115-64.
(52) Shively, J. M. (1974) Inclusion bodies of prokaryotes. *Annu Rev Microbiol 28*, 167-87.
(53) Shively, J. M., Bryant, D. A., Fuller, R. C., Konopka, A. E., Stevens, S. E., Jr., and Strohl, W. R. (1988) Functional inclusions in prokaryotic cells. *Int Rev Cytol 113*, 35-100.
(54) Codd, G. A., and Marsden, W. J. N. (1984) The carboxysomes (polyhedral bodies) of autotrophic prokaryotes. *Biol. Rev. 59*, 389-422.
(55) Yeates, T. O., Kerfeld, C. A., Heinhorst, S., Cannon, G. C., and Shively, J. M. (2008) Protein-based organelles in bacteria: carboxysomes and related microcompartments. *Nat Rev Microbiol 6*, 681-91.
(56) Drews, G., and Niklowitz, W. (1956) [Cytology of Cyanophycea. II. Centroplasm and granular inclusions of Phormidium uncinatum.]. *Arch Mikrobiol 24*, 147-62.
(57) Long, B. M., Badger, M. R., Whitney, S. M., and Price, G. D. (2007) Analysis of carboxysomes from Synechococcus PCC7942 reveals multiple Rubisco complexes with carboxysomal proteins CcmM & CcaA. *J Biol Chem*.

(58) Tanaka, S., Kerfeld, C. A., Sawaya, M. R., Cai, F., Heinhorst, S., Cannon, G. C., and Yeates, T. O. (2008) Atomic-level models of the bacterial carboxysome shell. *Science 319*, 1083-6.
(59) Tsai, Y., Sawaya, M. R., Cannon, G. C., Cai, F., Williams, E. B., Heinhorst, S., Kerfeld, C. A., and Yeates, T. O. (2007) Structural analysis of CsoS1A and the protein shell of the Halothiobacillus neapolitanus carboxysome. *PLoS Biol 5*, e144.
(60) Zaim, J., and Kierzek, A. M. (2003) The structure of full-length LysR-type transcriptional regulators. Modeling of the full-length OxyR transcription factor dimer. *Nucleic Acids Res 31*, 1444-54.
(61) Ezezika, O. C., Haddad, S., Clark, T. J., Neidle, E. L., and Momany, C. (2007) Distinct Effector-binding Sites Enable Synergistic Transcriptional Activation by BenM, a LysR-type Regulator. *J Mol Biol 367*, 616-29.
(62) Muraoka, S., Okumura, R., Ogawa, N., Nonaka, T., Miyashita, K., and Senda, T. (2003) Crystal structure of a full-length LysR-type transcriptional regulator, CbnR: unusual combination of two subunit forms and molecular bases for causing and changing DNA bend. *J Mol Biol 328*, 555-66.
(63) Muraoka, S., Okumura, R., Uragami, Y., Nonaka, T., Ogawa, N., Miyashita, K., and Senda, T. (2003) Purification and crystallization of a LysR-type transcriptional regulator CBNR from Ralstonia eutropha NH9. *Protein Pept Lett 10*, 325-9.
(64) Swaren, P., Maveyraud, L., Raquet, X., Cabantous, S., Duez, C., Pedelacq, J. D., Mariotte-Boyer, S., Mourey, L., Labia, R., Nicolas-Chanoine, M. H., Nordmann, P., Frere, J. M., and Samama, J. P. (1998) X-ray analysis of the NMC-A beta-lactamase at 1.64-A resolution, a class A carbapenemase with broad substrate specificity. *J Biol Chem 273*, 26714-21.
(65) Tyrrell, R., Verschueren, K. H., Dodson, E. J., Murshudov, G. N., Addy, C., and Wilkinson, A. J. (1997) The structure of the cofactor-binding fragment of the LysR family member, CysB: a familiar fold with a surprising subunit arrangement. *Structure 5*, 1017-32.
(66) Nishimura, T., Takahashi, Y., Yamaguchi, O., Suzuki, H., Maeda, S., and Omata, T. (2008) Mechanism of low CO2-induced activation of the cmp bicarbonate transporter operon by a LysR family protein in the cyanobacterium Synechococcus elongatus strain PCC 7942. *Mol Microbiol 68*, 98-109.
(67) Wintjens, R., and Rooman, M. (1996) Structural classification of HTH DNA-binding domains and protein-DNA interaction modes. *J Mol Biol 262*, 294-313.
(68) Brennan, R. G. (1993) The winged-helix DNA-binding motif: another helix-turn-helix takeoff. *Cell 74*, 773-6.
(69) Brennan, R. G., and Matthews, B. W. (1989) The helix-turn-helix DNA binding motif. *J Biol Chem 264*, 1903-6.
(70) Dubbs, J. M., and Tabita, F. R. (1998) Two functionally distinct regions upstream of the cbbI operon of Rhodobacter sphaeroides regulate gene expression. *J Bacteriol 180*, 4903-11.
(71) van Keulen, G., Ridder, A. N., Dijkhuizen, L., and Meijer, W. G. (2003) Analysis of DNA binding and transcriptional activation by the LysR-type transcriptional regulator CbbR of Xanthobacter flavus. *J Bacteriol 185*, 1245-52.
(72) Dangel, A. W., Gibson, J. L., Janssen, A. P., and Tabita, F. R. (2005) Residues that influence in vivo and in vitro CbbR function in Rhodobacter sphaeroides and identification of a specific region critical for co-inducer recognition. *Mol Microbiol 57*, 1397-414.
(73) Dubbs, P., Dubbs, J. M., and Tabita, F. R. (2004) Effector-mediated interaction of CbbRI and CbbRII regulators with target sequences in Rhodobacter capsulatus. *J Bacteriol 186*, 8026-35.
(74) Golic, N., Schliekelmann, M., Fernandez, M., Kleerebezem, M., and van Kranenburg, R. (2005) Molecular characterization of the CmbR activator-binding site in the metC-cysK promoter region in Lactococcus lactis. *Microbiology 151*, 439-46.
(75) Hryniewicz, M. M., and Kredich, N. M. (1991) The cysP promoter of Salmonella typhimurium: characterization of two binding sites for CysB protein, studies of in vivo

transcription initiation, and demonstration of the anti-inducer effects of thiosulfate. *J Bacteriol 173*, 5876-86.

(76) Lochowska, A., Iwanicka-Nowicka, R., Plochocka, D., and Hryniewicz, M. M. (2001) Functional dissection of the LysR-type CysB transcriptional regulator. Regions important for DNA binding, inducer response, oligomerization, and positive control. *J Biol Chem 276*, 2098-107.

(77) Monroe, R. S., Ostrowski, J., Hryniewicz, M. M., and Kredich, N. M. (1990) In vitro interactions of CysB protein with the cysK and cysJIH promoter regions of Salmonella typhimurium. *J Bacteriol 172*, 6919-29.

(78) van Keulen, G., Girbal, L., van den Bergh, E. R., Dijkhuizen, L., and Meijer, W. G. (1998) The LysR-type transcriptional regulator CbbR controlling autotrophic CO2 fixation by Xanthobacter flavus is an NADPH sensor. *J Bacteriol 180*, 1411-7.

(79) Zwieb, C. a. A., S. (1994) Improved plasmid vectors for the analysis of protein-induced DNA bending. *Methods Mol. Biol. 30*, 281-294.

(80) Thompson, J. F., and Landy, A. (1988) Empirical estimation of protein-induced DNA bending angles: applications to lambda site-specific recombination complexes. *Nucleic Acids Res 16*, 9687-705.

(81) Sambrook, j., and Russell, D. (2001) *Molecular Cloning; A Laboratory Manual*, Cold Spring Harbor Laboratory Press, Cold Spring Harbor, New York.

(82) Pluthero, F. G. (1993) Rapid purification of high-activity Taq DNA polymerase. *Nucleic Acids Res 21*, 4850-1.

(83) Jing, D., Agnew, J., Patton, W. F., Hendrickson, J., and Beechem, J. M. (2003) A sensitive two-color electrophoretic mobility shift assay for detecting both nucleic acids and protein in gels. *Proteomics 3*, 1172-80.

(84) Jing, D., Beechem, J. M., and Patton, W. F. (2004) The utility of a two-color fluorescence electrophoretic mobility shift assay procedure for the analysis of DNA replication complexes. *Electrophoresis 25*, 2439-46.

(85) Kaplan, A., and Reinhold, L. (1999) Co2 Concentrating Mechanisms In Photosynthetic Microorganisms. *Annu Rev Plant Physiol Plant Mol Biol 50*, 539-570.

(86) Badger, M. R., Hanson, D., and Price, G. D. (2002) Evolution and diversity of CO2 concentrating mechanisms in cyanobacteria. *Functional Plant Biology 29*, 161-173.

(87) Giordano, M., Beardall, J., and Raven, J. A. (2005) CO2 CONCENTRATING MECHANISMS IN ALGAE: Mechanisms, Environmental Modulation, and Evolution. *Annual Review of Plant Biology 56*, 99-131.

(88) Kaplan, A., Schwarz, R., Lieman-Hurwitz, J., and Reinhold, L. (1991) Physiological and Molecular Aspects of the Inorganic Carbon-Concentrating Mechanism in Cyanobacteria. *Plant Physiol. 97*, 851-855.

(89) Price, G. D., Badger, M. R., Woodger, F. J., and Long, B. M. (2008) Advances in understanding the cyanobacterial CO2-concentrating-mechanism (CCM): functional components, Ci transporters, diversity, genetic regulation and prospects for engineering into plants. *J. Exp. Bot. 59*, 1441-1461.

(90) Sainsbury, S., Lane, L. A., Ren, J., Gilbert, R. J., Saunders, N. J., Robinson, C. V., Stuart, D. I., and Owens, R. J. (2009) The structure of CrgA from Neisseria meningitidis reveals a new octameric assembly state for LysR transcriptional regulators. *Nucleic Acids Res 37*, 4545-58.

(91) Ogawa, T., and Togasaki, R. K. (1988) Carbonyl Sulfide: An Inhibitor of Inorganic Carbon Transport in Cyanobacteria. *Plant Physiol 88*, 800-804.

(92) Ogawa, T., and Kaplan, A. (1987) The Stoichiometry between CO(2) and H Fluxes Involved in the Transport of Inorganic Carbon in Cyanobacteria. *Plant Physiol 83*, 888-891.

(93) Sharkey, T. D., Stitt, M., Heineke, D., Gerhardt, R., Raschke, K., and Heldt, H. W. (1986) Limitation of Photosynthesis by Carbon Metabolism: II. O(2)-Insensitive CO(2) Uptake Results from Limitation Of Triose Phosphate Utilization. *Plant Physiol 81*, 1123-1129.

(94) Omata, T., and Ogawa, T. (1986) Biosynthesis of a 42-kD Polypeptide in the Cytoplasmic Membrane of the Cyanobacterium Anacystis nidulans Strain R2 during Adaptation to Low CO(2) Concentration. *Plant Physiol 80*, 525-530.

(95) Omata, T., and Ogawa, T. (1985) Changes in the Polypeptide Composition of the Cytoplasmic Membrane in the Cyanobacterium *Anacystis nidulans* during Adaptation to Low CO_2 Conditions. *Plant Cell Physiol*, 1075-1081.
(96) Ogawa, T., and Ogren, W. (1985) ACTION SPECTRA FOR ACCUMULATION OF INORGANIC CARBON IN THE CYANOBACTERIUM, *Anabaena variabilis*. *Photochemistry and Photobiology 41*, 583-587.
(97) Shibata, M., Ohkawa, H., Kaneko, T., Fukuzawa, H., Tabata, S., Kaplan, A., and Ogawa, T. (2001) Distinct constitutive and low-CO2-induced CO2 uptake systems in cyanobacteria: genes involved and their phylogenetic relationship with homologous genes in other organisms. *Proc Natl Acad Sci U S A 98*, 11789-94.
(98) Klughammer, B., Sultemeyer, D., Badger, M. R., and Price, G. D. (1999) The involvement of NAD(P)H dehydrogenase subunits, NdhD3 and NdhF3, in high-affinity CO2 uptake in Synechococcus sp. PCC7002 gives evidence for multiple NDH-1 complexes with specific roles in cyanobacteria. *Mol Microbiol 32*, 1305-15.
(99) Prommeenate, P., Lennon, A. M., Markert, C., Hippler, M., and Nixon, P. J. (2004) Subunit composition of NDH-1 complexes of Synechocystis sp. PCC 6803: identification of two new ndh gene products with nuclear-encoded homologues in the chloroplast Ndh complex. *J Biol Chem 279*, 28165-73.
(100) Zhang, P., Battchikova, N., Jansen, T., Appel, J., Ogawa, T., and Aro, E. M. (2004) Expression and functional roles of the two distinct NDH-1 complexes and the carbon acquisition complex NdhD3/NdhF3/CupA/Sll1735 in Synechocystis sp PCC 6803. *Plant Cell 16*, 3326-40.
(101) Woodger, F. J., Bryant, D. A., and Price, G. D. (2007) Transcriptional regulation of the CO2-concentrating mechanism in a euryhaline, coastal marine cyanobacterium, Synechococcus sp. Strain PCC 7002: role of NdhR/CcmR. *J Bacteriol 189*, 3335-47.
(102) Maddocks, S. E., and Oyston, P. C. (2008) Structure and function of the LysR-type transcriptional regulator (LTTR) family proteins. *Microbiology 154*, 3609-23.
(103) Schell, M. A. (1993) Molecular biology of the LysR family of transcriptional regulators. *Annu Rev Microbiol 47*, 597-626.
(104) Nishimura, T., Takahashi, Y., Yamaguchi, O., Suzuki, H., Maeda, S. I., and Omata, T. (2008) Mechanism of low CO(2)-induced activation of the cmp bicarbonate transporter operon by a LysR family protein in the cyanobacterium Synechococcus elongatus strain PCC 7942. *Mol Microbiol*.
(105) Myszka, D. G. (1999) Improving biosensor analysis. *J Mol Recognit 12*, 279-84.
(106) Hellman, L. M., and Fried, M. G. (2007) Electrophoretic mobility shift assay (EMSA) for detecting protein-nucleic acid interactions. *Nat. Protocols 2*, 1849-1861.
(107) Pattnaik, P. (2005) Surface plasmon resonance. *Applied Biochemistry and Biotechnology 126*, 79-92.
(108) Jones, R. B., Gordus, A., Krall, J. A., and MacBeath, G. (2006) A quantitative protein interaction network for the ErbB receptors using protein microarrays. *Nature 439*, 168-74.
(109) Teh, H. F., Peh, W. Y., Su, X., and Thomsen, J. S. (2007) Characterization of protein--DNA interactions using surface plasmon resonance spectroscopy with various assay schemes. *Biochemistry 46*, 2127-35.
(110) Shultzaberger, R. K., Roberts, L. R., Lyakhov, I. G., Sidorov, I. A., Stephen, A. G., Fisher, R. J., and Schneider, T. D. (2007) Correlation between binding rate constants and individual information of E. coli Fis binding sites. *Nucleic Acids Res 35*, 5275-83.
(111) Kimura, M., Yamamoto, T., Zhang, J., Itoh, K., Kyo, M., Kamiya, T., Aburatani, H., Katsuoka, F., Kurokawa, H., Tanaka, T., Motohashi, H., and Yamamoto, M. (2007) Molecular basis distinguishing the DNA binding profile of Nrf2-Maf heterodimer from that of Maf homodimer. *J Biol Chem 282*, 33681-90.
(112) Engohang-Ndong, J., Baillat, D., Aumercier, M., Bellefontaine, F., Besra, G. S., Locht, C., and Baulard, A. R. (2004) EthR, a repressor of the TetR/CamR family implicated in ethionamide resistance in mycobacteria, octamerizes cooperatively on its operator. *Mol Microbiol 51*, 175-88.

(113) Boozer, C., Kim, G., Cong, S., Guan, H., and Londergan, T. (2006) Looking towards label-free biomolecular interaction analysis in a high-throughput format: a review of new surface plasmon resonance technologies. *Curr Opin Biotechnol 17*, 400-5.
(114) Brockman, J. M., Nelson, B. P., and Corn, R. M. (2000) Surface plasmon resonance imaging measurements of ultrathin organic films. *Annu Rev Phys Chem 51*, 41-63.
(115) Campbell, C. T., and Kim, G. (2007) SPR microscopy and its applications to high-throughput analyses of biomolecular binding events and their kinetics. *Biomaterials 28*, 2380-92.
(116) Homola, J. (2003) Present and future of surface plasmon resonance biosensors. *Anal Bioanal Chem 377*, 528-39.
(117) Lee, H. J., Yan, Y., Marriott, G., and Corn, R. M. (2005) Quantitative functional analysis of protein complexes on surfaces. *J Physiol 563*, 61-71.
(118) Kyo, M., Yamamoto, T., Motohashi, H., Kamiya, T., Kuroita, T., Tanaka, T., Engel, J. D., Kawakami, B., and Yamamoto, M. (2004) Evaluation of MafG interaction with Maf recognition element arrays by surface plasmon resonance imaging technique. *Genes Cells 9*, 153-64.
(119) Papageorgiou, G., Tsimilli-Michael, M., and Stamatakis, K. (2007) The fast and slow kinetics of chlorophyll a fluorescence induction in plants, algae and cyanobacteria: a viewpoint. *Photosynthesis Research 94*, 275-290.
(120) Campbell, D., and Oquist, G. (1996) Predicting Light Acclimation in Cyanobacteria from Nonphotochemical Quenching of Photosystem II Fluorescence, Which Reflects State Transitions in These Organisms. *Plant Physiol. 111*, 1293-1298.
(121) Drath, M., Baier, K., and Forchhammer, K. (2009) An alternative methionine aminopeptidase, MAP-A, is required for nitrogen starvation and high-light acclimation in the cyanobacterium Synechocystis sp. PCC 6803. *Microbiology 155*, 1427-1439.
(122) Geitmann, M., and Danielson, U. H. (2004) Studies of substrate-induced conformational changes in human cytomegalovirus protease using optical biosensor technology. *Analytical Biochemistry 332*, 203-214.
(123) Mi, H., Klughammer, C., and Schreiber, U. (2000) Light-Induced Dynamic Changes of NADPH Fluorescence in Synechocystis PCC 6803 and Its ndhB-Defective Mutant M55. *Plant Cell Physiol. 41*, 1129-1135.
(124) Lieman-Hurwitz, J., Haimovich, M., Shalev-Malul, G., Ishii, A., Hihara, Y., Gaathon, A., Lebendiker, M., and Kaplan, A. (2008) A cyanobacterial AbrB-like protein affects the apparent photosynthetic affinity for CO by modulating low-CO-induced gene expression. *Environ Microbiol*.

APPENDIX A

Oligonucleotide Primers (PCR)

CcmR Protein Expression Construct (N-Term His-Tag)	
For: 5' GCGCAATATGATGCAAAGCAACCTTACACAA 3'	Rev: 5' GCGCCTCGAGTTAAAGAACTAACTTCACAGGGGTTT 3'
CcmR Protein Expression Construct (C-Term His-Tag)	
For: 5' GCGCCATATGCAAGCAACCTTACACCAATTAAAAG 3'	Rev: 5' GCGCCTCGAGAAGAACTAACTTCACAGG 3'
CmpR Protein Expression Construct (N-Term His-Tag)	
For: 5' GCGCGCCTCGAGATGAAAAATGCACCCTCC 3'	Rev: 5' GCGCGCCTCGAGTTAAAAAATTTGGGCAATGGA 3'
CmpR Protein Expression Construct (C-Term His-Tag)	
For: 5' GCGCCATATGAAAAATGCCACCCTCCAC 3'	Rev: 5' CGCCTCGAGAAAAATTTGGGCAATGGAAAC 3'
ycf30 Protein Expression Construct (N-Term His-Tag)	
For: 5' CTCGAGATGTCGGATATCCCGTTCAC 3'	Rev: 5' CTCGAGTTAAGTAACCGAGTCGATTTCAATG 3'
ycf30 Protein Expression Construct (C-Term His-Tag)	
For: 5' GCGCCATATGTCGGATATCCCGTTCACG 3'	Rev: 5' GCGCCTCGAGAGTAACCGAGTCGATTTCAATG 3'

GSx sequences are for the gel-shifting DNA targets. The numbers are relative to the translational start site unless otherwise indicated.

GS3 (394bp ccmR -194, +200 [transcriptional start site relative])	
For: 5' ATCGGGCCTCGGCCC 3'	Rev: 5' GTGGCTTCAAAAACTTTTAATTGG 3'
GS4 (347bp end bend ccmR -90, +257 [transcriptional start site relative])	
For: 5' ATCGGGCCTCGGCCC 3'	Rev: 5' GTGGCTTCAAAAACTTTTAATTGG 3'
GS5 (347bp ccmR -120, +227 [transcriptional start site relative])	
For: 5' TTAGTCAACAGTTCTGTCATGGG 3'	Rev: 5' GTTGCTTGCATTGTCCTTGA 3'
GS6 (347bp ccmR -140, +207 [transcriptional start site relative])	
For: 5' GCCGCCTAAGCTGATTTG 3'	Rev: 5' CGAAGATGGTGATTTAGATGGG 3'
GS7 (347bp ccmR -165, +182)	
For: 5' ACCTTTGGGTCCGGGTC 3'	Rev: 5' ACAATTTGAAGGGGCAGATTAA 3'
GS8 (300bp ndhF3 -400, -100)	
For: 5' AATTCGGATATTTATGTAATTCGGAT 3'	Rev: 5' GACTGCCAGAACCCAGACA 3'
GS9 (300bp ndhF3 -300, +1)	
For: 5' ATTCACTTAAGCAAATGGTTGTTG 3'	Rev: 5' TTGGGGGTTGTGGGAAAT 3'
GS10 (300bp ndhF3 -500, -200)	
For: 5' CAAGTTCCCTCACAACTGGTAGA 3'	Rev: 5' ACAATGGTATAACCTAGATGCATAGAA 3'
GS11 (300bp sbtA -425, -125)	
For: 5' TCCGCTAGAATCCTCCCC 3'	Rev: 5' ACTCTTGTCTATGCAGGTTTGAATG 3'
GS12 (300bp sbtA -325, -25)	
For: 5' GGGGGCCATTGAGCA 3'	Rev: 5' AATTTATGGGGATTGGGGTAGT 3'
GS14 (300bp psbA2 -297, +3)	

For: 5’ TCATTATTTCATCTCCATTGTCCC 3’	Rev: 5’ CATTTGGTTATAATTCCTTATGTATTTGTC 3’
GS15 (300bp psbA2 -550, -250)	
For: 5’ TGCCCAGATGCAGGCCTT 3’	Rev: 5’ AGGGGCGACACAACTGATTT 3’
GS16 (300bp psbA2 -800, -500)	
For: 5’ CCATAATGAAGTCGGAGTTTCG 3’	Rev: 5’ CCGCAATCGTTGCTCACC 3’
GS17 (300bp psbA2 -1050, -750)	
For: 5’ GGGAATCTCCTGCACTTTG 3’	Rev: 5’ CTTTATGTTGATCCCCATGATC 3’
GS18 (300bp cmpR -297, +3)	
For: 5’ GGCGGCGGAGGTGAG 3’	Rev: 5’ CATAGTGGATTAATTTTATAGACTAC 3’
GS19 (300bp cmpR -400, -100)	
For: 5’ ATCCCCGGCCGCTT 3’	Rev: 5’ TGGATTAGTCATTGTCCTCGG 3’
GS20 (300bp cmpR -700, -400)	
For: 5’ GGTAATCAATTGGGCCAATAC 3’	Rev: 5’ ATTAGCCCAGAAATGATGCC 3’
GS21 (300bp cmpR -1000, -700)	
For: 5’ GATGCGATAGGGCCAAGG 3’	Rev: 5’ CAGGGAAATGGTATTGCCGT 3’
GS22 (300bp ycf30 -297, +3)	
For: 5’ TTTGACCAGGGTGTTTAATGC 3’	Rev: 5’ CATAGATCCAGCCAAACGATG 3’
GS23 (300bp ycf30 -400, -100)	
For: 5’ CGTGGAAGCAGAAAAGGATT 3’	Rev: 5’ AATGGGAACCTAGTTAATATCAGGACT 3’
GS24 (300bp ycf30 -700, -400)	
For: 5’ TTACCGCCAAAAAGTTGGTC 3’	Rev: 5’ CCAATCTCAGCGGCAGC 3’
GS25 (300bp ycf30 -1000, -700)	
For: 5’ AGTTGTCCTTGCTTGTAGTGGAG 3’	Rev: 5’ TCCCCTGGCGGTTTTT 3’
GS26 (175bp ccmR -110, +65 [transcriptional start site relative])	
For: 5’ GTTCTGTCATGGGACTGAGAATC 3’	Rev: 5’ GTCAATAACTAAAATAGACCTAT 3’
GS27 (213bp slr0808 16s rRNA processing protein RimM homolog +30, +243)	
For: 5’ ACAGAAAATTGGCTGGAAATC 3’	Rev: 5’ TTCAGTAAAACGCAGAATATAAAGG 3’
GS28 (225bp ccmR -50, +175 [transcriptional start site])	
For: 5’ TCCCCGGACTAAGCTTGTC 3’	Rev: 5’ GAAGGGGCAGATTAATTTTTTTC 3’
GS29 (225bp ccmR -226, -1 [transcriptional start site])	
For: 5’ GGCTCCTTTCTGACTGAAATCTC 3’	Rev: 5’ AACCAATGATAGAATAAAGCCAATG 3’
GS30 (225bp ccmR -138, +87 [transcriptional start site])	
For: 5’ CGCCTAAGCTGATTTGCG 3’	Rev: 5’ CTTGGGTCTAGGATGTGCTGA 3’
GS31 (300bp ndhD5 -350, -50)	
For: 5’ GGAGCGGGCCATGGT 3’	Rev: 5’ GGCCAGTTTCATGGTGGC 3’
GS32 (300bp ubiX -350, -50)	
For: 5’ TGGCCTACGAAGATGTTATTGC 3’	Rev: 5’ ACAAACCAATCGACGTATTAGATCA 3’
GS33 (300bp cmpA -350, -50)	
For: 5’ GGGCTGGGTCAGAAACAATT 3’	Rev: 5’ AGCGCCATGGATATCCCC 3’
GS34 (300bp rbcL -350, -50)	
For: 5’ TCACCGGAGGAGTGGCAAT 3’	Rev: 5’ GAAATTTGGCAATATAAAGCCTACC 3’
GS35 (300bp G6P dehydrogenase -350, -50)	
For: 5’ CCGAAGTGTTAGATGTAAACCTGA 3’	Rev: 5’ TCCCGAAAGTTTTCTTTTTCTG 3’

GS36 (300bp G3P dehydrogenase -350, -50)	
For: 5’ AGCTAATGCTTTAGGGGATGC 3’	Rev: 5’ ATTAGGGAGAATGGGAAAAAATACTT 3’
GS37 (300bp Isocitrate dehydrogenase -350, -50)	
For: 5’ ATCCAAACTTGATTTTTGAAAAACG 3’	Rev: 5’ GAGGCTCTGATTGCATTGG 3’
GS38 (300bp Malate dehydrogenase -350, -50)	
For: 5’ CTGGGGAGAAACTAGCCAAA 3’	Rev: 5’ TCGATTTGGTCTAAGCGCA 3’
GS39 (100bp slr0808 16s rRNA processing protein rimM homolog +41, +141)	
For: 5’ GGCTGGAAATCGGTACCAT 3’	Rev: 5’ TTGACCCTTAGTCAAAAATCTAGCT 3’
GS40 (107bp slr0808 16s rRNA processing protein rimM homolog +3, +109)	
For: 5’ GGCAGAACCCATGACAGAACAACA 3’	Rev: 5’ CTGATGCTGAAAGAACCCGCACTT 3’
CmpA (305bp cmpA -510, -205)	
For: 5’ GCAATCACTTCCTGCAATTGATCC 3’	Rev: 5’ GCGCCCAATTTTTTATGTAATTTATAGTC 3’
GS42 (300bp ndhF3 -400, -100 [BamHI])	
For: 5’ GCGCGGATCCAATTCGGATATTTATGTAATTCGGAT 3’	Rev: 5’ GCGGATCCGACTGCCAGAACCCAGACA 3’
GS43 (305bp cmpA -510, -305 [BamHI])	
For: 5’ GCGGATCCGCAATCACTTCCTGCAATTGATCC 3’	Rev: 5’ GCGGATCCGCGCCCAATTTTTTATGTAATTTATAGTC 3’
GS44 (300bp cmpA -350, -50 [BamHI])	
For: 5’ GCGGATCCGGGCTGGGTCAGAAACAATT 3’	Rev: 5’ GCGGATCCAGCGCCATGGATATCCCC 3’
GS45 (301bp cmpA -558, -258 [BamHI])	
For: 5’ GGATCCTGGTAATAGTTGCTAGGCGCA 3’	Rev: 5’ GGATCCAATGCCACCCTCCACCAATTT 3’

Surface Plasmon Resonance Primers. Primers used to create DNA fragments for binding studies using the SPR machine.

SPR1 (300bp ndhf3 -400, -100) 5’ Modified (Amine)	For: 5’ AATTCGGATATTTATGTAATTCGGAT 3’
SPR2 (ccmR -138, +175) 5’ Modified (Amine)	For: 5’ CGCCTAAGCTGATTTGCG 3’
SPR3 (300bp rimM +3, +303) 5’ Modified (Amine)	For: 5’ GGCAGAACCCATGACAGAACAACA 3’
SPR4 (300bp rimM +3, +303)	Rev: 5’ GGTGGCGGGGACTAATAGTTGG 3’
SPR5 (300bp cmpA -275, +25) 5’ Modified (Amine)	For: 5’ TGGTGGAGGGTGGCATTTTTC 3’
SPR6 (300bp cmpA -275, +25)	Rev: 5’ AATTTACGTCGATTGAATGAACCCATAAC 3’
SPR7 (300bp ndhF3 -400, -100) 5’ Modified (Biotin)	For: 5’ AATTCGGATATTTATGTAATTCGGAT 3’
SPR8 (142bp ndhF3 -333, -191) 5’ Modified (Biotin)	For: 5’ TAGCCTGCCTCTTCCTC 3’
SPR9 (142bp ndhF3 -333, -191)	Rev: 5’ AGTCAAGCGACAATGGTATAACC 3’
SPR10 (cmpA -275, +25) 5’ Modified (Biotin)	For: 5’ TGGTGGAGGGTGGCATTTTTC 3’
SPR11 (300bp rimM +3, +303) 5’ Modified (Biotin)	For: 5’ GGCAGAACCCATGACAGAACAACA 3’
SPR12 (G3P -350) 5’ Modified (Biotin)	For: 5’ GCGCAGCTAATGCTTTAGGGGATGC 3’
SPR13 (197bp ccmR -110, +87) 5’ Modified (Biotin)	For: 5’ GCGTTCTGTCATGGGACTGAGAATC 3’
SPR14 (137bp ccmR -50, +87) 5’ Modified (Biotin)	For: 5’ GCTCCCCGGACTAAGCTTGTC 3’
SPR15 (150bp ndhD5 -327, -177) 5’ Modified (Biotin)	For: 5’ GGCTTGTATTTTTGTGACTGTGATC 3’
SPR16 (150bp ndhD5 -327, -177)	Rev: 5’ GGAGTAAGAAAGCCAGTGCGGG 3’
SPR17 (154bp sbtA -325, -171) 5’ Modified	For: 5’ GGGGGCCATTGAGCA 3’
SPR18 (154bp sbtA -325, -171)	Rev 5’ GCTAAAGTCTATATGTAAATCCG 3’
SPR19 (150bp ubiX -330, -180) 5’ Modified (Biotin)	For: 5’ CCACCATTCCCCCGTTGATTGAG 3’
SPR20 (150bp ubiX -330, -180)	Rev 5’ CTAGGGCTTCCAGCAAGGC 3’

Fusion PCR. Underlined sequences correspond to the resistance cassette.

UbiX_LF (-545, +26 nt Fusion PCR)	For: 5’ CGGACCCGACCATAGTGGAACC 3’
Kan_LR_UbiX_LR (-545, +26 nt Fusion PCR)	Rev: 5’ GAGATTTTGAGACACAACGTGGCT ACCCCCAAAATCAAAGGTTGT 3’
Kan_RR_UbiX_RF (+585, +1164 nt Fusion PCR)	For: 5’ GCAAAGCAAAAGTTCAAAATCACC TCCAGCGTTGGCAAGGGGGTAT 3’
UbiX_RR (+585, +1164 nt Fusion PCR)	Rev: 5’ TTTGCCGTAAAACTCACGGTAGTCATGTTG 3’
UbiD_LF (-540, +33 nt Fusion PCR)	For: 5’ AAGCCATTGGCCCCGCCAGTGA 3’
Kan_LR_UbiD_LR (-540, +33 nt Fusion PCR)	Rev: 5’ GAGATTTTGAGACACAACGTGGCTCAACTGGATGAATCCCCGTAAATCT 3’
Kan_RR_UbiD_RF (+1455, +2051 nt Fusion PCR)	For: 5’ GCAAAGCAAAAGTTCAAAATCACC ATATTAATTTAACCGAAGTTAATCCCAAC 3’
UbiD_RR (+1455, +2051 nt Fusion PCR)	Rev: 5’ ATCTTCTAAAGCTTTGGCGATCGTGGCCA 3’

APPENDIX B

Figure B1a

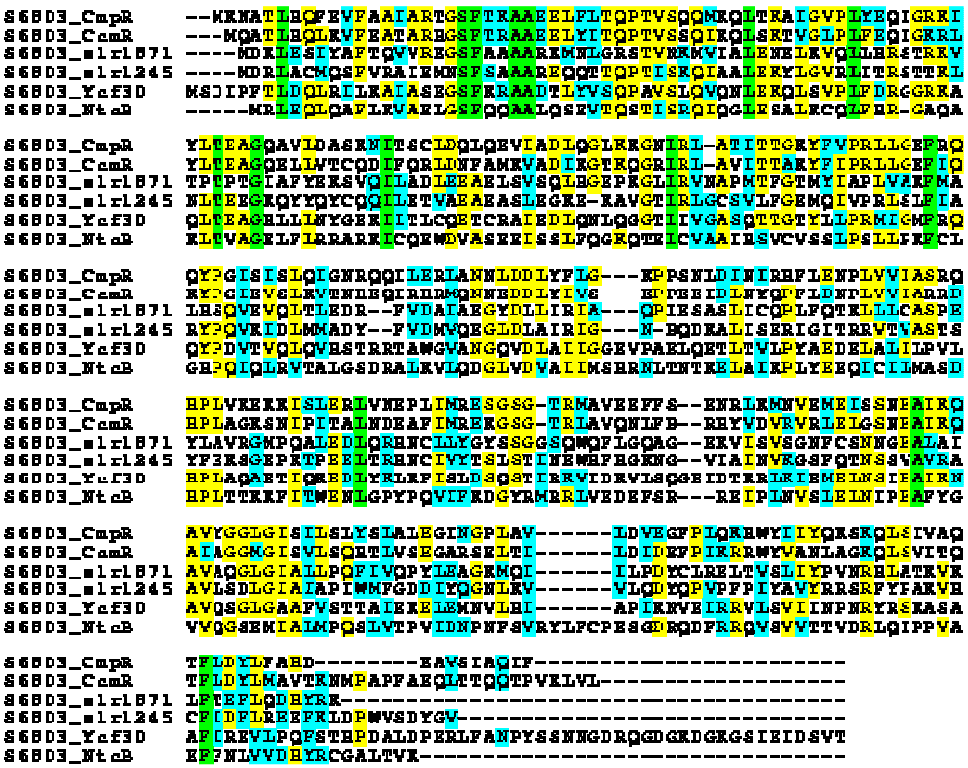

Figure B1a: Sequence alignments for all six LTTRs within *Synechocystis* sp. PCC 6803. Alignments were generated from the sequences available at the Cyanobase database, and processed using an alignment program available at the San Diego Super Computer.

Residues marked in green are conserved across all of the aligned proteins. Residues marked in yellow are identical among at least 2 of the sequences. Residues marked in cyan indicating strong conservation among at least 2 of the sequences.

Figure B1b

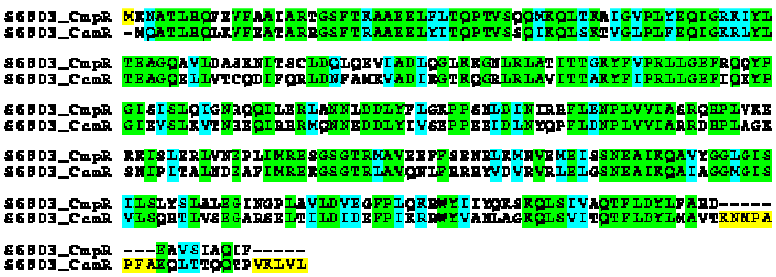

Figure B1b: Sequence alignments for the two inorganic carbon acquisition regulators within Synechocystis sp. PCC 6803. Alignments were generated from the sequences available at the Cyanobase database, and processed using an alignment program available at the San Diego Super Computer.

Residues marked in green are conserved across all of the aligned proteins.
Residues marked in cyan indicate strong conservation among the sequences.

Figure B1c

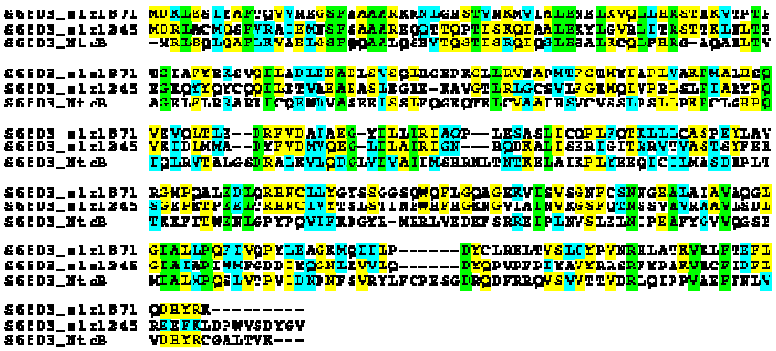

Figure B1c: Sequence alignments for three members of one branch (Figure B1e) of the paralogous regulators within *Synechocystis* sp. PCC 6803. Alignments were generated from the sequences available at the Cyanobase database, and processed using an alignment program available at the San Diego Super Computer.

Residues marked in green are conserved across all of the aligned proteins.
Residues marked in yellow are identical among at least 2 of the sequences.
Residues marked in cyan indicate strong conservation among at least 2 of the sequences.

Figure B1d

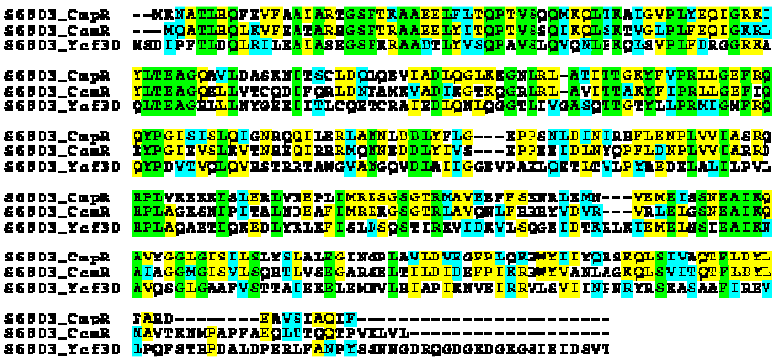

Figure B1d: Sequence alignments for three members of one branch (Figure B1e) of the paralogous regulators within *Synechocystis* sp. PCC 6803. Alignments were generated from the sequences available at the Cyanobase database, and processed using an alignment program available at the San Diego Super Computer.

Residues marked in green are conserved across all of the aligned proteins.
Residues marked in yellow are identical among at least 2 of the sequences.
Residues marked in cyan indicate strong conservation among at least 2 of the sequences.

Figure B1e

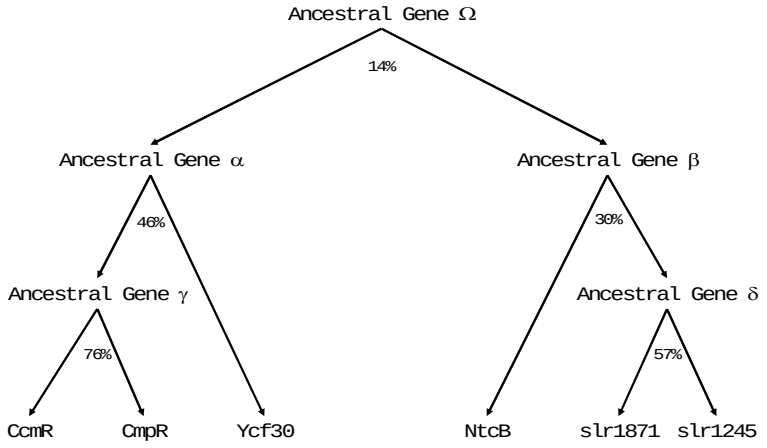

Figure B1e: Percentages are based on identity and strong conservation from the applicable sequence alignments. The 'ancestral genes' are hypothetical branch points for the gene duplication events (see main text). [See Figure B1a-d, B2]

Figure B2

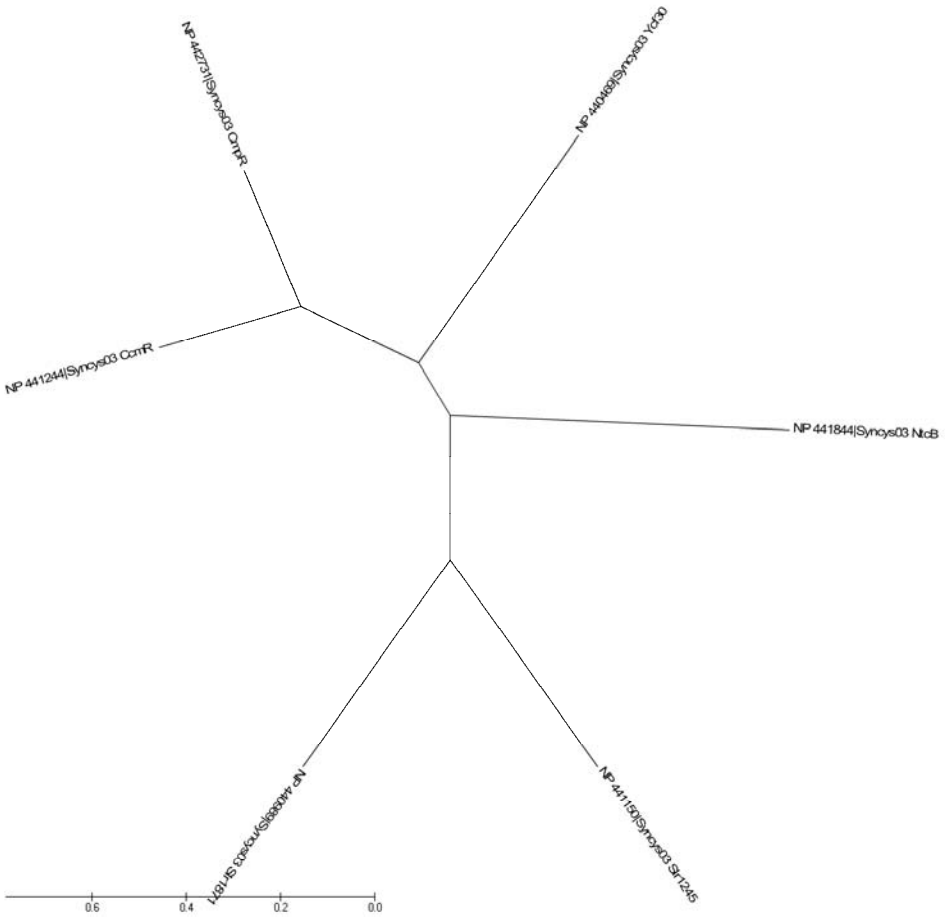

Figure B2: Unrooted tree generated from the sequence alignments (see Figure B1a) for all six LTTRs found within *Synechocystis* sp. PCC 6803.

Figure B3

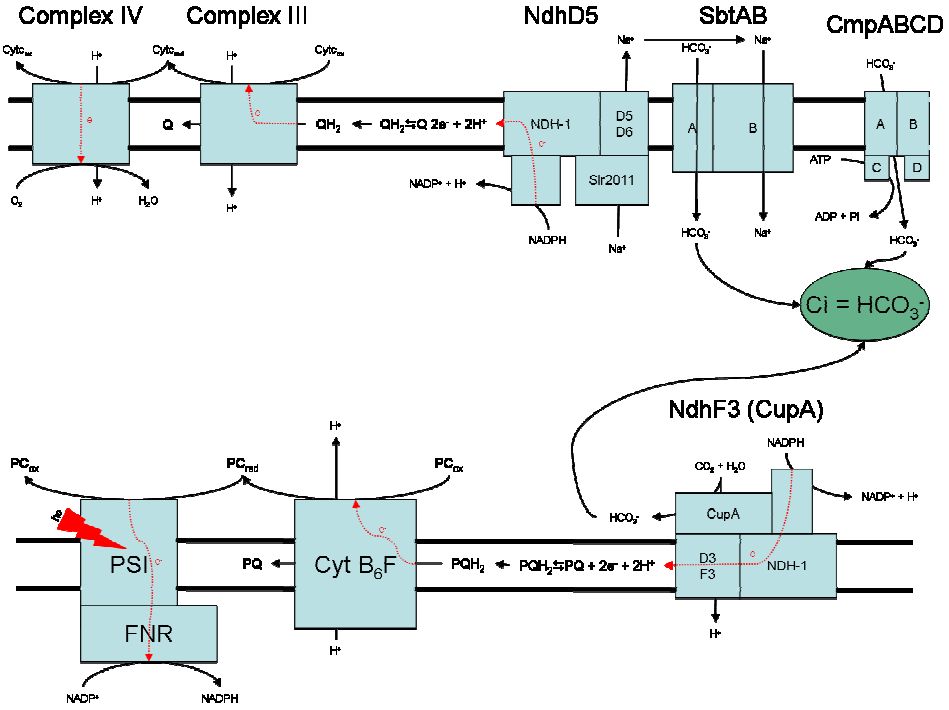

Figure B3. Theoretical diagram delineating electron usage within CCM (with links to photophosphorylation and oxidative phosphorylation).

APPENDIX C

Figure C1

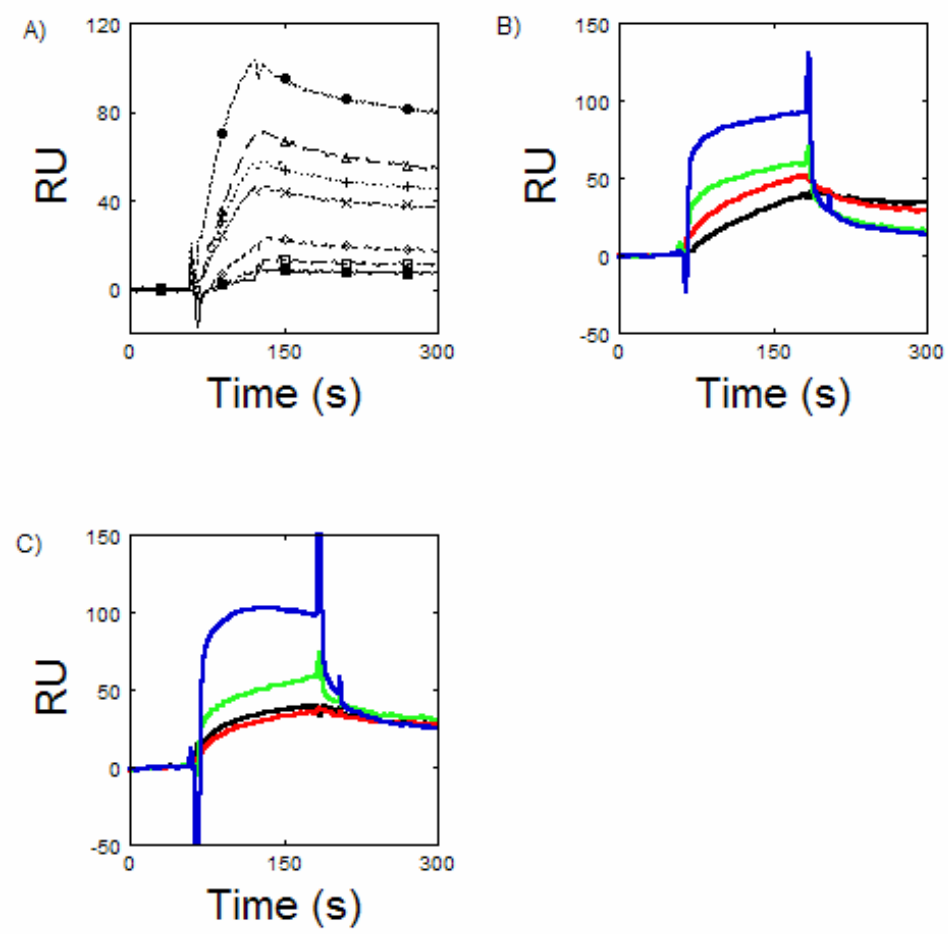

Figure C1

A) SPR curve showing the binding of Synechocystis CmpR to the promoter region of cmpA. Data markers for visualization purpose only. See Figure 2 in main text for details. Protein (CmpR) concentration for each target is as follows; 0 nM (Closed Square), 250 nM (Open Square), 500 nM (Open Diamond), 750 nM (X), 1000 nM (+), 2000 nM (Open Triangle), 3000 nM (Closed Circle). Protein was incubated with the indicated ligand molecule on ice for at least 5 minutes before injection. All injections contain 1.5 μM of CmpR and, for B and C, 0 μM (Black), 10 μM (Red), 100 μM (Green), or 500 μM (Blue) of the indicated ligand molecule.

B) 2PG

C) RuBP

Figure C2

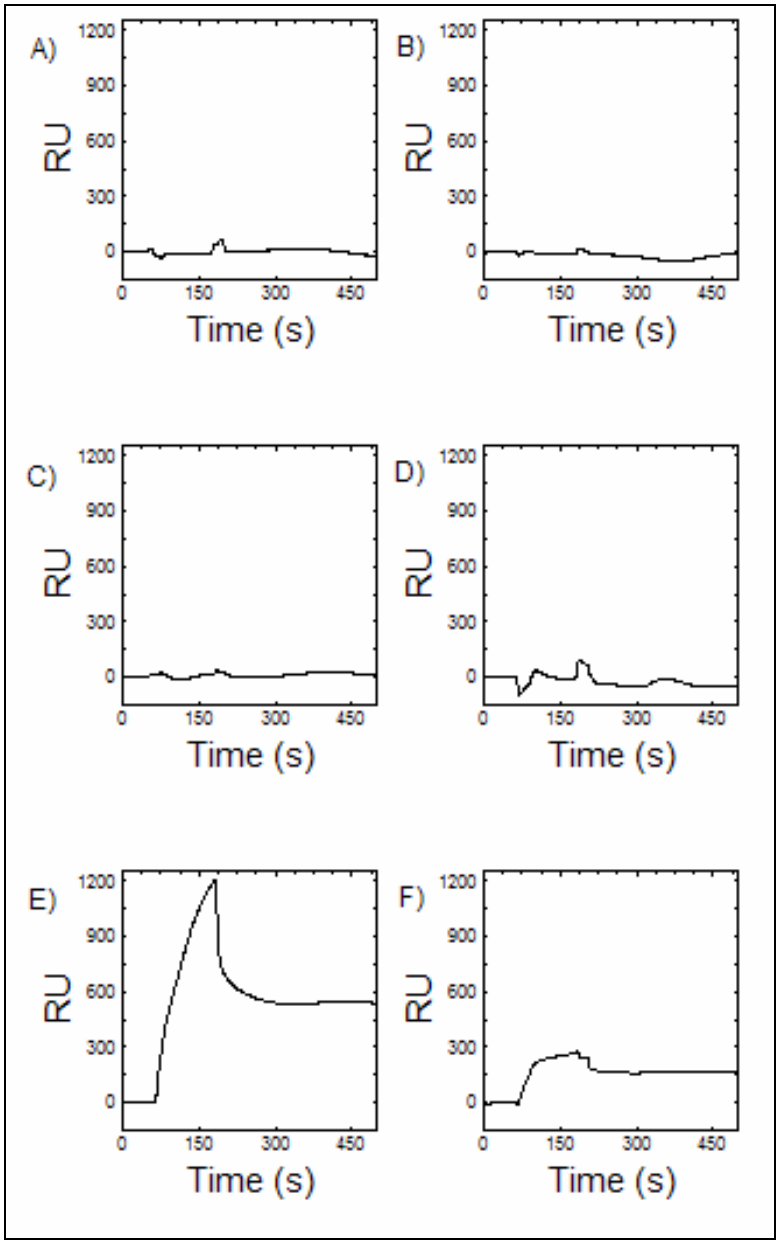

Figure C2
SPR curves illustrating ligand molecule screening using CcmR binding to immobilized biotinylated DNA fragment (pndhF3, see Table 1) with and without the indicated small molecule. DNA immobilization as described in Figure 2. For assay method see Figure 2. All small molecules were injected at 500 μM. All curves are double referenced (*90*).
A) Pyruvate.
B) PEP.
C) NADPH.
D) 2PG.
E) $NADP^+$.
F) α-KG.

Table C 1

SPR Kinetic Values							
Average Protein RU[1] 37.99 kDa[2]	Average Protein (pg)	Average Protein (pmol)	n	DNA RU[3,4] 92.868 kDa	DNA (pg)	DNA (pmol)	Protein:DNA Ratio (M)
111.79	111.79	2.93×10^{-3}	3	90.695	66.20	7.13×10^{-4}	4.13
112.268	112.268	2.95×10^{-3}	2	95.457	69.68	7.50×10^{-4}	3.94

[1]Protein: 1 RU = 1 pg/mm^2; [2]Each Monomer; [3]DNA: 1 RU = 0.73 pg/mm^2 (Engohang-Ndong *et al* 2008); [4]DNA Injected Only Once Per Set.

Table C 1
Data table of the CcmR:DNA molar ratio as determined using SPR.

APPENDIX D

EMSA Buffer 5x (Invitrogen Component E)

750 mM KCl; 0.5 mM DTT; 0.5 mM EDTA; 50 mM Tris pH 7.4

Native PAGE Buffer / Running Buffer 5x

250 mM Tris-Base (pH ~8.5 Don't adjust); 1.9 M glycine; 9.5 mM EDTA

Native Lysis/Wash Buffer

50 mM $Na_2PO_4^-$ pH 8.0; 750 mM NaCl; 20 mM imidazole; 20% sucrose ($^w/_v$)

Native Elution Buffer

50 mM $Na_2PO_4^-$ pH 8.0; 750 mM NaCl; 250 mM imidazole; 20% sucrose ($^w/_v$)

Protein Storage Buffers

50 mM Na_2HPO_4 pH 8.0; 300 mM NaCl; 30% Sucrose ($^w/_v$)

10 mM Pipes pH 7.4, 150 mM NaCl; 150 mM KCl; 5 mM $MgCl_2$; 0.01% Tween-20 ($^w/_v$)

SPR Running Buffer

10 mM Pipes pH 7.4, 150 mM NaCl; 150 mM KCl; 5 mM $MgCl_2$; 0.005% Triton X-100 ($^w/_v$)

10 mM Pipes pH 7.4, 300 mM NaCl; 0.02% Tween-20 ($^w/_v$)

VITA

Shawn Michael Edward Daley

Candidate for the Degree of

Doctorate of Philosophy

Dissertation: MODULATION OF THE TRANSCRIPTIONAL CONROL OF THE CARBON CONCENTRATION MECAHNISM WITHIN *SYNECHOCYSTIS* SP. PCC 6803

Major Field: Biochemistry and Molecular Biology

Biographical:

Education:
Completed the requirements for the Bachelors of Science in Biochemistry at Colorado State University, Fort Collins, Colorado in December 2002.

Experience:

- Research Associate, Professor Robert Burnap, Oklahoma State University, Stillwater OK, Summer 2004, Spring 2008 – Present
- Teaching Associate, Dept. Biochemistry & Molecular Biology, Oklahoma State University, Stillwater OK, Fall 2004 – Fall 2005, Spring 2009
- Bioinformatics Specialist, Professor Robert Burnap, Oklahoma State University (College of Arts & Sciences), Stillwater OK, Spring 2006 – Spring 2008
- Lab Technician, Associate Professor Karolin Luger, Colorado State University, Fort Collins CO, Spring 2003
- Undergraduate Student Researcher, Assistant/Associate Professor Karolin Luger, Colorado State University, Fort Collins CO, Fall 2002

Professional Memberships:

- American Chemical Society (2009 – Present)
- Sigma Xi [Associate Member, OSU Chapter] (2009 – Present)
- International Society for Photosynthesis Research (2006 – Present)
- American Association for the Advancement of Science (2001 – Present)
- American Society for Microbiology (2007)
- Oklahoma Academy of Sciences (2006 – 2007)

Name: Shawn Michael Edward Daley Date of Degree: July, 2010

Institution: Oklahoma State University Location: Stillwater, Oklahoma

Title of Study: MODULATION OF THE TRANSCRIPTIONAL CONROL OF THE CARBON CONCENTRATION MECAHNISM WITHIN *SYNECHOCYSTIS* SP. PCC 6803

Pages in Study: 123 Candidate for the Degree of Doctorate of Philosophy

Major Field: Biochemistry and Molecular Biology

Scope and Method of Study:

This study involved looking at paralogous proteins (CcmR and CmpR), which function as transcriptional regulators of the carbon concentration mechanism within the cyanobacteria *Synechocystis* sp. PCC 6803. Techniques used include electrophoretic mobility shift assay, Dynamic Light Scattering, gel-filtration chromatography, and surface plasmon resonance.

Findings and Conclusions:

For the first time the identification of the ligand molecules for CcmR, $NADP^+$ and α-KG, and their subsequent modulation of the binding characteristics for the protein and to target DNA. Additionally, the ligand molecules have been identified for CmpR, 2PG and RuBP. This allows for the first time the construction of a regulatory network or pathway for the carbon concentration mechanism and the apparent *in vivo* small molecule regulators.

ADVISER'S APPROVAL: Dr. Robert Burnap